Faculty of Engineering and Science
Department of Mechanical Engineering

Flow Physics Modelling and Design Optimization of an Exhaust-air Energy Extractor in the Cooling Tower Applications

Reuben Brandon Lee Huan Chung
(0000-0002-0521-4775)

This thesis is presented for the Degree of

Master of Philosophy

of

Curtin University

June 2023

ABSTRACT

In Malaysia, the demand for power generation increases annually as the country continuously moves towards the technology realm. Currently, the main source of generation is generated from non-renewable energy sources. For example, coal, gas, and petroleum are used in a vast variety of fields to meet the demand for power generation to combat climate change and global warming the country is turning to renewable energy to meet the demand for power generation. This research is carried out to support renewable energy in Malaysia, particularly the energy recovery sector, Specifically the waste recovery sector of the cooling tower applications often used in the industry. There is a lack of understanding of the reasoning behind the low efficiency of the air energy extractor. To underline the reasons for the low efficiency, this research investigates the flow physics and aerodynamics of the air energy extractor using both numerical and experimental methods. The main region studied is the region above the cooling tower region. The numerical study will be conducted in Ansys Fluent on a three-dimensional model. The wind velocity of 5m/s, 10m/s, and 15m/s and the selected Tip Speed Ratio (TSR) are used to determine the optimum coefficient of the moment for H-Darrieus, helical Darrieus, semi-elliptical savonious and the helical savonious turbines. The result of the numerical study shows the H-Darrieus VAWT with airfoil number S1046 achieved the maximum power coefficient of 0.39 at the TSR 3.0 and wind speed of 15m/s. Further study was conducted on the H-Darrieus by testing different airfoils, which are the S1048 and S1221 airfoil numbers. The maximum power coefficient achieved for the S1046, S1048, and S1221 airfoil profile are 0.36, 0.33 and 0.32 for respectively. In addition, the S1046 H-Darrieus was printed and tested on the experimental setup. An average error of 24.99% was found from the results of the numerical study and the experimental result. The best overall performing turbine is the H-Darrieus VAWT with the airfoil profile of S1046 both in numerical and experimental study.

Acknowledgement

I would personally like to thank my thesis committee. My principal supervisor, Professor Vincent Lee together with my co-supervisor Associate Prof. Dr Law Ming Chiat. Also, Associate Prof. Dr Sukanta Roy and Dr Yam Ke San for their continuous support in this study.

My thesis committee had given me a lot of support and guidance to ensure the completion of the thesis. Also, I would like to thank Curtin Malaysia Graduate School for their never-ending support to ensure that the study was conducted smoothly during the Covid-19 Pandemic. I would like to thank my lovely wife, Yeo Hui Hui for her continuous support throughout the entire process of making this thesis a success.

I would also like to thank the Fundamental Research Grant (FRGS) for its financial support.

Table of Contents

List of Figures

List of Tables

Nomenclature

Symbol	Definition	Unit
V_{in}	Inlet Velocity	m/s
V_{∞}	Freestream Velocity	m/s
V_{rel}	Relative Velocity	m/s
F_L	Lift force	N
F_D	Drag force	N
α	Wind angle of attack	°
γ	Blade pitch angle	°
θ	Azimuth angle	°
Ω	Angular Velocity	rad/s
C_M	Coefficient of Moment	
C_L	Lift Coefficient	
Cd	Drag Coefficient	
C_τ	Torque Coefficient	
C_P	Power Coefficient	

CHAPTER 1: INTRODUCTION

1.0 Introduction

Solar and wind are free, non-perishable, and are easily obtained sources of energy throughout the world. These energies provide a better economical substitute to fossil fuel-based sources and aid in healing the world's atmosphere and climate. Due to the increase in the demand for energy in the world, many countries are investing in studies of renewable energy systems to ensure the supply would meet the demand. Thus, in the year 2017, the world recognized the installation of solar energy extractor of 98 GW. This added to the cumulative capacity of 402GW for the year 2017. Meanwhile, for wind energy, 52 GW of wind energy systems were added to the total cumulative capacity of 539 GW (REN21 2019). Figure 1.1 shows the graph of the growth of the power capacity from wind generation at an increasing capacity from the year 2008 till 2018.

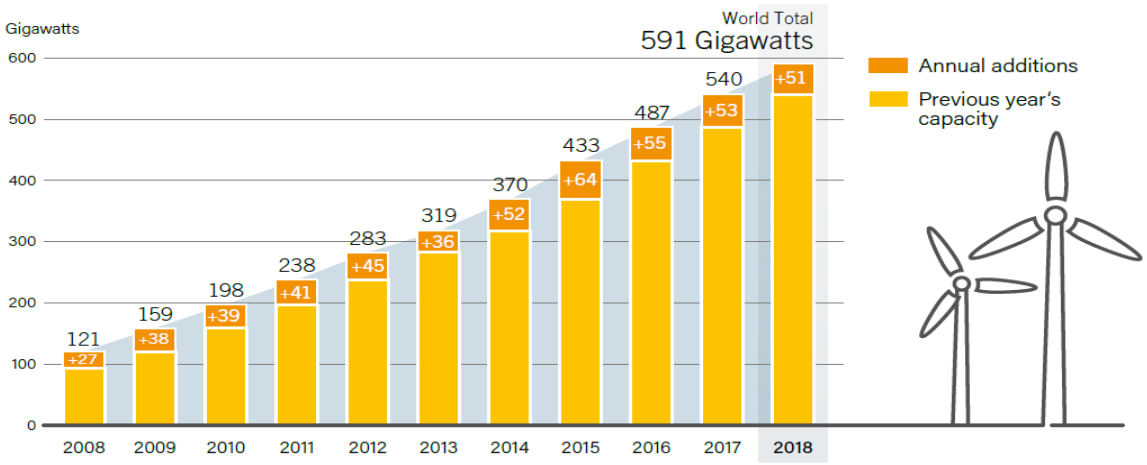

Figure 1.1:Wind Power Global Capacity and Annual Additions, 2008-2019 (REN21 2019)

There are many renewable energy resources available such as solar, wind, biomass, hydro, geothermal, and tidal wave power. However, Malaysia is a country known for its low velocity of wind when compared to other regions of the world. An average wind velocity of 1.5m/s and 4.5m/s is recorded for the lower altitude area and higher altitude areas, it can be in the range of 9 to 11m/s (Abdullah et al. 2019). To obtain the most output from a wind turbine, it would require a wind velocity of 8.5m/s to 10.99m/s (Razali et al. 2010). Although the average wind flow in Malaysia is light and non-uniform, it has the potential to generate a high amount of energy as the East

Coast States in Malaysia namely, Sabah and Sarawak can experience a strong wind speed of 15.4m/s (Borhanazad et al. 2013). Thus, there is a need to study other innovative methods to harvest wind energy in Malaysia as the wind speed in the region is considered light wind and is non-uniform.

In addition, wind energy provides a non-polluting and readily available throughout the world non-perishable source of renewable energy. It is also a key to reducing harmful gaseous emissions compared to using fossil-fuel to harvest energy. Current-day wind turbines are grouped into two major categories, horizontal wind axis and vertical axis wind turbine. These different wind turbine categories are shown in Figure1.2.

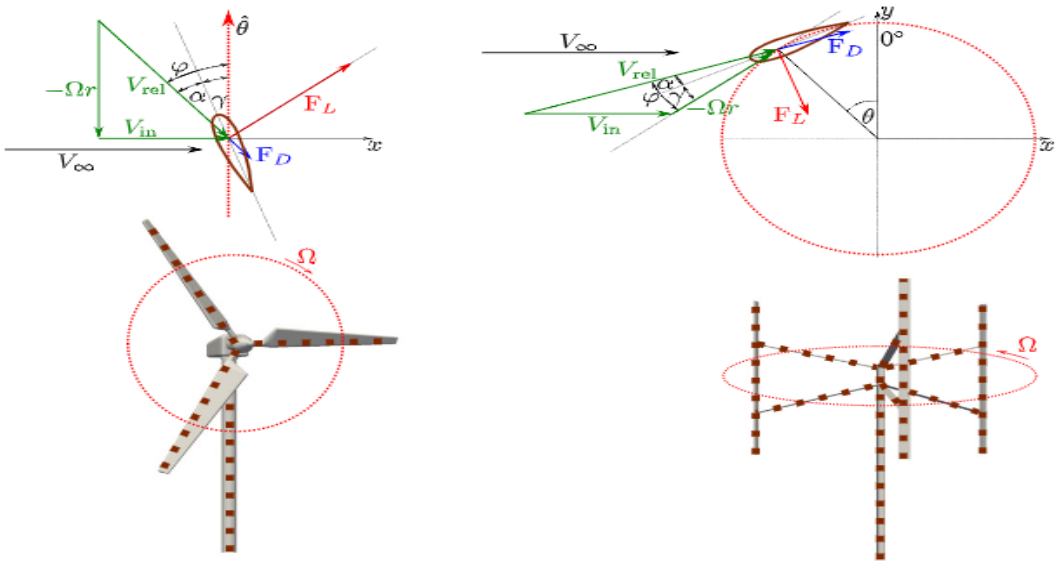

Figure 1.2:Horizontal axis wind turbine (HAWT) (left) and Vertical axis wind turbine (VAWT)(right).(Mendoza, Chaudhari, and Goude 2019)

1.1 Research Problem

There is a demand for a deeper understanding and innovative development of green energy technology to harvest energy from natural resources while leaving zero to no carbon footprint in Malaysia. The focus of this thesis is to analyse the flow physics of the air energy extractors through the usage of the Vertical Axis Wind Turbine (VAWT). The VAWT was employed to draw out maximum energy from the cooling towers. Cooling towers were used for many different purposes such as heating, ventilation, and air- conditioning (HVAC) systems in a wide industry. Combining the

VAWT with the region where the exhaust air escapes from the cooling tower, would enable an energy recovery system and would aid in combating climate change.

However, based on the study conducted by Fazlizan et al. (2015), the maximum efficiency of the Vertical Axis Wind Turbine (VAWT) in the cooling tower application could reach a low efficiency of approximately 13%. Thus, there is a serious need to study the flow physics and aerodynamics of the turbine to identify the reasons behind the low efficiency obtained in the cooling tower application. It is also important to study the turbine design. This would ensure a maximum efficiency could be achieved by extracting the energy from the cooling towers.

1.2 Research Questions

The research questions to be answered in this study are as follows:

1. What is the main cause of the low efficiency, 13% of the Vertical Axis Wind Turbine in the cooling tower application?

2. What is the associated aerodynamics and flow physics related to the current existing air energy extractor and what is the impact of it towards efficiency?

3. How can the flows physics aid in optimizing the design of the air energy extractor?

1.3 Research Objectives

The objectives for this research are as follows:

1. To determine the associated flow physics through velocity, and pressure surrounding the existing air energy extractor in the cooling tower application.
2. To determine the moments, aerodynamic forces and mechanical power generation by the air energy extractor via numerical studies.
3. To optimise the design of the air energy extractor with the aid of the flow and aerodynamic modelling by testing different type of airfoil on the best performing Vertical Axis Wind Turbine.
4. To validate the optimized air energy extractor in the experimental study and results will be compared with the numerical studies.

1.4 Novelty

Two types of VAWT (Darrieus and Savonius type) were employed in the study for the cooling tower application. The study included the H-Darrieus VAWT, Helical Darrieus VAWT, semi-elliptical Savonius VAWT, and the Helical Savonius VAWT. The improvement in the efficiency of the best-performance VAWT was studied. This was done through the optimization of the turbine blade air foil type. In addition, the flow physics of the vorticity, velocity, and pressure around the air energy extractor were developed with the aid of computational flow visualization and the calculations of the flow properties. Presentation of velocity profile and pressure profile to provide a better visualization of the flow physic. Thus, with the optimized design and understanding of the flow physics and aerodynamics, the reduction of carbon footprint in energy production can be calculated.

1.5 Scope of Work

The scope of this study was to further investigate the reason behind the low efficiency of the current existing VAWT in the cooling tower application through both qualitative and quantitative analysis of flow physics which have not been established in the cooling tower-controlled flow conditions. Also, the effect of aerodynamic forces on the VAWT under a cooling tower-guided flow setup will be addressed through this investigation. A new design of an air energy extractor would be deployed specifically for cooling tower application through the optimization of the turbine aspect ratio, solidity ratio, airfoil thickness, number of blades, blade chord, and chambers. The parameters were important and widely used when designing the VAWT.

With the new design, the flow physics around the air energy extractor was studied. Fabrication of a cooling tower to conduct experiments on the air energy extractor. The experimental result would be used to be compared with the numerical results.

Lastly, the study was expected to solve the air exhaust energy recovery problem of the cooling tower application and to analyze the fluid flow and aerodynamics related to the cooling tower applications.

1.6 Thesis Outline

Chapter 1 is the introduction which includes the introduction of VAWT in the cooling tower application. It also consists of the problem statement, objective, novelty and the scope of the research.

Besides, chapter 2 is the literature review. This chapter includes a brief literature review on the two types of VAWT (Darrieus and Savonious type). It also consists of the description of the VAWT in the cooling tower applications.

The chapter 3 focuses on the numerical methodology. All four of the selected VAWT CAD are shown in this chapter. The setting and meshing are discussed together with the appropriate turbulence model. Also, this chapter portrays the grid independence of the VAWT that is being studied.

In addition, chapter 4 spotlights the experimental methodology. The block diagram of the cooling tower is shown. The initial calibration result of the cooling tower fan is plotted. The set up for the experimental works are further discussed.

Chapter 5 is the results and discussion. This chapter includes the result, discussion of the result obtained through the simulation from Ansys Fluent and the experimental results.

Lastly, chapter 6 is the conclusion and recommendations. This chapter includes the conclusion of the overall research and the recommendation for any future research or projects.

CHAPTER 2: LITERATURE REVIEW

2.0 Introduction

This section presents the studies conducted by researchers in the past on the types of VAWT and the developments of the VAWT. The section discusses the fundamental principles of VAWT and their applications in the cooling tower. Some of the data from these studies are employed as the benchmark for our study.

Throughout the years, many researchers turned their attention towards the conventional HAWT used in the global market with high efficiency of electrical production in open areas with steady wind velocity (Ma et al. 2018). Despite having high efficiency, the downfall of the HAWT was that it required a large amount of space to generate a large amount of electricity. The spanwise of the turbine was a major factor when calculating the useful output power generation adapted from Euler's turbine equation (Sørensen 2016). Also, a study was conducted by Oerlemans et al. (2007) to determine the noise source of a HAWT, and the noise produced by the blades increased faster than the noise produced by the hub with increasing wind speed. It was also noted an approximate 800Hz and the A-weighted level was recorded near 85dB (A).

On the contrary, the VAWT would provide a much more positive impact on the global scale. This was mainly because the VAWT does not need a large space and it produces less noise (Armstrong, Fiedler, and Tullis 2012). Also, the VAWT does not depend on wind orientation and area cheaper (Pope et al. 2011).

2.1 Design of Darrieus Vertical Axis Wind Turbine

The VAWT could be grouped into the Darrieus wind turbine relying on the lift force of the turbine and the Savonius wind turbine was dependent on the drag force of the turbine (Thé and Yu 2017). The two main designs of the Darrieus wind turbine were the Phi (ϕ)-rotor type and the H-rotor type. The H-rotor of the Darrieus VAWT would have higher wind power coefficient and with a wider application capability resulting in modified designs such as the helical H-rotor, fixed-pitch H-rotor, tilted H-rotor and also a combination of Savonious type rotor (Kumar et al. 2018). Figure 2.1 portrays the Darrieus's turbine and its configurations.

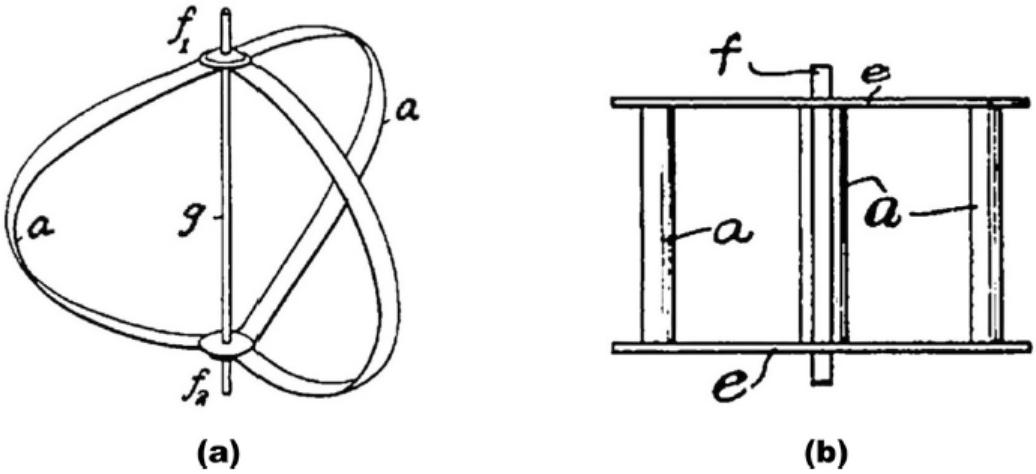

Figure 2.1:Darrieus's patent showing the turbine with (a) curved blades (b) straight blades. Annotations refer to a. blades e. support structure f. hub g. shaft. (Darrieus 1931)

A study was conducted by Yusri et al. (2023) on the 2-Dimensional numerical simulation of the H-type Darrieus VAWT. Their study employs the airfoil NACA4415 with an inlet velocity of 7m/s. The study also set the turbulent intensity to 5% and the turbulent viscosity ratio to 10. This gave a result of the highest torque 0.9365Nm and the highest power recorded 19.6658W. In addition, a Computational Fluid Dynamic (CFD) study on the effective parameters of the H-rotor Darrieus wind turbine was conducted by Mehrpooya et al. (2023). The outcome of the study deduced that the increase in the inlet velocity would increase the efficiency of the turbine. The 3-bladed turbine had the highest efficiency at the inlet velocity of 12m/s and the TSR of 2.5.

Furthermore, a study conducted by Qamar and Janajreh (2017) using a Computational Fluid Dynamic in a two-dimensional simulation to study the eddy viscosity model and compared three airfoils' effect on a straight three-bladed H-rotor turbine with a limiting TSR of 1 to 7. The airfoils employed for this study were symmetrical geometry, NACA0012 and another two cambered airfoils of NACA4512 and NACA7512. The airfoils employed for the study were shown in Figure 2.2.

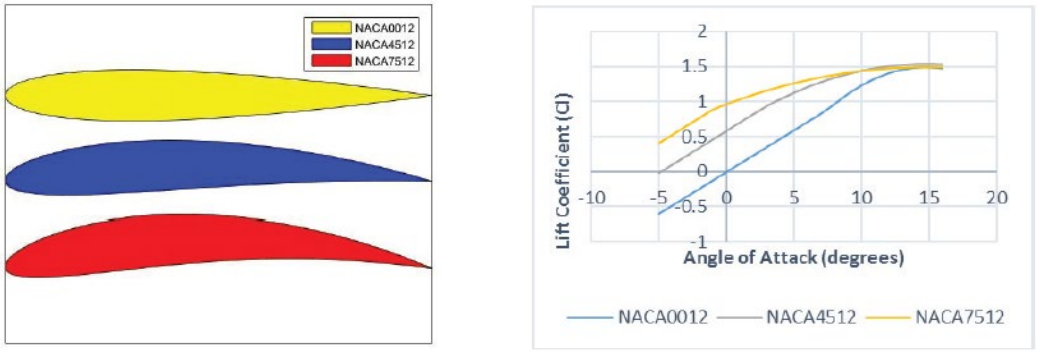

Figure 2.2: Left: NACA Airfoil (0012,4512 &7512); Right: Lift coefficients for NACA0012,4512 & 7512 (Qamar and Janajreh 2017)

The outcome of the study indicated the turbine with cambered airfoils produced an increase C_p of 42%. However, the maximum C_p reached at a lower TSR as compared to the symmetrical geometry NACA0012. One of the important notices of the study was the cambered airfoils turbine indicated better self-starting behaviour and the aerodynamic performance had less fluctuation in instantaneous torque with no changes between positive and negative value as it was in the symmetric airfoil NACA0012 blade turbine. The results from the study are portrayed in Figure 2.3.

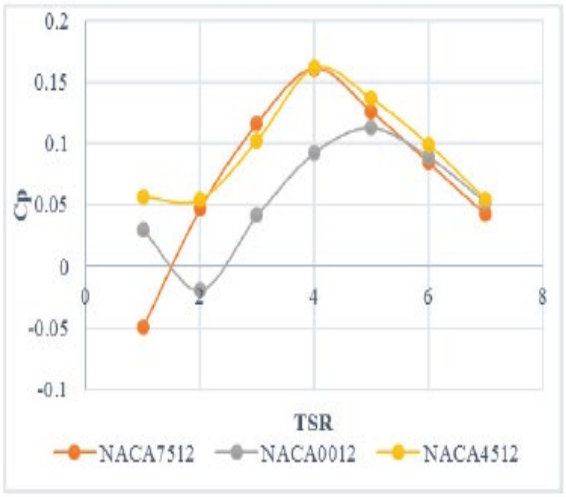

Figure 2.3: Cp plot for the tested NACA bladed VAWT (Qamar and Janajreh 2017)

This study clearly shows the cambered airfoils of the turbine blade have an impact on the efficiency of the turbine power output due to the better self-starting behaviour. It is also clear the cambered airfoil will give a better power output due to the increase C_p and it would require less TSR to achieve its maximum C_p. There is also a downfall that needs to be addressed for the cambered airfoil as the higher camber causes a

negative impact on the turbine's ability to self-rotate due to the interactions between the blades.

A further dive into the study of the airfoil study on a two-dimensional simulation by employing Unsteady Reynolds-Averaged Navier-Stokes (URANS) condition on the different airfoils used in the three-bladed H-rotor was conducted by Hashem and Mohamed (2018). The main aim of the study was to hike the output power coefficient of the straight-bladed Darrieus wind turbine. The study was conducted with several new airfoils (24 airfoils) with symmetric and non-symmetrical profiles of the Darrieus turbine blade. The 24 airfoils can be seen in Figure 2.4. It was found the S1046-type performed best with TSR value ranges from 2 to 7. This is portrayed in Figure 2.5.

The maximum power coefficient $C_{p,max}$ of 0.3463 was achieved by the airfoil S1046. The study also tested on diffuser type mainly, flat-pane, curved-surface and cycloidal surface diffuser. With power generation as the main aim, the results concluded by adopting the diffuser with the cycloidal surface shown a better power output as compared to the other two diffusers. This showed a higher maximum power coefficient of 1.3662, an increase by the factor of 3.9 as compared to the test conducted on an open Darrieus turbine.

Another study was conducted by Sagharichi, Zamani, and Ghasemi (2018) to understand the relationship between the blade solidity and the performance of the variable-pitch VAWT. It was aimed to enhance the self-starting characteristic of the turbine and the aerodynamic performance of the system. It was conducted with CFD simulation with two types of pitch with variations of solidities. The two types of pitch that were employed in this study namely, the fixed pitch and the variable pitch. To increase the accuracy of the result of the variable-pitch VAWT, the computational model chosen for the study was a two-dimensional transient flow. The model was employed around the VAWT with solidities ranges between 0.2 and 0.8 with turbine blades of two to four. The simulation models the flow field surrounding the turbine with no similarities to the URANS and SST k-ω turbulence model. It was reported from this study the blades with higher solidity, σ would have higher power generation with lower rotor speed. This is shown in Figure 2.6. It was reported, that the fixed-blade turbine with a solidity of 0.8 would provide more power at a lower rotor speed.

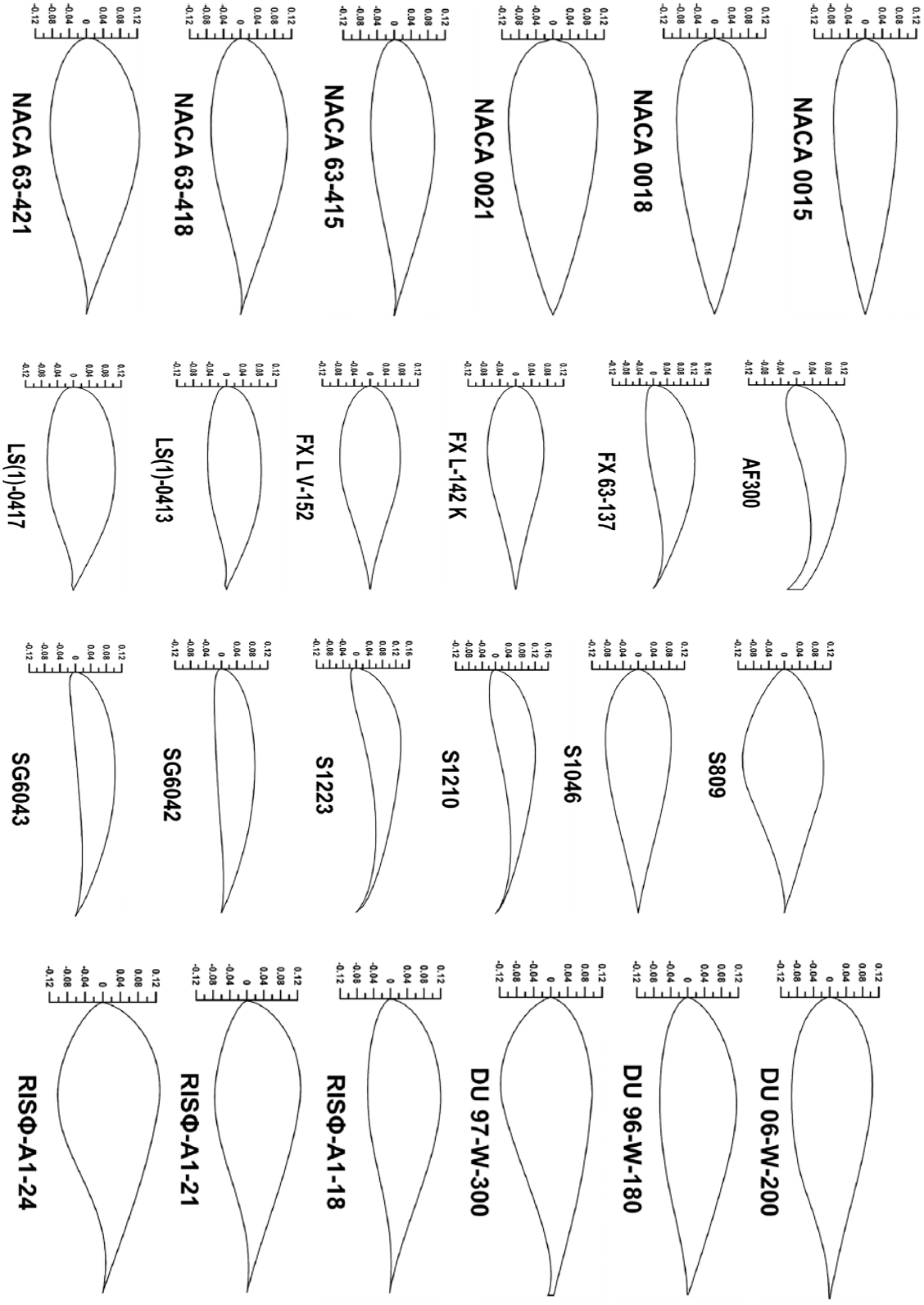

Figure 2.4 Tested airfoil shape (Hashem and Mohamed 2018)

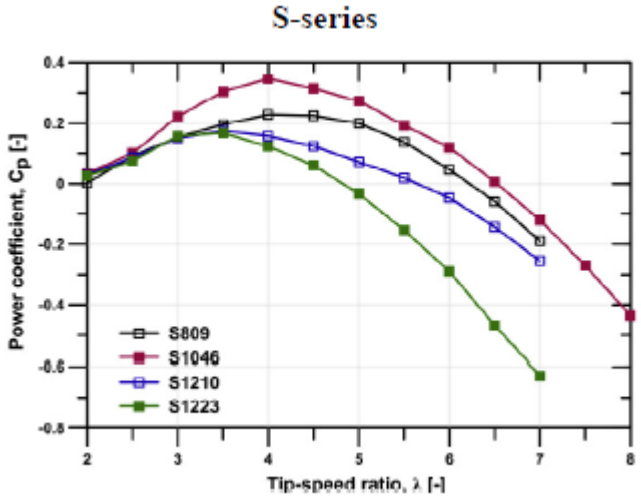

Figure 2.5:Power coefficient of H-rotor Darrieus rotor using S-series airfoils (Hashem and Mohamed 2018)

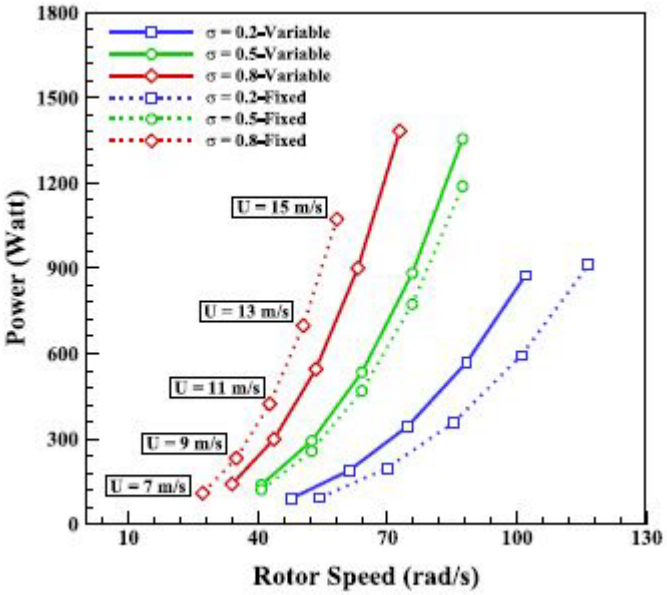

Figure 2.6:Fixed and variable pitch wind turbine for different solidities, σ (Hashem and Mohamed 2018)

This study conducted by Sagharichi, Zamani, and Ghasemi (2018) also underlines the downfall of turbines with more than three blades. It was reported that more blades would have an impact on other external factors, such as cost, weight, and inertia. Also, the greater number of blades would increase the vibration. It was also clearly underlined the increase in cord length will significantly impact the increase of the

weight. With a lesser blade number and with high rotational speed, the value of the maximum torque will be reduced.

The results indicated blades with high solidity were more favorable when studying the initial self-starting torque. In addition, variable pitch blades tend to produce higher torque values during high solidities. Thus, a reduction of the vortex was formed between the upwind vortices and the blades in the downwind stream.

Another study was done on the effect of the number of blades on the power performance of the turbine. The study conducted by Li et al. (2015) with the blade profile of NACA0021 with increasing blade numbers from two to five. The pressure on the surface of the blade was taken during the rotation by a multiport pressure device and was sent to a computer through the wireless LAN. The investigation was also conducted with loads to compare the experimental data. It was found that the power absorbed from the wind was in close relationship with the upstream area of the azimuth angle of $\theta=0°$ to 180°. In addition, the power coefficient decreased with an increase in blade numbers. The maximum power coefficient was 0.410 for two blades and the maximum power output for five blades is 0.326. An important factor to note from this experiment in high wind velocities, the blade configuration could generate more energy but for low wind velocity areas, the five-blade design could have a greater generating capacity. This study indicated the blade number was a factor in determining the maximum capacity which was dependent on the wind velocity area. In a cooling tower, the wind speed was classified as high wind velocity and thus, our study would employ the two-blade configuration of the VAWT as it would be placed in the cooling tower application having a high wind velocity region. Li et al. (2015) also noted and evaluated the number of blades with a full 3D result which was very important for further research.In addition, another study was conducted by Subramanian et al. (2017) focuses on the effect of the airfoil solidity on the performance of small scale vertical axis wind turbine by using a three dimensional CFD model. This study was conducted with ANSYS Fluent by selecting 4 airfoils namely as shown in Figure 2.7. The inlet wind velocity was set to be at 10m/s with varying Tip Speed Ratio (TSR) from 1 to 2.5. To test the solidity, the study compared the VAWT with 2 blades and 3 blades for the airfoil NACA0012 and NACA 0030 blade profiles with the fixed chord length for the studies. To test the solidity, the study ranges the TSR from 1 to 3.

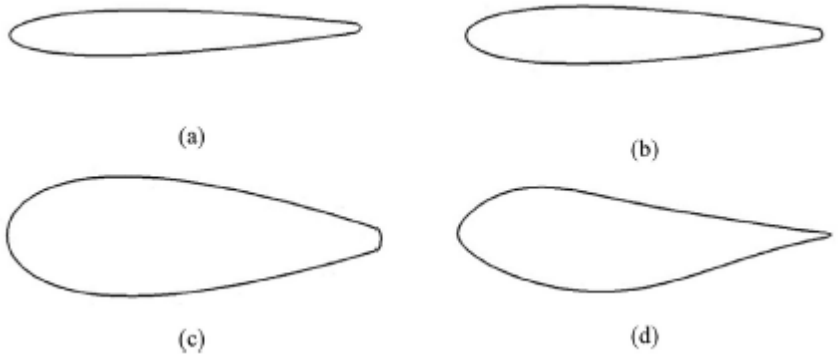

Figure 2.7: Representation of Airfoil profiles- (a) NACA 0012; (b) NACA 0015; NACA 0030: and (d) AIR 001 (Subramanian et al. 2017)

In the study, the y+ value for the model was 2.90 and this is done by meshing the blades with a prism layer with the first level thickness of 0.05mm. The blades and shaft were set to be solid walls with no-slip boundary conditions. The top surface had been set to be a symmetric boundary together with the sides to have zero shear stress. The study also set every simulation to run until the flow becomes cyclic. This was reflected in the plot of the moment coefficient. The study found the 5th and 6th rotation of the turbine would not have much variation in the moment coefficient. Therefore, the study takes the 5th and 6th rotation to calculate their average torque which was then used to calculate the power generation of the turbine. The graph of the variation moment coefficient of the 5th and the 6th rotation azimuthal angle is shown in Figure 2.8.

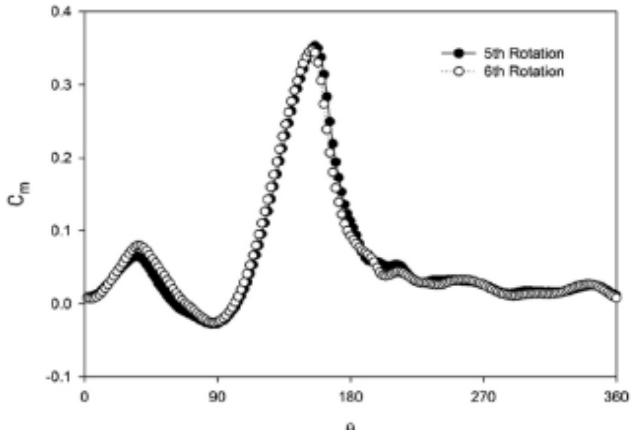

Figure 2.8:Variation of Cm for the 2 bladed NACA0015 profile with TSR of 1.3. (Subramanian et al. 2017)

c

2.2 Summary of Darrieus turbine Vertical Axis Wind Turbine Design

In this subchapter, we will discuss on the primary parameters which would be employed in our study of the Darrieus VAWT in the cooling tower application. The primary parameters listed here were used as a guideline and are modified, if necessary, to fit to the experimental part of our study. Thus, table 2.1 summarizes the important parameters used in this study when designing the Darrieus VAWT.

Table 2.1: Summary of parameter for Darrieus Vertical Axis Design

Design Parameter	Author (year)	Title	Aim	Finding
Blade chord and Chamber	Qamar and Janajreh (2017)	Investigation of Effect of Cambered Blades on Darrieus VAWTs	To compare three airfoils effect on a straight three-bladed H-rotor turbine with limiting TSR of 1 to 7.	• Cambered airfoil increases Cp by 42%. • Cambered airfoil has better self-starting behaviour. • Cambered airfoil has better aerodynamic performance (less fluctuation in instantaneous torque)
Airfoil Thickness	Hashem and Mohamed (2018)	Aerodynamic performance enhancement of H-rotor Darrieus wind turbine	To hike the power output of the straight-bladed Darrieus wind turbine with 24 new airfoil profiles.	• S1046-type performed best for TSR range from 2 to 7. • S1046 maximum power coefficient is 0.3463.
Solidity Ratio	Sagharichi, Zamani, and Ghasemi (2018)	Effect of solidity on the performance of variable-pitch vertical axis wind turbine	To aid the self-starting capability and aerodynamic performance of the VAWT.	• Solidity range of 0.2 and 0.8. • Solidity of 0.8 shows more power generation. • Higher solidity will have higher power generation with lower rotor speed. • Higher power generation caused by isolated vortices from either the inlet or the outlet at higher solidity is reduced. • Greater blade number, the more impact on the cost, weight, inertia and increase in vibration.

Number of blades	Li et al. (2015)	Effect of number of blades on aerodynamic forces on a straight-bladed Vertical Axis Wind Turbine	To study the aerodynamic forces depending on the blade number	• Blade numbers used from 2 blades to 5 blades. • Two blade maximum power coefficient is 0.410. • Five blade maximum power coefficient is 0.326. • Number of blades will be a factor to determine the maximum power coefficient is dependent on wind velocity. • Since we are looking at a high wind velocity region in the Cooling tower application, a two bladed configuration is appropriate.
Airfoil type and solidity	Subramanian et al. (2017)	Effect of airfoil and solidity on performance of small-scale vertical axis wind turbine using three dimensional CFD model	To study the effect of solidity and airfoil profile on the performance of Vertical Axis Wind Turbine	• 5^{th} and 6^{th} rotation of the turbines are to be used to obtain the Coefficient of Moment. • The shed vortex dissipates much faster to the thinner airfoils as compared to the thicker airfoils at the higher TSR values. • The thickness of each turbine blades must be selected wisely to suit the high TSR value in our study.

2.3 Design of Savonius Vertical Axis Wind Turbine

Savonius VAWT was known to require lesser wind speed to start generating electricity from the rotational moment. It was usually made with two extruded semi-circles facing opposite directions to form almost an S-shape. It was best known for the unique features of simple assembly, not having high sound decibels, the ability to rotate at lower cuts in the wind, and also low manufacturing and operating costs (Chan, Bai, and He 2018). However, the main drawback of the Savonius VAWT was the poor aerodynamics and performance (Emmanuel and Jun 2011) but it was preferred if power reliability was the main concern over the turbine efficiency. Research has been conducted by Roy and Saha (2013) with the aid of computational methods to further understand the operating parameters of the Savonius VAWT. It was concluded the drag force spinning the turbine was the primary reason for the poor aerodynamic effect. The VAWT was widely used in rural areas to generate electricity to reduce the carbon footprint of fossil fuels. The VAWT could be installed in places with limited space, on top of skyscrapers, and even on the top of lamp posts to generate electricity in a particular place (Kumar et al. 2018). Figure 2.9 shows a simple Savonius solid view from Tian et al. (2018).

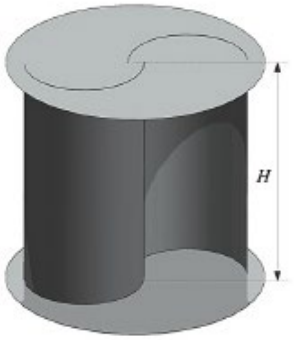

Figure 2.9:Solid view of a Savonius wind turbine where H is the height (Tian et al. 2018)

To further understand the Savonius VAWT, Lee, Lee, and Lim (2016) conducted a research to study the helical type Savonius wind turbine with different helical angles. The study aimed to obtain the power coefficient, C_p at multiple tip speed ratios (TSR) and the torque coefficient, C_T was obtained from azimuth angle for the helical blades

angled at 0°, 45°,90°, and 135° respectively. Figure 2.10 shows the blades used for this study.

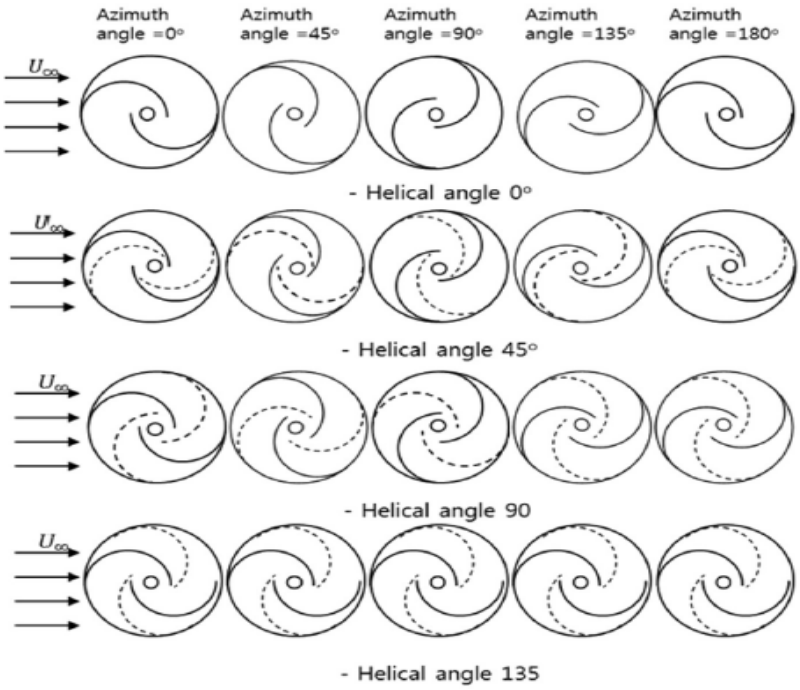

Figure 2.10:Blade shape of azimuth angle (Solid line: contact lines to the upper plate, Dashed line: Lower endplates) (Lee, Lee, and Lim 2016)

This study was conducted with limitations of a fix projection area and aspect ratio. The numerical results were obtained by employing the incompressible unsteady Reynolds average Navier-Stokes (k-ϵ RNG) model. The numerical analysis was examined with the flow characteristics with 1° interval from 0° to 360°. The experiment was then conducted in a wind tunnel. The reported results from both numerical and experimental was compared and has similar results of maximum power coefficient $C_{p,max}$ for the TSR range was defined in the study. From this study, the maximum power coefficient, $C_{p,max}$ was obtained at a twist angle of 45° and it then decreases by 25.5% at the 90° and the 135°. This was obtained from the results of their study shown in Figure 2.11 and 2.12.

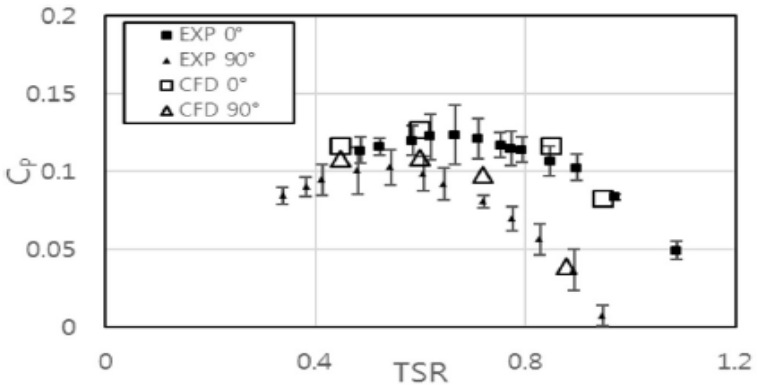

Figure 2.11:Plot of Power coefficient against TSR for 0° and 90° angle of twist (Lee, Lee, and Lim 2016)

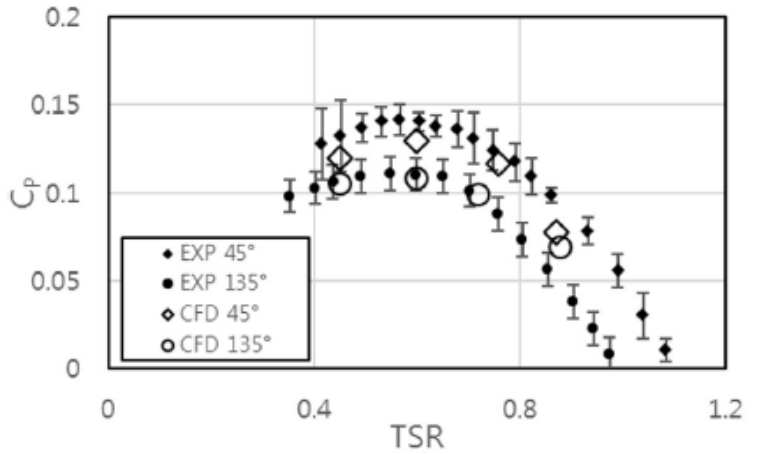

Figure 2.12:Plot of Power coefficient against TSR for 45° and 135° angle of twist (Lee, Lee, and Lim 2016)

For the torque coefficient,C_T, the result indicated the peak-to-peak coefficient of torque in the profile of 0° and 45° where greater than those profiles with 90° and 135°.

Thus, from this study, it is vital for the pitch angle of a Savonius VAWT to be kept in a range of 0° to 45°. When designing a Savonius VAWT in this study, the angle of twist will be kept at a constant of 45°. This would ensure the maximum power coefficient $C_{p,max}$ and the greater torque coefficient C_T would be achieved to gain a better power output from our system. This would then ensure a greater energy is harvested from the air would increase the efficiency of the system.

Furthermore, a study was conducted by Saad et al. (2020) with the focus on the twisted-bladed Savonius vertical axis wind turbines. This study focused on several

design parameters. The design parameters were the endplates size ratio, twist angle and overlap ratio. This study gave a better overview of the geometrical variables would affect the aerodynamic performance for the twisted Savonius rotor. The study was conducted with a three dimensional with the incompressible unsteady Reynolds-averaged Navier-Stokes model together with the k-ω shear-stress transport turbulence model by using ANSYS Fluent 17.2. The data obtained from the numerical study are validated with experiments and the data from the literature review. The study set the free stream wind velocity of 4m/s to 18m/s. Several configurations of the overlap ratios and end plate size ratios are used in the study. This can be seen in Figure 2.13 and Figure 2.14.

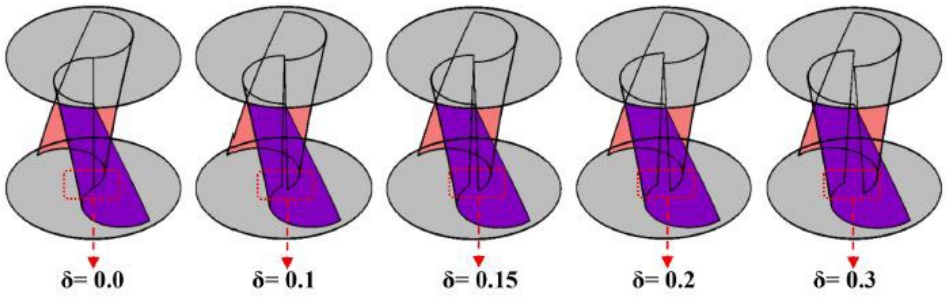

Figure 2.13:Schematic Drawing for the overlap ratio (Saad et al. 2020)

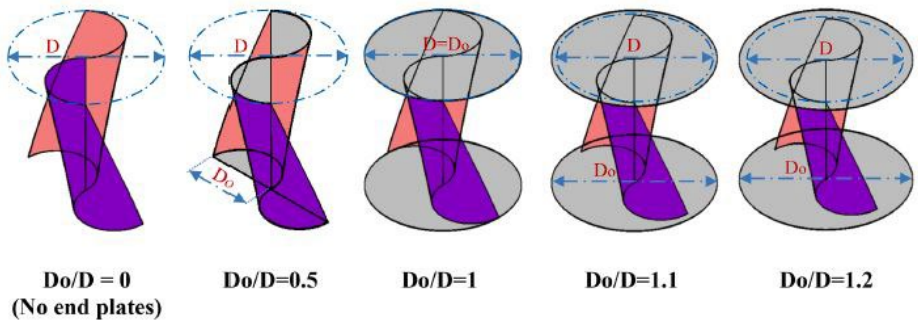

Figure 2. 14:Schematic Drawing for the end plate ratio (Saad et al. 2020)

This study found that a twisted-bladed Savonius turbine twist angle of 45°, zero overlapping ratio and the 1.1 endplates size ratio gave the greatest output power. At the wind velocity of 6m/s, the rotor gained a maximum power coefficient of 0.233. An increase of wind velocity to 10m/s would enable the maximum power coefficient to be 0.231. A further step taken by the study conducted by Saad et al. (2020), was to look into the untwisted design. The maximum power coefficient was 0.174 with the

0.15 overlapping ratio and the same endplate size ratio. They have noted the presence of a negative value of static torque coefficient which prevents the self-staring ability.

To underline the cause of the low ability to self-rotate the study from Saad et al. (2020), a study was done on the effect of various straight blade angles on the modified Savonius wind turbine would give a better understanding of the relationship of the turbine designs and the flow physics. This study was done by Anwar et al. (2018) using a simulation of the two-dimensional flow analysis. It was done based on the RANS equation and the SST k-ω turbulence model to study the airflow on the turbine blades. The study investigated both static and dynamic simulations and focused on the Bach Type Savonius wind turbine, the straight blade region. The study modified the Bach-type Savonius turbine by bending inwards and outward to form an angle (β) that varies from 70° to 110° with an interval of 10° for each set. Other parameters such as rotor diameter (D), blade angle (Φ), straight blade length (S1), blade radius (S2), and the distance between the blades (a) are kept constant. Figure 2.15 shows the variation of blades tested in this study.

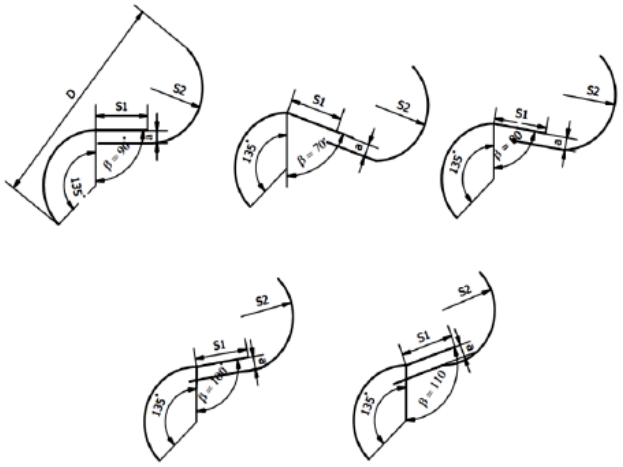

Figure 2.15:Change of geometry of tested blades with different angle of β (Anwar et al. 2018)

It was found from the static simulation the drag and lift coefficient of the Savonius turbine can be obtained at other angular position. The static simulations were conducted to understand the performance of the modified blades at different angular position which begins from 0° to -150° with an interval of 30°. Thus, Figure 2.16 and

Figure 2.17 shows the results for the drag and lift coefficient with to the selected angular positions.

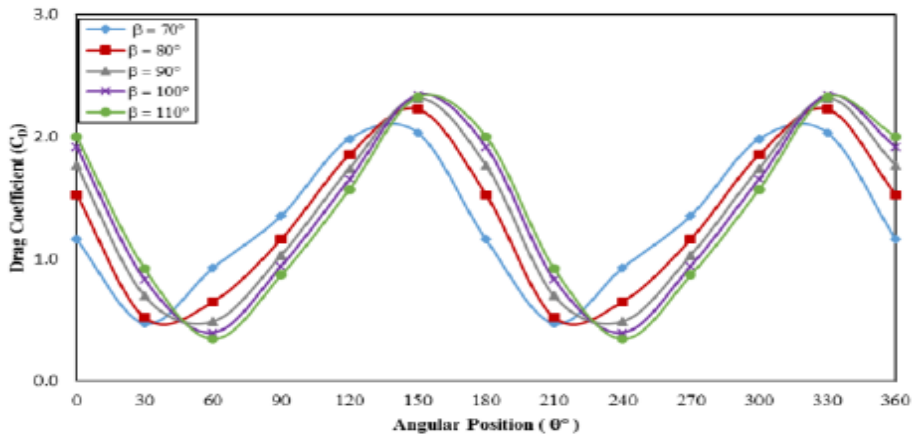

Figure 2.16:Drag coefficients at selected angular position (Anwar et al. 2018)

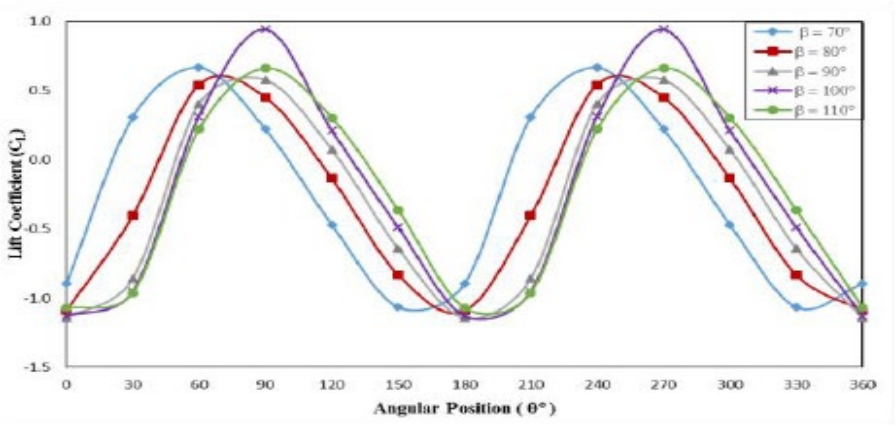

Figure 2.17:Lift coefficient at selected angular position (Anwar et al. 2018)

A high value for the drag coefficient was seen for the blades with the angle β of 100° and 110°. For the lift coefficient, there was a huge increase from 60° to 90°. Thus, this indicated the presence of lift forces on the blade at the two positions of 60° and 90°. From this study, it was noted the turbine did not depend on drag force as the contributing force, but it depended on the lift force to aid in the increase of power. The greatest lift coefficient was gained when the bend angle β equals 100° with the angular position of 90° and 270°.

However, for the dynamic simulations were conducted by setting a rotational speed to the region assigned to be the rotating zone. However, the study was limited

to the range of TSR from 0.2 to 1.4 only. In Figure 2.18 and Figure 2.19 shows the graphs of moment coefficient and power coefficient against the TSR value respectively.

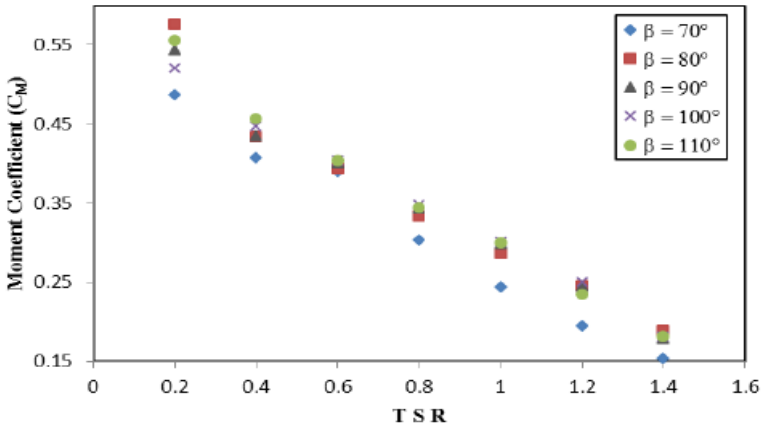

Figure 2.18:Moment coefficient at different TSRs (Anwar et al. 2018)

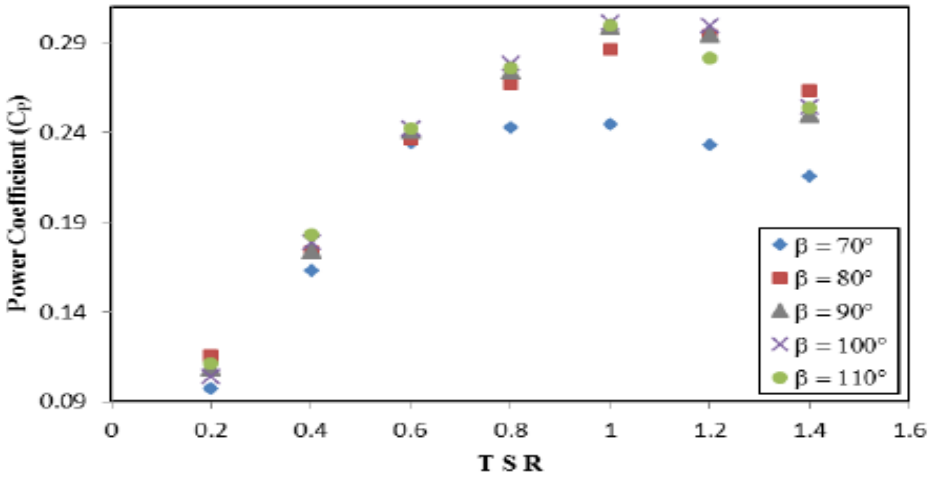

Figure 2.19:Power coefficients at different TSRs (Anwar et al. 2018)

From Figure 2.18, it is clear the design with the bend angle, β equal to 80° has the greatest torque coefficient with lower tip speed ratio of 0.2. But for higher TSR value (TSR>0.8), the design with the bend angle, β of 100° has the highest torque coefficients. Meanwhile in Figure 2.19, the maximum value of power coefficient for each bend angle is obtained from the TSR value of 1.

This study also shows the low efficiency of the Savonius turbine is caused by the counter moment on the blade is on the returning region. Thus, the Bach type would reduce the counter effect caused by the backflow passing through the protruding region

and the flow acceleration towards the returning blade side. It was found when the straight blades are bent inward with bend angles of 70° and 80°, the blade overlap gap is lesser in distance than the baseline of the blade. But in the case of the bend angle of 100° and 110°, the blade overlap gap is extended in excess of the baseline blade. This study verified the shorter the overlap distance, the area of the return flow is also shorter. This results in a reduced aerodynamic performance. However, in the case of a longer overlap distance, it may also have a negative cause direct implication on the performance of the Savonius turbine since the time taken for the back flow is longer and would prevent a positive effect on the return blade. Thus, a velocity vector plot was conducted, and found the bend angle of 100° is the optimal distance. This is because it can maximize the return flow to the overlap area and have the highest power coefficient of 0.302.

The study also highlighted the five flow conditions of the Savonius rotor which are the free flow region at the inlet, the acceleration flow region at the edge of the returning blade, the overlap flow region in between the blades, the lift flow on the convex of the advancing blade and the return flow region. The overlap flow region is the region that provides the forward effect for the advancing blades. However, for the returning flow, it is the stream that moves toward the inner side of the blade. This will aid in the increment of the torque for the rotor. Due to the bend on the straight blade with equal distance between blades and different overlap distances, the overlap region is different in between the blades. This is caused by the flow acceleration effect that continues to provide thrust to the advancing blades. Besides, the thrust is low on the bending blades due to the short overlap gap. But for a higher overlap gap which is caused by a higher bend angle (β=110°), it would create a blockage. This blocks the return flow to the concave side and decreases the performance. The best blade design is from the bending angle of 100°. Thus, in our study, the design of the Savonius turbine will use a bend angle of 100° in line with the previous literature. This is to ensure the results obtained from our study will be the optimized results for the Savonius Turbine design.

To understand how the blade numbers would affect the Savonius Turbine, a study was conducted by Emmanuel and Jun (2011) to understand the ways to boost the performance of a six-bladed Savonius rotor. The improvement is done by increasing the blade numbers and using an external cover to prevent winds from impinging on

the surfaces of the blade. The aspect ratio of the study was kept at 2 while the number of blades used was 2 and 6 blades. The outcome of the study was the rotor has a better ability to self-starting when compared to the two bladed rotors. Thus, to determine the optimized number of blades for the Savonius turbine, a study was conducted by Mahmoud et al. (2012). This study was done on an experimental basis and tested on Savonius turbine with configurations of two blades, three blades, and four blades Savonius turbine. With considerations of the aspect ratio of 0.5, 1,2,4, and 5 and with overlap ratios from 0 to 0.35, the optimized geometry of the Savonius turbine is obtained. Thus, the study concluded the rotor with two blades has better efficiency as compared to the three-bladed and the four-bladed rotors.

Furthermore, an optimization study was conducted by Haddad et al. (2023)with additional blades with the aid of a surrogate model with artificial neural networks. The study employs the design of experiment (DOE) on four variables namely the arc angle of the original blade, the shape factor, the arc angle of the additional blades, and the additional blade radii ratio. Their study was conducted with ANSYS FLUENT and the results were fed to the artificial neural network (ANN). The outcome of this study was an increase in the overall power coefficient of 0.2836 at the TSR of 0.75. This had the parameters of blade arc of 77.0033, the blade shape factor of 0.3185, the additional blade angle of 112.534°, and the additional blade radii ratio of 0.5818.

2.4 Summary of Savonius turbine Vertical Axis Wind Turbine Design

In this chapter, we will discuss on the primary parameters employed in this study of the Savonius VAWT in the cooling tower application. The primary parameters listed here were used as a guideline and were modified, if necessary, to fit to the experimental part of our study. Thus, table 2.2 summarizes the important parameters used in this study when designing the Savonius VAWT.

Table 2.2: Summary of parameter for Savonius Vertical Axis Design

Design Parameter	Author (year)	Title	Aim	Finding
Twist Angle	Lee, Lee, and Lim (2016)	Effect of twist angle on the performance of Savonius wind turbine.	To obtain the power coefficient at multiple TSR and torque coefficient.	• Constant project area and Aspect ratio. • Maximum power coefficient at 45° then decrease by 25.5% at the 90° and 135°. • Torques coefficient is greatest at 45° followed by 90° and 135°.
Overlap ratio and end pate size ratio	Saad et al. (2020)	Performance enhancement of twisted-bladed Savonius Vertical axis wind turbines.	To improve the efficiency of the twisted-bladed Savonius VAWT.	Twisted Turbine • Greatest power output obtained at the following parameter: Twist angle:45° Overlap ratio:0. endplate size ratio:1.1 • At wind velocity of 6m/s, the power coefficient is 0.233. • At wind velocity of 10m/s, the power coefficient is 0.231. Untwisted turbine • Maximum power coefficient of 0.174 with overlap ratio of 0.15 and equal endplate size ratio. • Lower self-starting ability.

Straight blade angle	Anwar et al. (2018)	Numerical investigation of Modified Savonius Wind Turbine with Various Straight Blade Angle.	To determine the effect of various straight blade angle on the modified Savonious wind turbine (Bach type).	• All parameters are kept constant except of the inward and outward bending angle, β. • Limited TSR range of 0.2 to 1.4 only. For Static simulation: • Static simulation can calculate the drag and lift coefficient at every angular position. • Higher Drag coefficient was seen for the blades with angle β of 100° and 110°. • Lift coefficient large at 60 ° to 90 ° For Dynamic simulation: • Higher TSR value (TSR >0.8) bend angle β of 100 ° has highest torque coefficient. • Bend angle of 100 ° also give the highest power output. • Shorter overlap distance will reduce the aerodynamic performance. • 100 ° bend angle has the optimized design.

Number of Blades	Emmanuel and Jun (2011)	Numerical study of a six-bladed Savonius wind turbine.	To understand the methods to improve the efficiency of a six-bladed Savonius rotor.	• Aspect ratio is kept at 2. • Blade number used:2 and 6 blades. • Six bladed rotors have better self-starting ability.
	Mahmoud et al. (2012)	An experimental study on improvement of Savonius rotor performance.	To determine the optimized blade numbers for the Savonius turbine.	• Aspect ratio of 0.5,1,2,4 and 5. • Overlap ratio ranging from 0 to 0.35. • Two bladed rotors have better efficiency than three bladed and four bladed.
Arc blade angle and shape factor	(Haddad et al. 2023)	Optimization of Savonius wind turbine with additional blades by surrogate model using artificial neural networks	To obtain the optimum configuration of Savonious wind turbine with Surrogated-based optimization	• Arc blade angle of 77.0033 • Blade shape factor of 0.3185

2.5 Cooling tower Application of VAWT

In the cooling tower application, research were conducted either in experimental or numerical methods. The basic idea was to reap the wind energy from the cooling tower which was then transformed to electrical energy. At the early stage of the study in Malaysia, an experiment was done by Chong et al. (2013) to understand the efficiency of the VAWT and the implications in the cooling tower efficiency. It was conducted with two methods. The first was a lab test by building a small-scale cooling tower model and mounting a Giromill VAWT above it. The second method was a field test on an induced-draft cooling tower. For the lab test, a 5-bladed H-rotor VAWT with FX 63-137 airfoil was employed while the field test used a two-stage Savonious rotor mounted at the center shaft of a 3-blaed Darrius VAWT. The results then portrayed no negative impact on the cooling tower performance but then displayed an increment of 0.39% of the power consumed by the cooling tower fan. The efficiency of the experiment in the lab also shows a 30.4% improvement in the rotating speed of the VAWT with the aid of diffuser plates. Figure 2.20 shows the experimental setup.

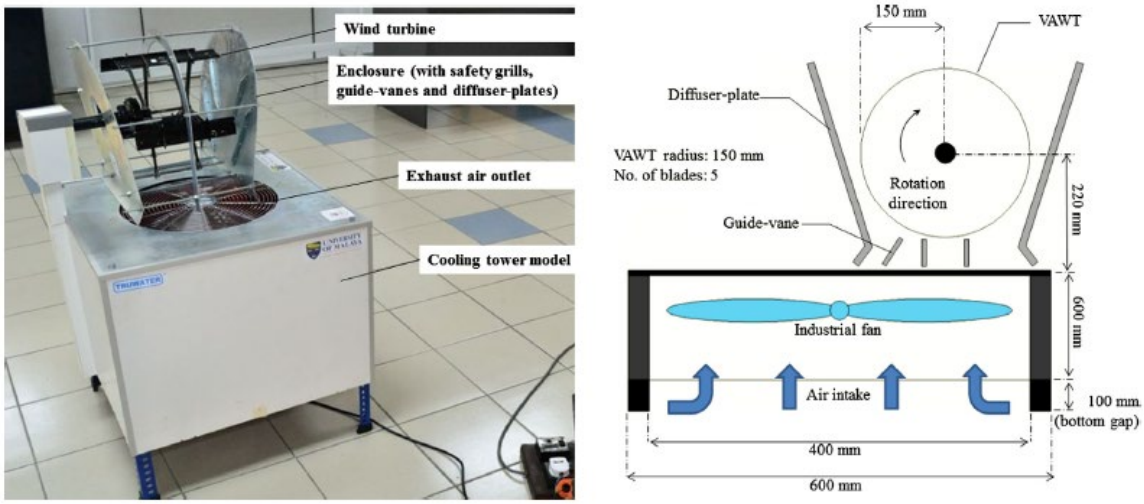

Figure 2.20:Test model with its set-up dimensions. (Chong et al. 2013)

The study from Chong et al. (2013) attracted increasing interest of researchers and further studies were conducted on the cooling tower application. A study was then conducted by Chong, Hew, et al. (2014) on the use of VAWT on exhaust air recovery in commercial buildings. The experiment was set up with two VAWTs in a crosswind configuration which are placed within an enclosure for safety purposes. It is then mounted at a fixed distance and positioned on the outlet of the cooling tower. This experiment is conducted with a 5-bladed H-rotor with a 0.3m in diameter generator. This experiment then produced a result indicating a

power reduction drained by the fan motor in the cooling tower and the intake air speed increases. As for the VAWT, it shows an increment of 7% in rotating speed and a 41% reduction in the time required to achieve maximum rotational speed. Further study with various VAWT was yet to be studied as it could enable better efficiency in energy recovery at lower wind speed countries. The study also showed no negative impact of the application of the VAWT when employed in the cooling tower.

In addition, a study was conducted with the numerical method to underline the comprehensive flow behavior study of the two Giromill VAWTs. This study was conducted by Tabatabaeikia, Bin Nik-Ghazali, et al. (2016), with the aid of numerical simulation. The results were then compared with those from the experimental ones. The results obtained from the study showed the power output of the wind turbine was improved by 5% when the diffusers were introduced and 34% when the guided vanes were installed when compared with the VAWT alone. The results were in line with the experimental results. The data collected from our study should have a variation of less than 34%. This may be caused by the experimental setup and other external forces causing a fluctuation in the result obtained.

Optimization of a particular system was crucial to enable a better gain of the output or product of the system. Thus, a study was led by Tabatabaeikia, Ghazali, et al. (2016) to study the optimization of the exhaust air recovery wind turbine generator with numerical study. It was targeted at the optimization of the entire system energy generation with a condition that did not go against the efficiency of the cooling tower. The optimization of the system was done by positioning the wind turbine rotor, modified diffuser plates and the introduction of the separator plates to the design is shown in Figure 2.21. This study employed the response surface methodology (RSM) as an analytical method used in multivariate static techniques. The CFD meshing of the rotating region is shown in Figure 2.22.

The result obtained from the study shows an increase of generated power by 48.6% shown in Figure 2.23. This enables lower fan motor power consumption and increase the fan intake airflow. The simulation result and the experimental result were compared and a small percentage difference of 6-8.5% is obtained.

Figure 2.21:Experimental apparatus. (Tabatabaeikia, Ghazali, et al. 2016)

.

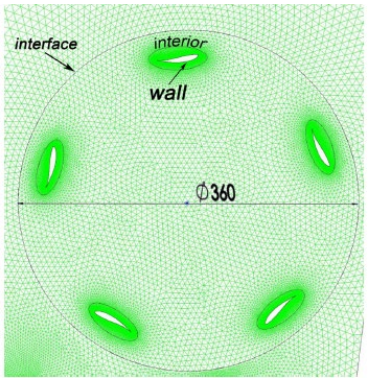

Figure 2.22:Mesh of rotating area. (Tabatabaeikia, Ghazali, et al. 2016)

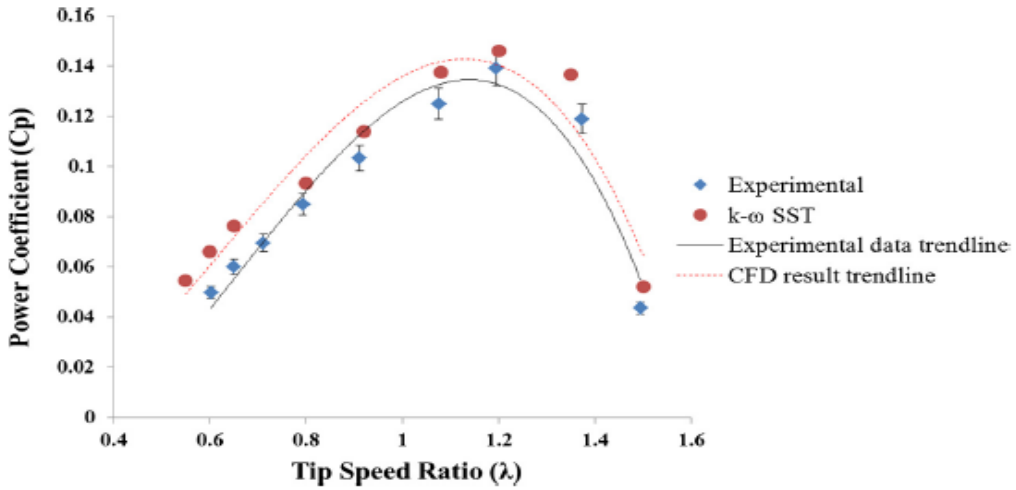

Figure 2.23:Comparison of power coefficient calculated by CFD simulations and experimental results. (Tabatabaeikia, Ghazali, et al. 2016)

2.6 Summary of the air energy extractor in cooling tower application

In this chapter, it summarized the important studies of the air energy extractor in the cooling tower application shown in table 2.3.

Table 2.3:Summary of air energy extractor in cooling tower applications

Author (year)	Title	Method	Aim	Finding
Chong et al. (2013)	Early development of an energy recovery wind turbine generator for exhaust air system.	Experimental	Experimental study on the efficiency of the VAWT and the effect of the system in the cooling tower efficiency.	• No negative impact on the cooling tower performance. • Increment of 0.39% of the power consumed in the cooling tower fan. • Improve by 30.4% of the rotational speed with the aid of diffuser-plates.
Chong, Yip, et al. (2014)	Design of an exhaust air energy recovery wind turbine generator for energy conservation in commercial buildings.	Experimental	Usage of VAWT on the exhaust air recovery in commercial buildings.	• Two VAWT in a crosswind orientation. • VAWT shows an increment of 7% in rotational speed. • VAWT shows a 41%-time reduction to reach maximum rotational speed.
Tabatabaeikia, Ghazali, et al. (2016)	Computational and experimental optimization of the exhaust air energy recovery wind turbine generator.	Numerical & Experimental	To study the optimization of the exhaust air recovery wind turbine generator conditioned to not violate the cooling tower performance.	• With modified diffuser plates, an increase of power generation by the VAWT of 48.6%. • Results from both methods are compared and have a minimal difference of 8.5%

CHAPTER 3: NUMERICAL METHODOLOGY

3.0 Introduction

In this chapter, the principles of operation of the VAWT in the cooling tower application and the numerical methodology are conducted. The design of the VAWT was done with Computer Aided Design (CAD) Solidwork software. To design blades with a complex blade profile of the S1046 blade profile for the H-Darrieus and helical Darieus turbine. For the Savonious turbines, the semi-elliptical Savonious and the helical Savonious are drawn. In addition, the cooling tower parameter employed in the simulation is drawn in the CAD software. The simulation parameters for the numerical methodology are also discussed in this chapter. A grid independence test is conducted to optimize the simulation time.

3.1 Vertical Axis Wind Turbine Design

The four types of turbines, namely, H-darrieus, helical darrieus, semi-elliptical Savonius, and helical Savonius VAWT were chosen to be studied based on the literature review. For the Darrieus type of VAWT, three bladed configurations were chosen due to better self-starting capability. This was mainly supported by the study conducted by Li et al. (2015) on the effect of blade numbers on the aerodynamic forces on the VAWT. The study was conducted with blade numbers of 2 to 5 and it was found the turbine with the 5-blade configuration had the lowest efficiency while the 2-blade configuration had the best efficiency. Therefore, this explained the low efficiency of 13% from the study conducted by Fazlizan et al. (2017) as their study was conducted with a 5-blade configuration. The pressure difference would decrease as the number of blades increases. The pressure difference was directly proportional to the efficiency of the turbine. Thus, the greater the number of blades, the lower the efficiency of the turbine.

Furthermore, for the Savonious VAWT, the number of blades was set to 2 blades which was supported by the study conducted by Emmanuel and Jun (2011) and Mahmoud et al. (2012). For the semi-elliptical end plate size and overlap ratio, it was referred to the study by Saad et al. (2020). The twist angle of the helical Savonious, it was set to be 45° with reference to the study conducted by Lee, Lee, and Lim (2016).

The turbines for this study were drawn with Computer Aided Design (CAD) in the Solidwork software and are shown in Figure 3.1.

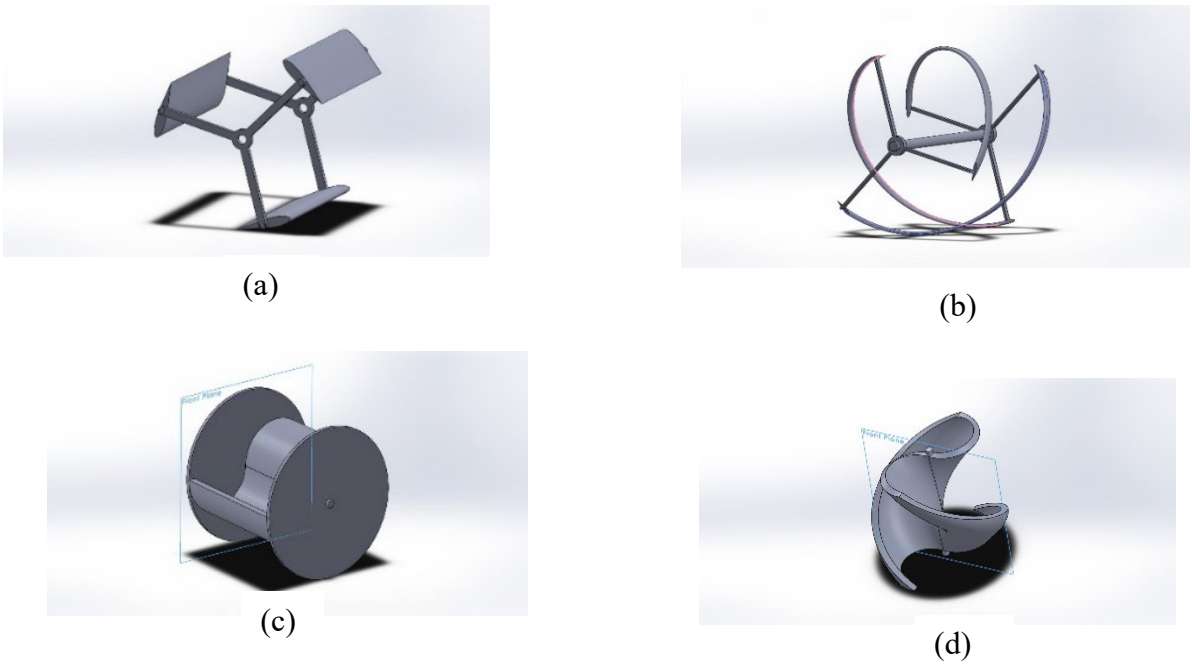

Figure 3.1:Turbine design (a) H-Darrieus (b) Helical Darrieus (c) Semi elliptical Savonious (d) Helical Savonious

3.2 Cooling Tower Design

The cooling tower was drawn in the Solidwork software. The cooling tower parameters would be based on the cooling tower from Liu, Zhang, and Ishihara (2018) shown in table 3.1. The cooling tower is shown in Figure 3.2.

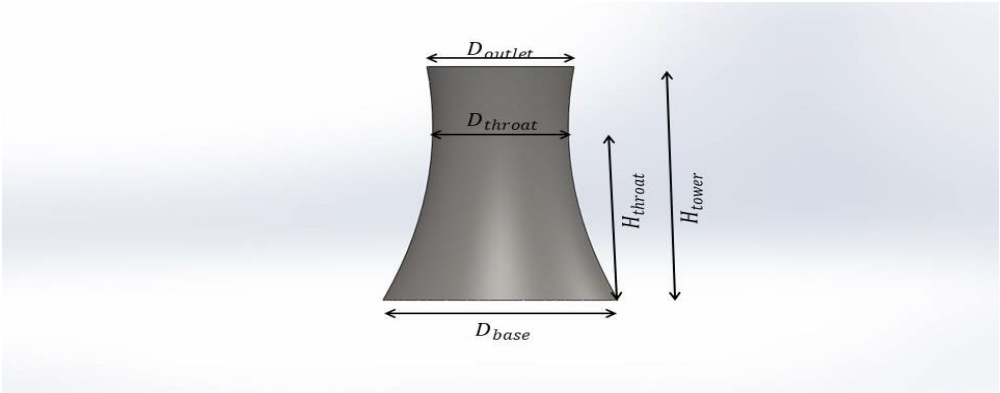

Figure 3.2:Adopted cooling tower adopted from Liu, Zhang, and Ishihara (2018)

Table 3.1: Cooling tower dimension from Liu, Zhang, and Ishihara (2018)

Parameter	Symbol	Dimension (mm)
Tower height	H_{tower}	1175
Base diameter	D_{base}	910
Outlet diameter	D_{outlet}	570
Throat diameter of tower	D_{throat}	525
Height of throat from base	H_{throat}	881

3.3 Mathematical Calculations

In this section, we will discuss the crucial mathematical that had a significant impact on the aerodynamic performance of the turbines of our study listed in section 3.1. The turbine solidity ratio, σ was the main parameter to be taken into consideration when optimizing the VAWTs. It is expressed in equation 1 as the ratio of the number of blades, N multiplied with the chord length, C, and is divided by the turbine diameter, D

$$\sigma = \frac{Nc}{D} \tag{1}$$

The tip speed ratio, TSR is a crucial design parameter as it is the ratio of the translational speed of the tip of the blade to the wind speed. The TSR can be expressed in the equation 2.

$$TSR = \frac{\omega R}{V_\infty} \tag{2}$$

Where,

ω is angular velocity

R is the radius of the turbine

V_∞ is the wind velocity

In order to determine the coefficient of moment of the turbine, we must first determine the torque of the turbine, T expressed in equation 3.

$$T = \frac{1}{2}\rho A R {V_\infty}^2 \tag{3}$$

Where,

ρ is the density of air

A is the turbine swept area

Thus, once the torque is obtained, then the coefficient of moment, C_m can be determined. The coefficient of moment of the turbine was an important parameter as it determined the start-up characteristic of the turbine. The coefficient of moment of the turbine can be expressed in equation 4.

$$C_m = \frac{2T}{\rho A R V_\infty^2} \tag{4}$$

The vital design parameter of the wind turbine was the coefficient of power, C_P. The coefficient of power is used to determine the efficiency of the wind turbine when extracting the kinetic energy from the wind to be converted into electrical power. Therefore, the coefficient of power was defined as the ratio of the turbine power output to the wind power output, or it can be simply expressed as the coefficient of moment multiply with the tip speed ratio as shown in equation 5.

$$C_p = \frac{P_{turbine}}{P_{available}} = \frac{2P}{\rho A V_\infty^3} = C_m \times TSR \tag{5}$$

3.4 Simulation Parameters

In this study, the diameter, D of all 4 turbines will be kept at a constant of 200mm. It was also important to note that 3 main wind speed, V_∞ of 5m/s, 10m/s and 15m/s respectively are employed in this study. Each turbine had 4 TSR values as shown in table 3.2 with the H-Darieus VAWT and the Helical Darieus VAWT. In addition, table 3.3 shows the design parameters for the Semi-elliptical Savonius VAWT and table 3.4 shows the design parameter for the Helical Savonious VAWT. These turbine parameters would be used in our numerical studies.

Table 3.2: Parameters for H-Darrieus VAWT and Helical Darieus VAWT

TSR	Wind Velocity, V (m/s)	Angular Velocity, ω (rad/s)
3	5	150
	10	300
	15	450
3.8	5	190
	10	380
	15	570
4.6	5	230
	10	460
	15	690
5.4	5	270
	10	540
	15	810

Table 3.3: Parameters for Semi-elliptical Savonius VAWT

TSR	Wind Velocity, V (m/s)	Angular Velocity, ω (rad/s)
1.5	5	75
	10	150
	15	225
2.2	5	110
	10	220
	15	330
3	5	150
	10	300
	15	450
3.8	5	190
	10	380
	15	570

Table 3.4:Parameters for Helical Savonius VAWT

TSR	Wind Velocity, V (m/s)	Angular Velocity, ω (rad/s)
0.4	5	20
	10	40
	15	60
0.6	5	30
	10	60
	15	90
0.7	5	35
	10	70
	15	105
1	5	50
	10	100
	15	150

3.5 Simulation flow chart

Figure 3.3 shows the simulation flowchart of the overall simulation would lead up to the selection of the airfoil of which would be used in the experimental section.

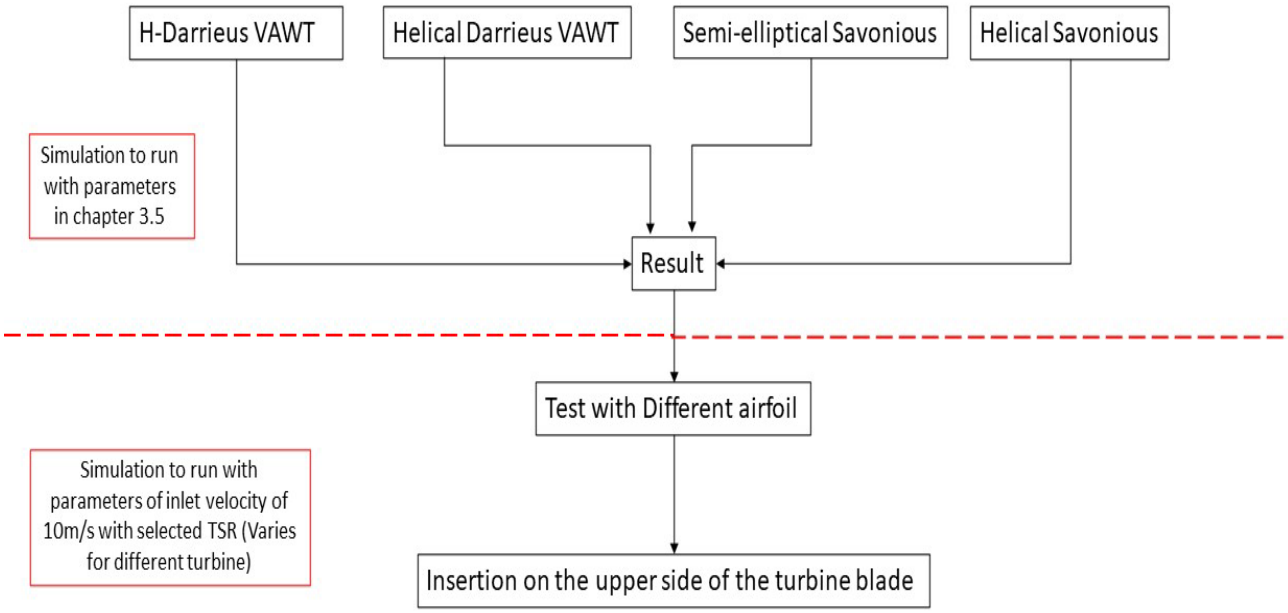

Figure 3.3: Simulation flow chart

3.6 Computational Methodology

In our research, the four turbine types will be investigated with the method of Computational Fluid Dynamics (CFD) to determine the best-performing turbine in the cooling tower application. A three-dimensional computational simulation would be done with the CFD solver ANSYS Fluent software that implemented the equation of the Reynolds-averaged Navier-Stokes. A three-dimensional approach was selected to ensure that all sides and axis of the turbines were captured to ensure an accurate and reliable result. Unsteady Reynolds-Averaged Navier Stokes equation (URANS) was used to solve the governing integral conservation of mass and momentum equations. It could also accurately capture the continuous change in the aerodynamic performance of the turbine at each rotating angle. In addition, for the unsteady-state in the simulation, the sliding mesh technique is employed to capture the rotational effect of the wind turbines. Figure 3.4 shows the workflow of ANSYS Fluent to ensure an accurate result is obtained for our research.

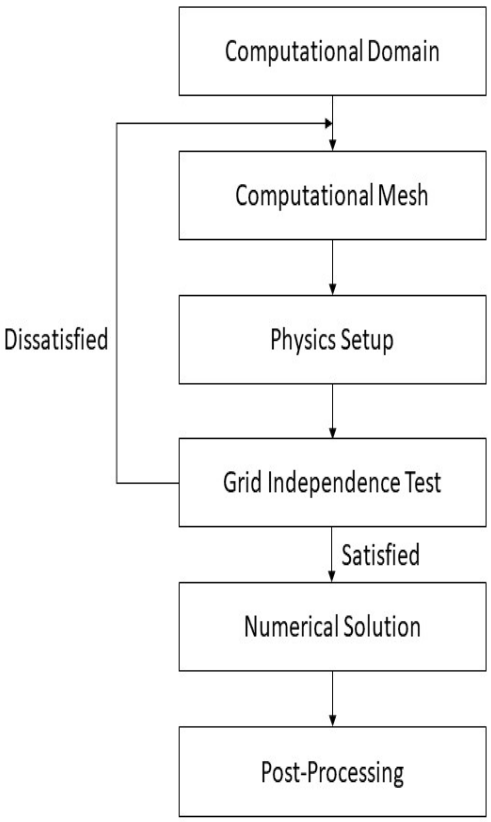

Figure 3.4:ANSYS-Fluent Workflow

3.7 Governing Equation

The selection of the turbulence model in this study plays a crucial part. The appropriate turbulence model would have an impact on the results and determine the success of the study. The k-ω SST turbulence model would be employed in the study. This was mainly due to the accuracy of the two-equation of the k-ω SST turbulence model. The SST transition model was a combination of the Wilcox k-ω model and the k-ϵ model. This combination was a promising approach to simulate different pressure flow and flow separation because it had a balanced performance for modeling near the wall region and also the far-field region used in the account of the transport of the principal shear stress (Asnaghi, Svennberg, and Bensow 2019). This was completed with the multiplication of the blending function with the standard k-ω and k-ϵ models. The two models were then added and the k-ω was set to be near the wall region and the k-ϵ was placed in the far-field region (Asnaghi, Svennberg, and Bensow 2019). Thus, employing the k-ω SST turbulence model together with the URANS method to solve the simulation will be a great balance for the fidelity modeling and the computational cost. The mathematical formulas related to the k-ω SST turbulence model are listed below:Continuity equation:

$$\frac{\partial \rho}{\partial t} + \frac{\partial (\rho U_i)}{\partial x_i} = 0 \quad (6)$$

Momentum equation:

$$\frac{\partial (\rho U_i)}{\partial t} + \frac{\partial (\rho U_i U_j)}{\partial x_j} = -\frac{\partial p}{\partial x_i} + \frac{\partial (\tau_{ij} - \rho \overline{U_i U_j})}{\partial x} \quad (7)$$

Where, the viscous tensor is expressed as:

$$\tau_{ij} = \mu \left(\frac{\partial U_j}{\partial x_i} + \frac{\partial U_i}{\partial x_j} - \frac{2}{3} \delta_{ij} \frac{\partial U_i}{\partial x_i} \right) \quad (8)$$

Transport equation for turbulent kinetic energy (k):

$$\frac{\partial (\rho k)}{\partial t} + \frac{\partial (\rho \overline{u_i} k)}{\partial x_i} = P_k + D_k + \frac{\partial}{\partial x_i} \left[(\mu + \sigma_k \mu_t) \frac{\partial k}{\partial x_i} \right] \quad (9)$$

Specific dissipation rate (ω):

$$\frac{\partial (\rho \omega)}{\partial t} + \frac{\partial (\rho \overline{u_i} \omega)}{\partial x_i} = P_\omega + D_\omega + \frac{\partial}{\partial x_i} \left[(\mu + \sigma_\omega \mu_t) \frac{\partial \omega}{\partial x_i} \right] \quad (10)$$

Where production terms are:

$$P_k = \mu_t \bar{S}^2 - \frac{2}{3}\rho k \frac{\partial(\overline{u_l})}{\partial x_i} - \frac{2}{3}\mu_t \left(\frac{\partial(\overline{u_l})}{\partial x_i}\right)^2$$
(11)

$$P_\omega = \rho\gamma \bar{S}^2 - \frac{2}{3}\rho\gamma\omega \frac{\partial(\overline{u_l})}{\partial x_i} - \frac{2}{3}\rho\gamma \left(\frac{\partial(\overline{u_l})}{\partial x_i}\right)^2$$
(12)

Where the term:

$$\bar{S}_{ij} = \frac{1}{2}\left(\frac{\partial \overline{u_l}}{\partial x_j} + \frac{\partial \overline{u_J}}{\partial x_i}\right)$$
(13)

Destruction terms:

$$D_k = -\rho\beta^* k\omega$$
(14)

$$D_\omega = -\rho\,\beta\omega^2$$
(15)

Model coefficients are,σ_k, σ_ω, β^* and β. Where, μ is the dynamic viscosity of the fluid.

3.8 Computational Domain and Boundary Conditions

In Ansys fluent, three main configurations, cuboid control volume, the cooling tower and the turbine. For the configurations of the cooling tower and the turbine were imported into the system from Solidworks. However, the cuboid control volume was a ratio of $8D_o$ for the height of the cuboid control volume and $6D_o$ for the width where D_o was the outlet diameter of the cooling tower. The downwind cuboid was set at $8D_o$ in height was the pressure outlet. The four walls surrounding the cuboid control volume region was set to have symmetry wall condition. In addition, the ambient velocity inlet was set at the outlet of the cooling tower (with wind velocity of 5m/s, 10m/s or 15m/s) and the area surrounding it was to be the natural airflow would be set at a constant of 2m/s.

The boundary domains for the blades are set to have no-slip conditions on the blade surface. Application of sliding mesh is used in the circular region of the turbine for rotation. This was to be enclosed with an interface surface that would distinct the rotating and non-rotating region of the turbine. The enclosure diameter was 1.5 times larger than the span area of the turbine.

3.9 Mesh generation and convergence

The 3-Dimensional CAD geometries of all the turbines were drawn in Solidworks. It was then imported into Ansys Workbench. The computational domain and the boundary conditions are then constructed in Ansys Workbench with the aid of Spaceclaim. The parameters for the computational domain and the boundary conditions were adopted from Chapter 3.8 of the study.

In this study, we had two domains, fixed domain and a rotating domain. The fixed domain would reflect the cuboid control volume meanwhile the rotating domain would be the enclosure surrounding the turbines.

3.10 Mesh generation for H-Darrieus VAWT

The fixed domain and the rotating domain are shown in Figure 3.5. A significant amount of effort was dedicated to refining the mesh in the rotating domain to achieve a minimum size of 0.03mm. This was done to ensure the flow field of the rotating domain was captured accurately. In addition, a very fine mesh was generated near the turbine blade surface. This was done by having 12 boundary layers having a normal growth rate of 1.2 with the first layer thickness of 0.058mm. The pressure-based solver named Semi-Implicit Method for Pressure-linked Linked Equations (SIMPLE) with an absolute velocity formation was employed for solving the velocity and pressure. The governing equations were solved by the finite volume method for the entire domains in our study.

Figure 3.6 shows the close-up view of the rotating domain and Figure 3.7 shows the boundary layers around the turbine.

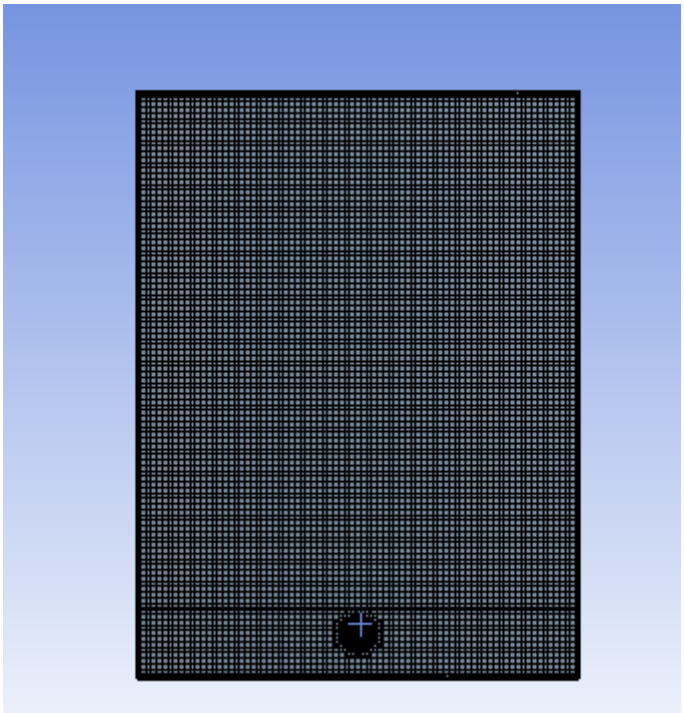

Figure 3.5:Fixed Domain

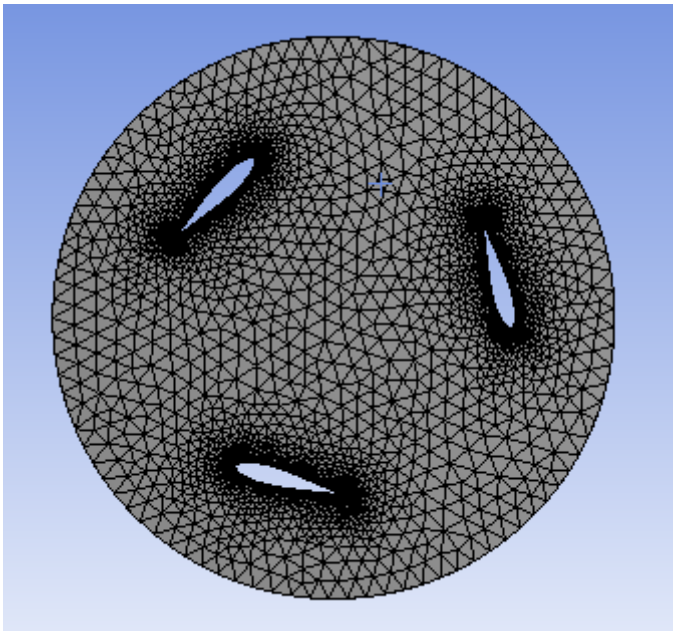

Figure 3.6:Rotating Domain

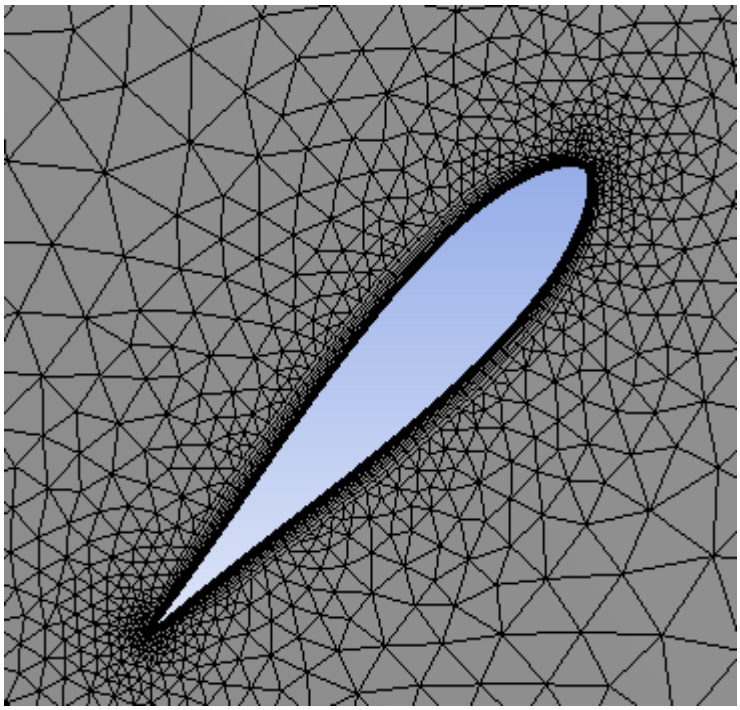

Figure 3.7:Turbine boundary layer mesh

3.11 Grid Independence Test For H-Darrieus VAWT

The quality of the mesh is an important factor affecting the accuracy of our numerical simulations. The mesh quality is strongly affected by the distribution and the size of the mesh of the study. In the study, we vary the number of elements by controlling the element size. The element size was set to be 0.09mm and decreased by 0.01mm until the element size reached 0.02mm. Table 3.5 below shows the number of elements created by the element size. All element size was refined to achieve a maximum skewness of 0.98.

Table 3.5: Element size and Number of elements

Element size (mm)	Number of elements
0.09	963366
0.08	1092015
0.07	1262510
0.06	1830844
0.05	2303919
0.04	3105103
0.03	4822413
0.02	8916760

As shown in Figure 3.8, the grid analysis showed it required at least 6,000,000 cells to achieve an error of less than 1% as compared to the finest grid. This shows the maximum cell size for this study would be 0.03mm to achieve the desired error of less than 1%. Therefore, the total number of 4,822,413 cells was selected for the current computational study as it has the least percentage of error as compared with the other number of cells. the criterion for the moment, continuity together with the transport equation from the SST k-ω turbulence model is defined by the RMS value less than. The coefficient of moment was taken from the last two rotations after the results converged.

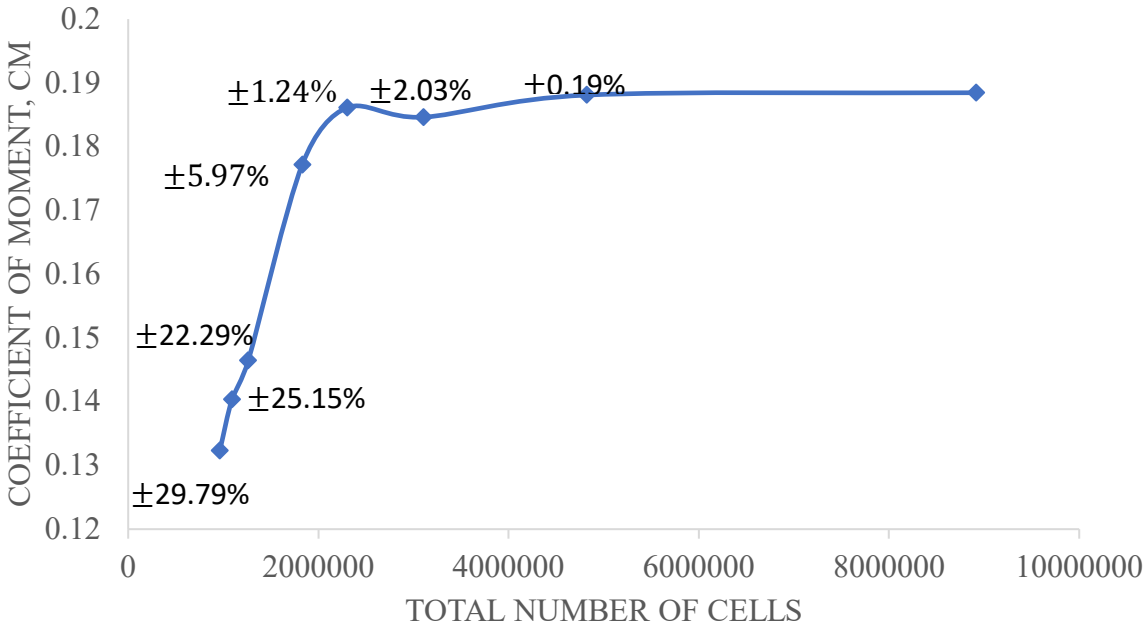

Figure 3.8:Grid Independence Test

3.12 Grid validation for H-Darrieus VAWT

An important criterion of the study is to validate the current grid study with other previous study. Thus, the same mesh conditions in the grid independence study in section 3.11 but the cooling tower domain was removed. The validation simulation was conducted with NACA 0021 turbine with the turbine parameter was tabulated as shown in table 3.6. The obtained results are compared to the experimental and 3D numerical study of Castelli, Englaro, and Benini (2011) and a 3D numerical study by Hashem and Mohamed (2018).

Table 3.6: Validation parameters

Physics setup	Values
Airfoil profile	NACA 0021
Inlet wind speed ($\boldsymbol{V_{in}}$)	9.00 m/s
Turbine diameter ($\boldsymbol{D}$)	0.515 m
Turbine span (H)	0.200 m
Solidity ratio ($\boldsymbol{\sigma}$)	0.25
Tip speed ratio (TSR)	1.44, 1.68, 2.04, 2.33, 2.51, 2.63, 3.01, 3.30

Figure 3.9 portrays the comparison of the current numerical outcome of the power coefficient with the numerical and experimental study of Castelli, Englaro, and Benini (2011) and another numerical study by Hashem and Mohamed (2018). Both the numerical study) conducted overestimated the experimental results. This may be caused by some 3-dimensional effects such as blade tip losses, missing struts and turbine shafts. In addition, the interactions between the boundary layers of the blades and the end plates were employed in the experimental study might have propagated a complex 3-dimensional flow. The validation from our validation study was approximately 8% higher on average as compared to the results from the experiment conducted by Castelli, Englaro, and Benini (2011) in their experimental study and is 5% lower than the computational study conducted by Hashem and Mohamed (2018). The result from our study is closer to the experiment conducted by Castelli, Englaro, and Benini (2011) because the ambient wind was taken into consideration which simulated the actual flow of the air in the cooling tower application. However, the coefficient of power obtained from the present CFD agreed to the conditions used in our current study.

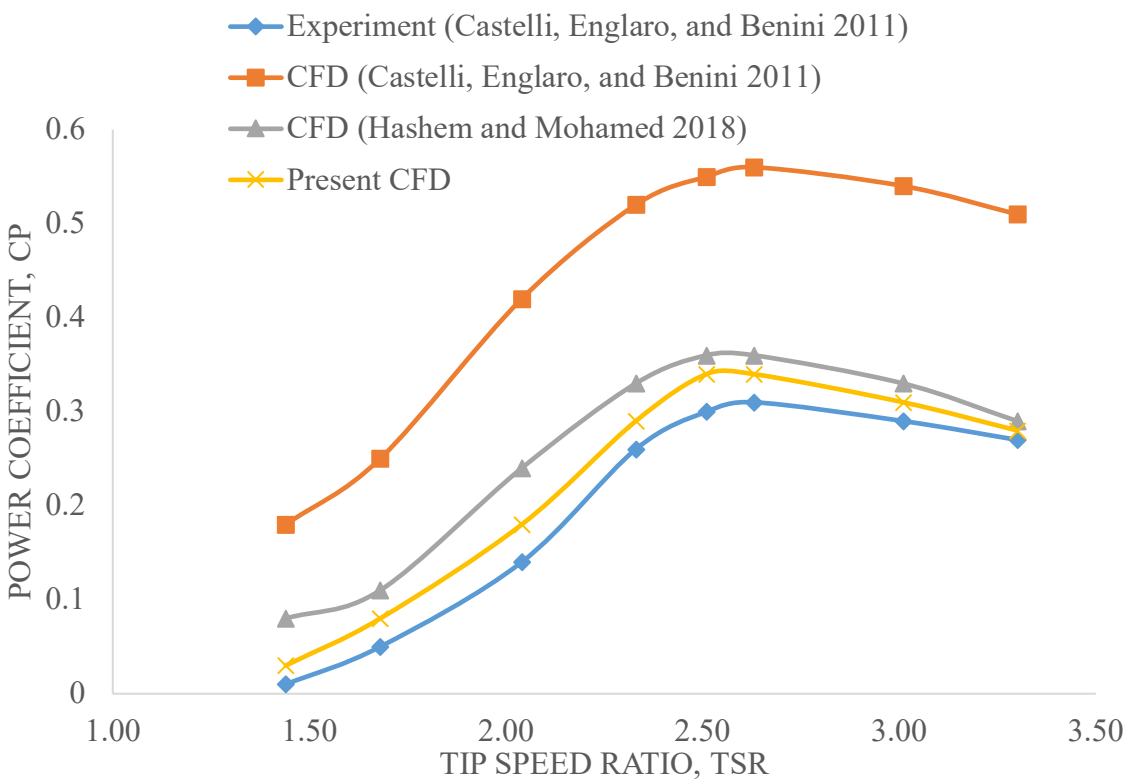

Figure 3.9:Validation of present study with past studies

CHAPTER 4: EXPERIMENTAL METHODOLOGY

4.0 Introduction

In this chapter, the experimental methodology and set up is discussed. The components of the cooling tower are discussed. The implication of the torque sensor and the velocity sensor are also shown. In addition, the initial calibration of the cooling tower fan was conducted. This calibration will help in determining the frequency of the 3 Phase alternating current that is required for the fan to produce the required amount of wind velocity at the outlet of the cooling tower.

4.1 Experimental study

A cooling tower was built based on the cooling tower design by Liu, Zhang, and Ishihara (2018). This was mainly due to the scaled-down factors of the cooling tower. At the bottom of the cooling tower, a fan with a voltage regulator was installed. A honey-comb structured screen was also placed at the bottom of the cooling tower above the fan to prevent vorticity from occurring in the cooling tower. This would reflect the airflow profile of the numerical study. The weldments of the cooling tower were done with the least impact on the overall structure. This was to prevent any surface friction that may occur during the experimental study affecting the results obtained. The fabricated cooling tower was installed in Curtin University in a confined space to prevent disturbance on the wake region by the natural wind flow.

The designed turbine in the CAD was then fabricated with the 3D printing machine available in Curtin University. Then, the test turbine was then installed onto the upper region of the outlet of the cooling tower with 200mm from the base of the turbine and the outlet. A pully was installed at the end of the turbine shaft to apply mechanical load. In addition, the torque sensor was attached to the turbine shaft. Figure 4.1shows the torque sensor used in the study and the Figure 4.2 shows the setup of the torque sensor.

Three points namely, the inner of the cooling tower, the turbine line of centre and the upper part of the turbine (wake region) were placed with velocity sensor. The

results from the velocity sensors and the torque sensor were then used to calculate the systems overall efficiency. The entire configuration for this experimental study can be portrayed in Figure 4.3 in a 3-dimensional view while the Appendix A shows the line diagram.

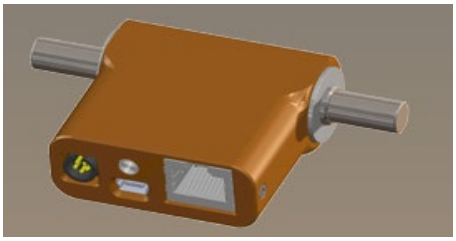

Figure 4.1: Torque sensor (ng-TTR200-ci)

Figure 4.2:Set up of the torque sensor with the pulley.

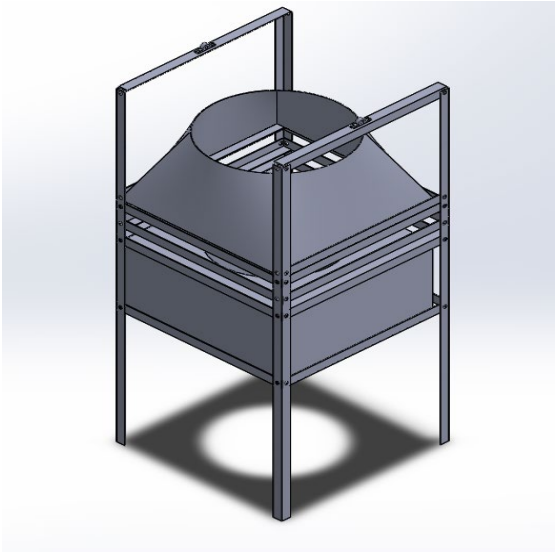

Figure 4.3:Experimental Set up

In this experimental study, the conditions are set as follow:

- Heat and chemical properties will be neglected in the study.
- Air is the working fluid in the experimental set up with atmospheric condition.

The results obtained from the numerical study and the experimental study will then be compared to validate the results to be accurate and precise.

4.2 Calibration of the cooling tower

In this subchapter, the calibration of the cooling tower was done by adjusting the frequency of the 3-phase frequency regulator. A grid shown in Figure 4.4 shows the grid of 30cm X 30cm with each individual square of 5 cm x 5cm respectively. The frequency tested was from 5Hz to 50Hz with a 5Hz interval. At each interval, the fan was allowed to run for 2 minutes before taking the wind velocity. The 2-minute runtime of the fan was to allow the wind velocity to stabilize before taking the reading from the wind velocity sensor. Once the 2 minutes were up, the wind velocity sensor took the average reading of 1 minute for each grid. The results were then converted into a graph of frequency against wind velocity as shown in Figure 4.5 and Table 4.1.

Figure 4.4: Grid of 30cm X 30 cm

Table 4.1: Frequency against wind velocity

Frequency (Hz)	Velocity (m/s)
0	0
5	0.9688
10	2.1572
15	3.3432
20	4.3464
25	5.7952
30	7.166
35	8.2968
40	9.6024
45	10.67
50	11.732

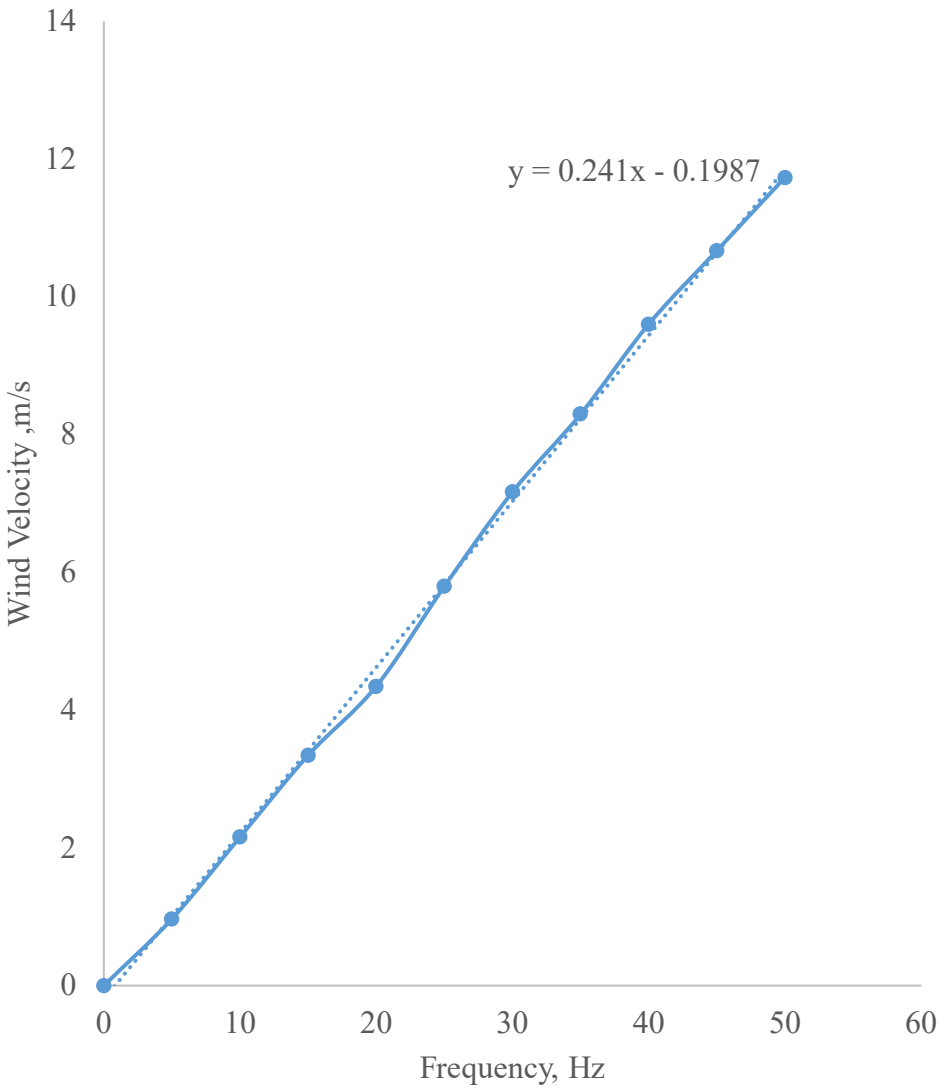

Figure 4.5: Graph of frequency against wind velocity

CHAPTER 5: RESULTS AND DISCUSSIONS

5.0 Numerical result

In this chapter, the flow physics of each selected VAWT type; H-Darrieus VAWT, Helical H-Darrieus VAWT, Savonius VAWT and Helical Savonious VAWT were studied in terms of the coefficient of moment and the coefficient of power. In addition, the 3-dimensional static pressure and velocity contours portrayed the flow characteristics in the turbine were also presented. The static pressure and velocity contours were presented at critical azimuth angles in the range from 30° to 120°. This chapter also discussed the optimized VAWT for the cooling tower application. This was generally done by studying the optimized coefficient of power of each type of VAWT turbine in the study. The numerical results also presented the static pressure contour and velocity contour for the optimized VAWT to further justify the results of the coefficient of power.

5.1 H-Darrieus VAWT Numerical Result

In this section of the study, the overall performance of the H-Darrieus VAWT is studied by first analysing the coefficient of moment and power coefficient. The graphs of the coefficient of moment and the coefficient of power were plotted against the selected tip speed ratio of 2.0, 2.5, 3.0 and 3.8. Further studies were conducted on the turbine by studying the velocity contour and pressure contour.

5.1.1 Coefficient of moment and coefficient of power for H-Darrieus VAWT

In this numerical study, the performance of the H-Darrieus VAWT is analyzed by studying the coefficient of the moment and the coefficient of power. Both are important and are plotted against the Tip Speed Ratio. Therefore, Figures 5.1 and 5.2 show the graph of the coefficient of moment and the graph of power coefficient with distinctive inlet velocity for the H-Darrieus VAWT. The graphs were obtained from the simulations with TSR of 2.0, 2.5, 3.0, and 3.8 together with a wind velocity of 5m/s, 10m/s, and 15m/s respectively.

As shown in Figure 5.1, the velocity achieved the highest coefficient of moment for the H-Darrieus turbine is the wind velocity of 15m/s throughout the selected range

of TSR. This was then followed by the wind velocity of 10m/s and lastly, the wind velocity of 5m/s gave the lowest coefficient of moment. There was a noticeable trend in the graph, where after a TSR of 2.5 to a higher TSR of 3.8, the coefficient of moment decreased for all the 3 wind velocities. This simply reflected at TSR2.5 the maximum Coefficient of moment was achieved at a lower rotational speed.

Furthermore, as the wind velocity increased by 5m/s for each wind velocity, the graph showed the percentage difference in the average Coefficient of Moment for 5m/s and 10m/s was 54.06% while the percentage difference of the 10m/s and the 15m/s was 12.96%. This indicates as the wind velocity increases after the 15m/s wind speed, the difference in coefficient of moment decreases to a certain point to an extent that even with the increase of wind velocity, the maximum Coefficient of moment will be achieved.

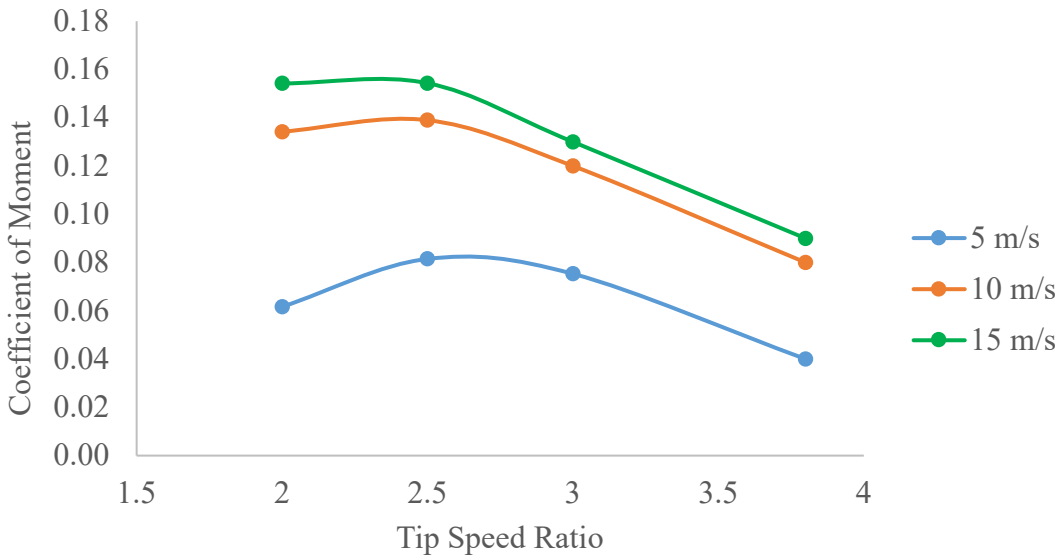

Figure 5.1:Coefficient of Moment for H-Darrieus at various wind velocity

In addition, the peak coefficient of moment for the three wind velocities were all located at the TSR 2.5. Overall, the graph points out the highest achieved coefficient of moment was from the wind velocity of 15m/s at TSR 2.5 with the peak coefficient of moment of 0. 1543.The peak coefficient of moment of the wind velocity of 5m/s and 10m/s were 0.0815 and 0.1390. From the graph, the trend of the 10m/s and the 15m/s graph were almost similar as compared to the 5m/s because the 10m/s and 15m/s wind velocity caused the turbine to have a more stable wake region at an earlier time as compared to the 5m/s.

Figure 5.2 shows the power coefficient graph as a function of TSR for the H-Darrieus VAWT with various wind velocities. The numerical results portray the coefficient of power increases till it reaches the peak at the TSR of 3.0 and then it decreases with the increase of the TSR. The maximum coefficient of power at TSR of 3.0 is 0.2260, 0.3614, and 0.3877 respectively for 5m/s, 10m/s, and 15m/s. The peak coefficient of power comes from the 15m/s wind velocity The difference between the peak coefficient of power for the 10m/s and the 15m/s wind velocity is approximately 37.25% and the difference for the 5m/s and the 10m/s wind velocity is 7.14%. With the percentage difference in the graphs, it is clear the changes power coefficient of the H-Darrieus VAWT for the increment of wind speed will decrease as the wind velocity increases.

The results from this study were well agreed with the results conducted by Ali, Lee, and Jang (2018) in their the power curve showed the power increase until it reached the wind speed of 14m/s and the power became a horizontal flat line. This was reflected in this study as the wind speed increases, the power coefficient increases regardless of the TSR. In addition, the results obtained was similar to the study conducted by Singh, Roy, and San (2020). However, there was an increase in the maximum coefficient of power due to the higher wind speed of 15m/s employed in this study as compared to the 9m/s case.

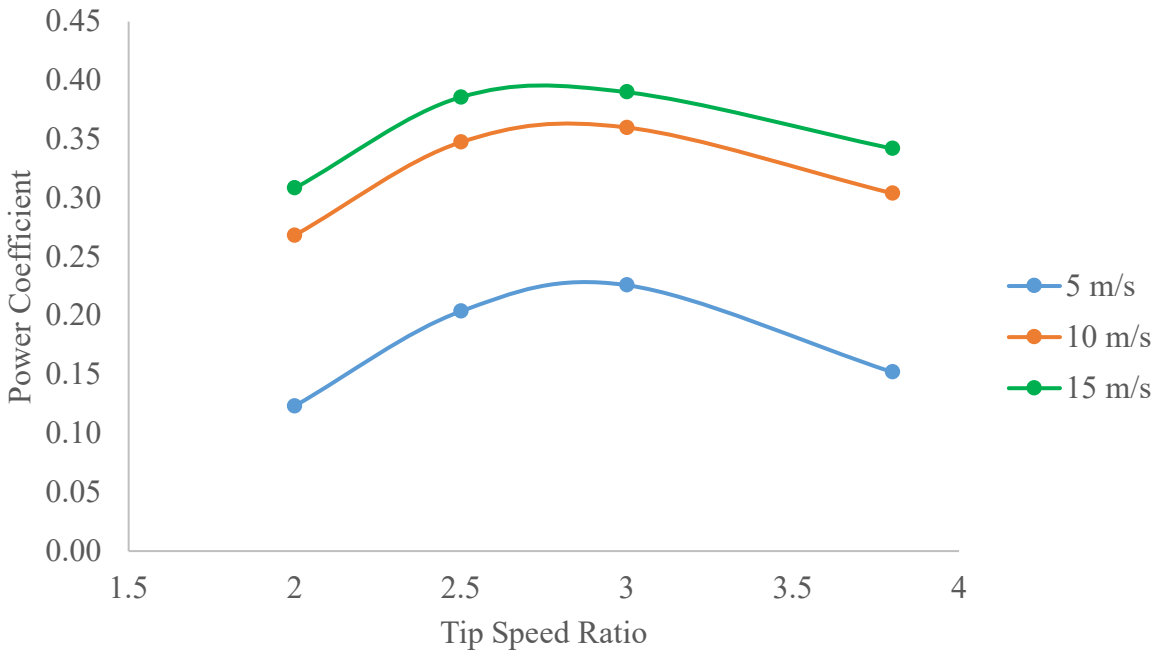

Figure 5.2: Power Coefficient for H-Darrieus at various wind velocity

5.1.2 Instantaneous Coefficient of moment for H-Darrieus

The radial graph of instantaneous coefficient of moment was deployed focusing on the point of the maximum coefficient of moment and the minimum coefficient of moment in Figure 5.3(A) and Figure 5.3(B) respectively.

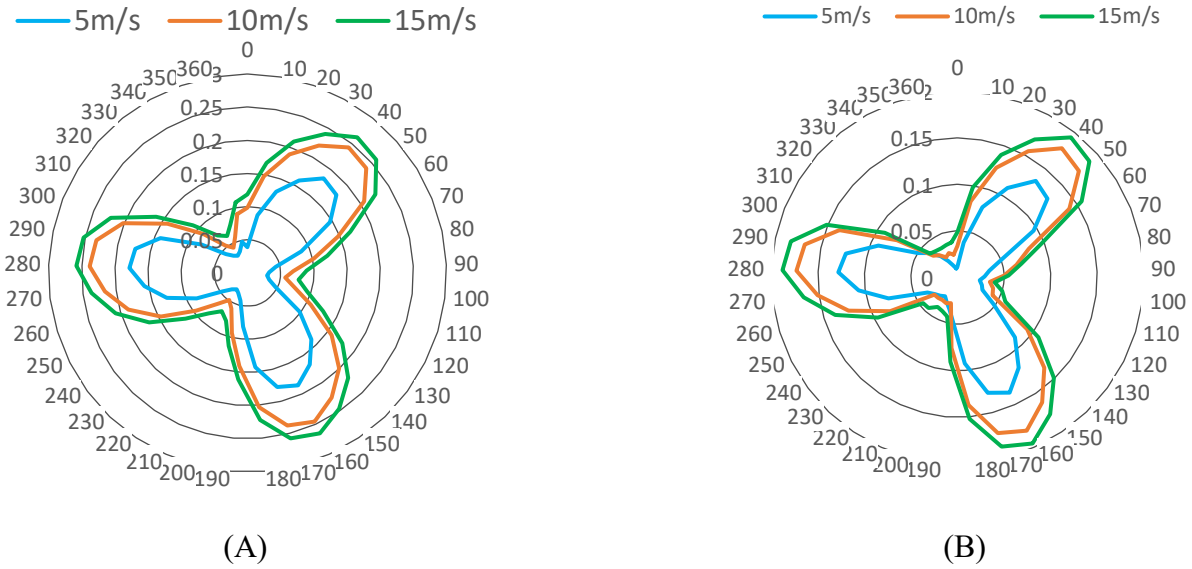

(A) (B)

Figure 5.3:Graph of Instantaneous coefficient of moment (A) Maximum (B) Minimum

5.1.3 Velocity Magnitude Contour of H-Darrieus

The velocity contour of the airflow for the maximum and minimum power coefficient of the turbines is shown in Figure 5.4. The critical azimuthal angles of θ=30°, 60°, 90° and 120°. The maximum power coefficient was at TSR3.0 with a wind velocity of 15m/s shown in Figure 5.4(A) and the minimum power coefficient at TSR2.0 with a wind velocity of 5m/s shown in Figure 5.4(B). For the maximum power coefficient, it was noticeable that high-velocity regions of approximately 15m/s were formed at the lower surface of the airfoil at azimuthal angle of θ=30° and 60°. However, as the azimuthal angle increases to 90° and 120°, a higher velocity region approximately 23m/s was seen at the lower part of the airfoil. As the velocity gets higher, the pressure decreases. Thus, the higher velocity region indicated the formation of the lower pressure region at the lower surface of the airfoil. This portrayed the higher-pressure difference of the upper and lower surfaces of the airfoil. This stipulated more lift was being generated for the higher power coefficient. On the contrary, for the minimum power coefficient, no visible abrupt change in the velocity

throughout the critical azimuthal angle from 30° to 120°. As a result of the lesser velocity difference, the power coefficient was smaller.

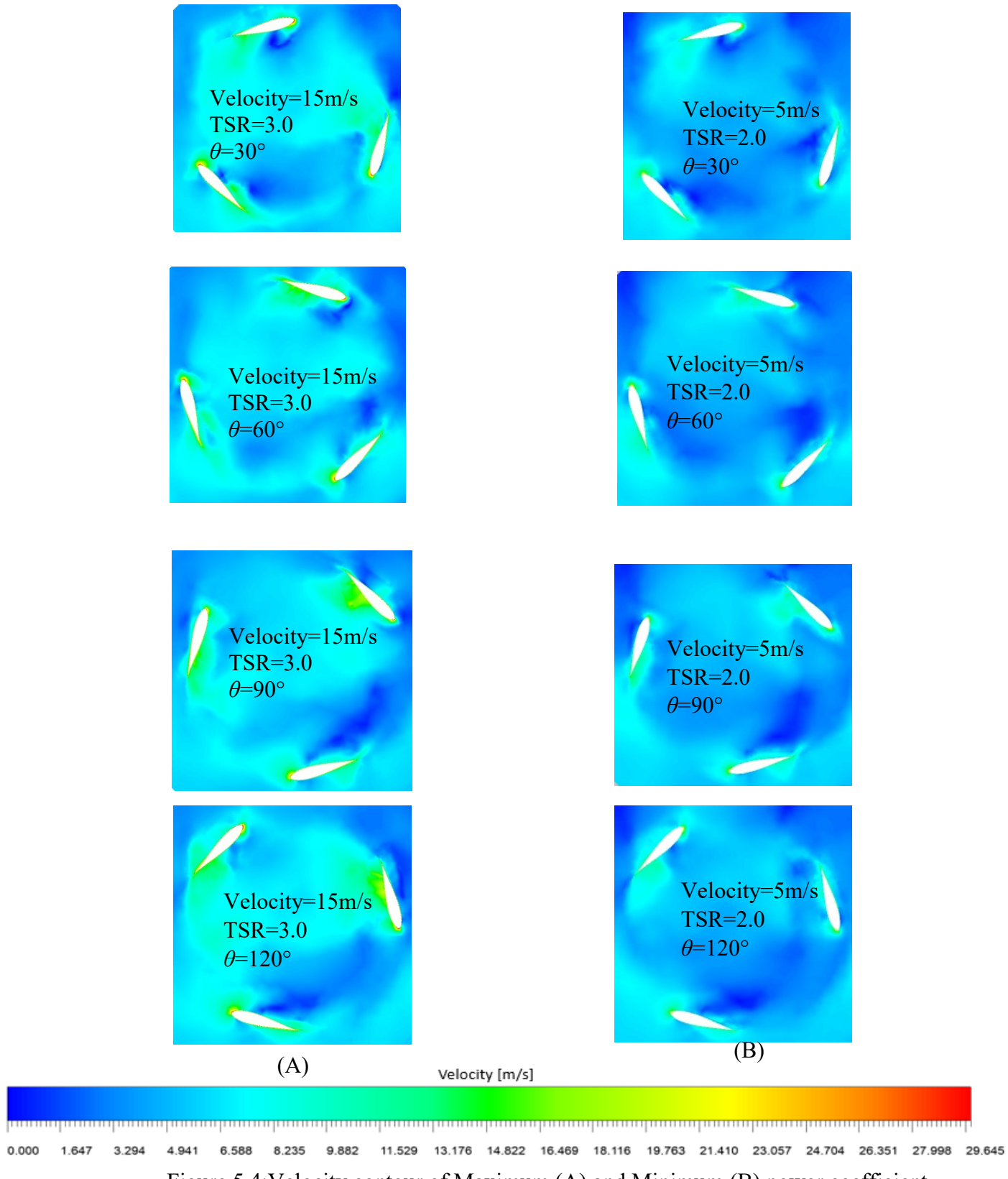

Figure 5.4:Velocity contour of Maximum (A) and Minimum (B) power coefficient

5.1.4 Static Pressure Contour of H-Darrieus

Figure 5.5 (A) showed the pressure contour for the maximum CP for H-Darrieus of TSR 3.0 with the wind velocity of 15m/s and Figure 5.5 (B) portrayed the pressure contour for the minimum coefficient of power for the H-Darrieus of TSR2.0 with the wind velocity of 5m/s. The positive regions were highly concentrated at the leading edge of the airfoil with the highest power coefficient indicates a higher drag force was being experienced at the leading edge.

As seen in Figure 5.5 (A), the turbine produced a maximum coefficient of power caused by the positive pressure with the lower pressure difference. The trailing edge of the turbine blades for θ=30° and 60° is approximately 397pa whereas for the azimuthal angle of θ=90° and 120°, it showed the trailing edge experiences about 110pa. It was also noticeable for all the blades in the selected azimuthal angle, the pressure difference between the outer side and the inner side of the blades was significantly small. This causes the lift force to be small. Therefore, the overall coefficient of power for the H-Darrieus turbine with TSR3.0 and wind velocity of 15m/s were the highest.

In addition, with reference to Figure 5.5(B), the trailing edge of the blades experienced a high-pressure region at the inner side for the azimuthal angle of θ=30° to 120°. This indicated a high drag force was being exerted on the blades, causing it to have an impact on the aerodynamic performance of the turbine. There is also a large pressure difference between the outer surface and the inner surface of the blade. The larger pressure difference caused a high drag-to-lift ratio and affected the turbine's aerodynamic performance. This was the main cause of the low coefficient of power being generated.

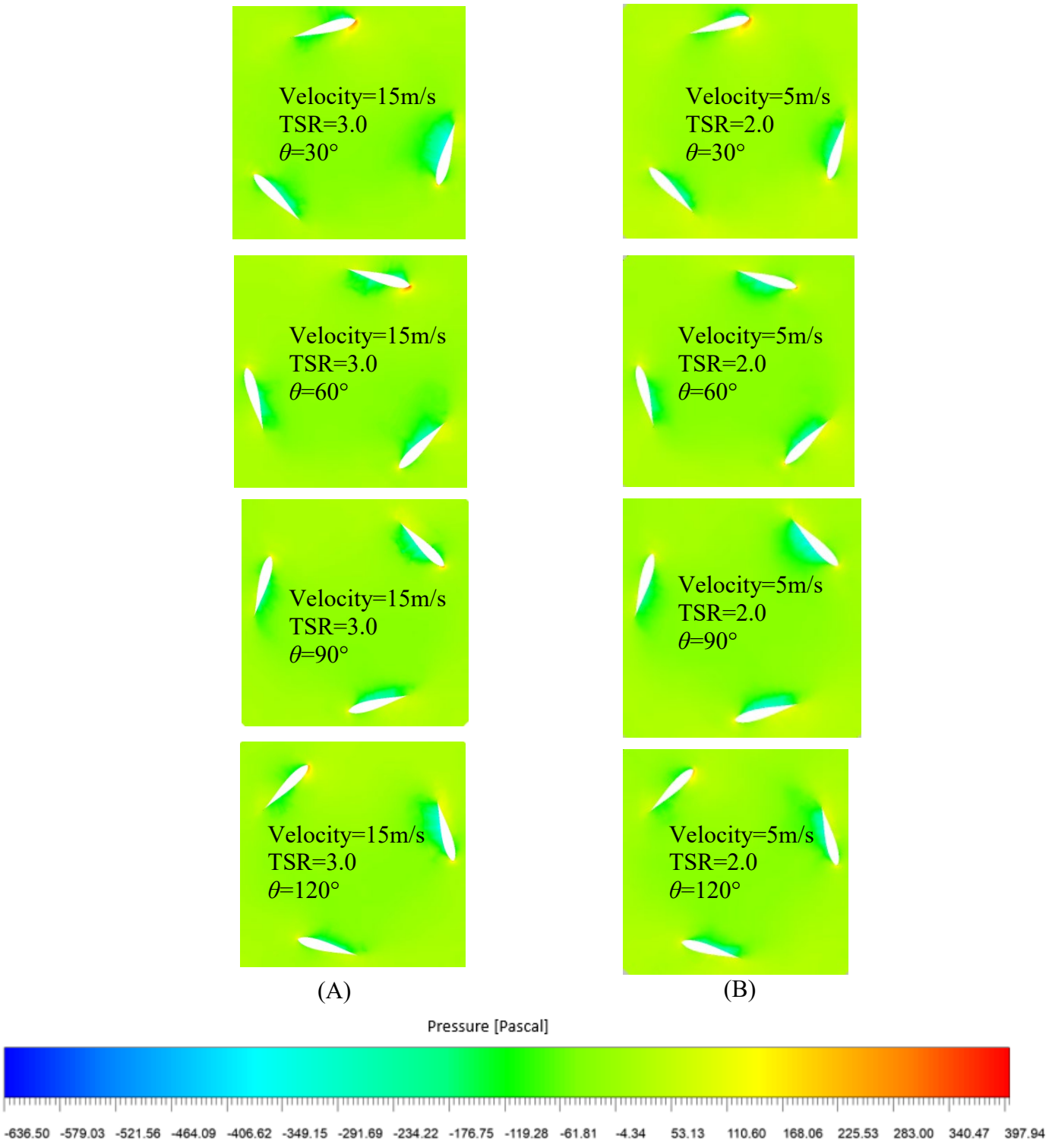

Figure 5.5:Static Pressure Contour for Maximum (A) and Minimum (B) Power Coefficient

5.2 Numerical results for Helical H-Darrieus VAWT

In this section of the study, the overall performance of the Helical H-Darrieus VAWT was studied by first analysing the coefficient of moment and coefficient of power. The graphs of the coefficient of moment and the coefficient of power were plotted against the selected tip speed ratio of 2.0, 2.5, 3.0 and 3.8. Further studies were conducted on the turbine by studying the velocity contour and pressure contour.

5.2.1 Coefficient of moment and power for Helical Darieus VAWT

Figure 5.6 shows the coefficient of moment for the Helical Darrieus VAWT. From the selected wind speed of 5m/s, 10m/s and 15m/s, the wind speed producing the highest coefficient of moment is the 15m/s wind speed. A similar trend was portrayed in the graph, where the coefficient of moment continued to increase from the tip speed ratio of 2.0 to 3.0 where at the tip speed ratio of 3.0, it reached the maximum coefficient of moment. Followed by a decrease in all three graph lines as it approached the tip speed ratio of 3.8.

Furthermore, the peak coefficient for all the three wind speeds were at the tip speed ratio of 3.0. The graph shows the maximum coefficient of moment is the wind speed of 15m/s with a peak coefficient of moment of 0.1184. However, for the wind speed of 10m/s and 5m/s, the peak coefficient of moment was 0.1086 and 0.07541 respectively.

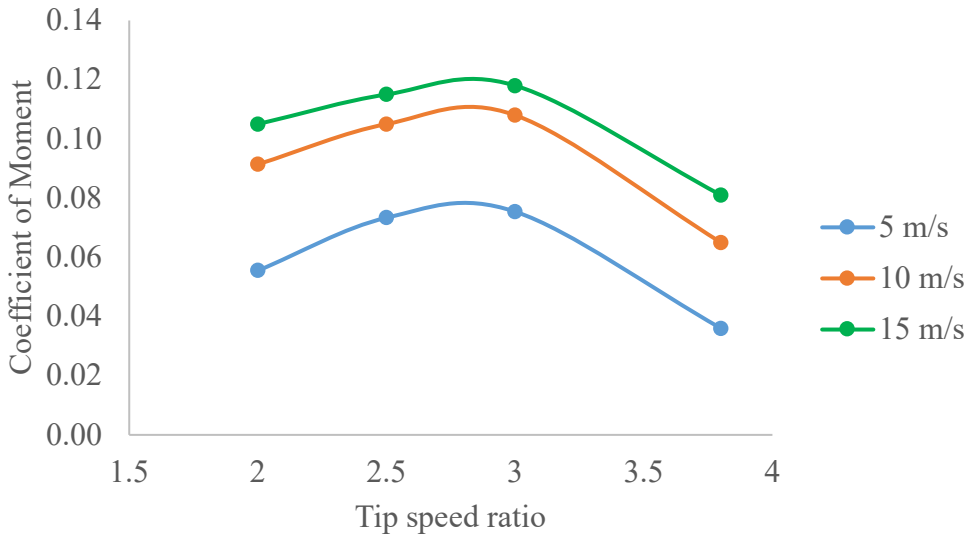

Figure 5.6: Coefficient of Moment for Helical H-Darrieus at various wind velocity

In addition, Figure 5.7 indicates the graph of the power coefficient for the Helical H-Darrieus VAWT. The graph showed the maximum power coefficient was achieved with the wind speed of 15m/s as compared to the other two wind speed. Similar behaviour was seen where the power coefficient increased from the TSR of 2.0 to 3.0 and then decreased to the 3.8 tip speed ratio. All graphs indicated the peak power coefficient was at TSR of 3.0. Overall, the maximum power coefficient achieved was 0.3541 at the wind speed of 15m/s and the TSR of 3.0.

Furthermore, the results produced for the Helical Darrieus were compared to the study conducted by Castelli and Benini (2012). The behaviour of the power coefficient graph was similar where the coefficient of power continued to increase until it reached TSR3.0 and then it decreased. When comparing the data from the wind speed of 10m/s from the current study and the data from Castelli and Benini (2012) where the wind speed was 9m/s, the data from both study had about 8% difference. This was acceptable due to the difference of 1m/s in the wind velocity.

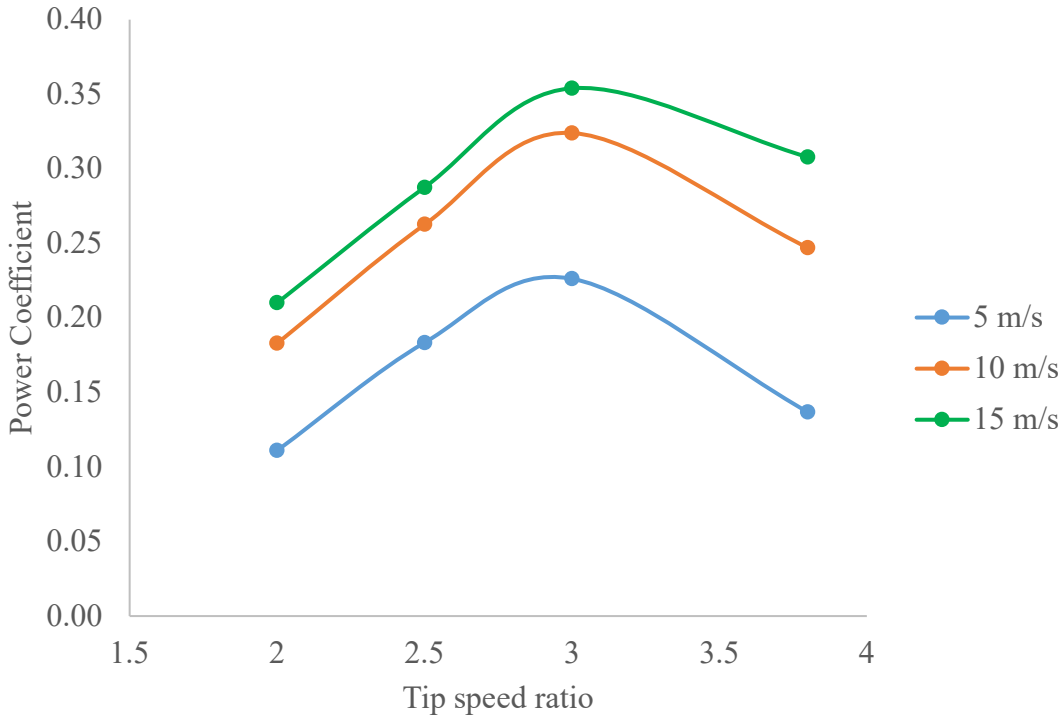

Figure 5.7:Power Coefficient for Helical Darrieus at various wind velocity

5.2.2 Instantaneous Coefficient of moment for Helical Darrieus VAWT

The maximum coefficient of moment and the minimum coefficient of moment are shown in Figure 5.8(A) and Figure 5.8(B) respectively. To determine the coefficient of moment at each angle of the final rotation of the simulation. For the maximum coefficient of moment in Figure 5.8(A), It was visible the difference of the maximum and minimum coefficient of moment was smaller. This indicates lesser fluctuation in the coefficient of moment. On the other hand, for Figure 5.8(B), it can be seen the difference in the coefficient is larger, this causes the increase of the fluctuation of the coefficient of moment and thus decreases the overall coefficient of moment.

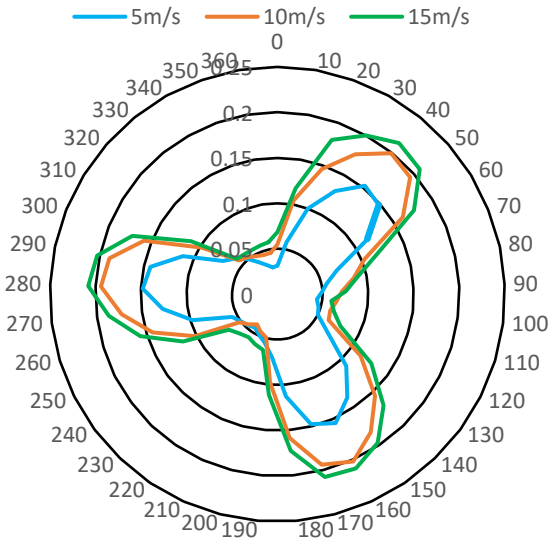

(A)TSR 3.0

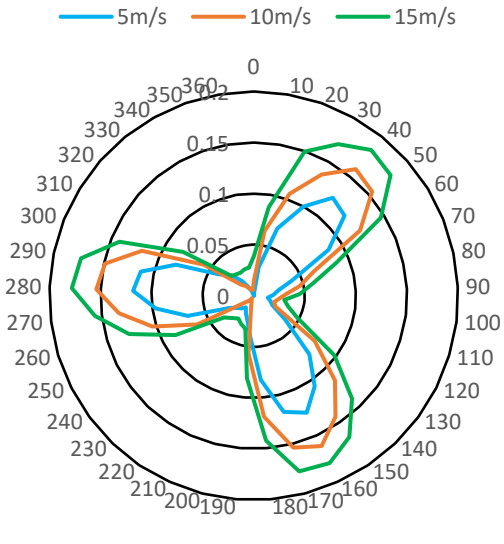

(B)TSR 3.8

Figure 5.8:Graph of Instantaneous coefficient of moment (A) Maximum (B) Minimum

5.2.3 Velocity Magnitude Contour of Helical Darrieus

The velocity contour for the maximum and minimum power coefficient is shown in Figure 5.9. The selected azimuthal angle of θ= 30°, 60°, 90°, and 120° are employed to study the velocity contour. The maximum power coefficient was at TSR 3.0 with a wind velocity of 15m/s and the minimum power coefficient was at TSR 3.8 with a wind velocity of 5m/s. The contours are seen in Figure 5.9(A) for the maximum and the Figure 5.9(B) for the minimum.

For the maximum coefficient of power, it showed the azimuthal angle of 30°, 90°, and 120°, all three blades of the turbine show similar characteristics of the inner

surface of the turbine had higher velocity. As this is a helical type of turbine, the higher velocity was at the inner surface of the leading part of the turbine. However, for the azimuthal angle of 60°, a larger velocity of 42m/s was seen at the inner surface of the trailing edge for one of the blades. As the turbine was forced with a wind speed of 15m/s the curvature of the helical surface of the blade improved the air flow acting as a guide causing the increase in the wind speed at the blade.

Besides, for the minimum coefficient of power, the selected azimuthal angle of 30°,60°, 90° and 120° shows the similar flow. The inner surface of the blades shows higher velocity as compared to the outer region. The trailing edge has a longer velocity contour due to better flow separation at the centre of the turbine blades.

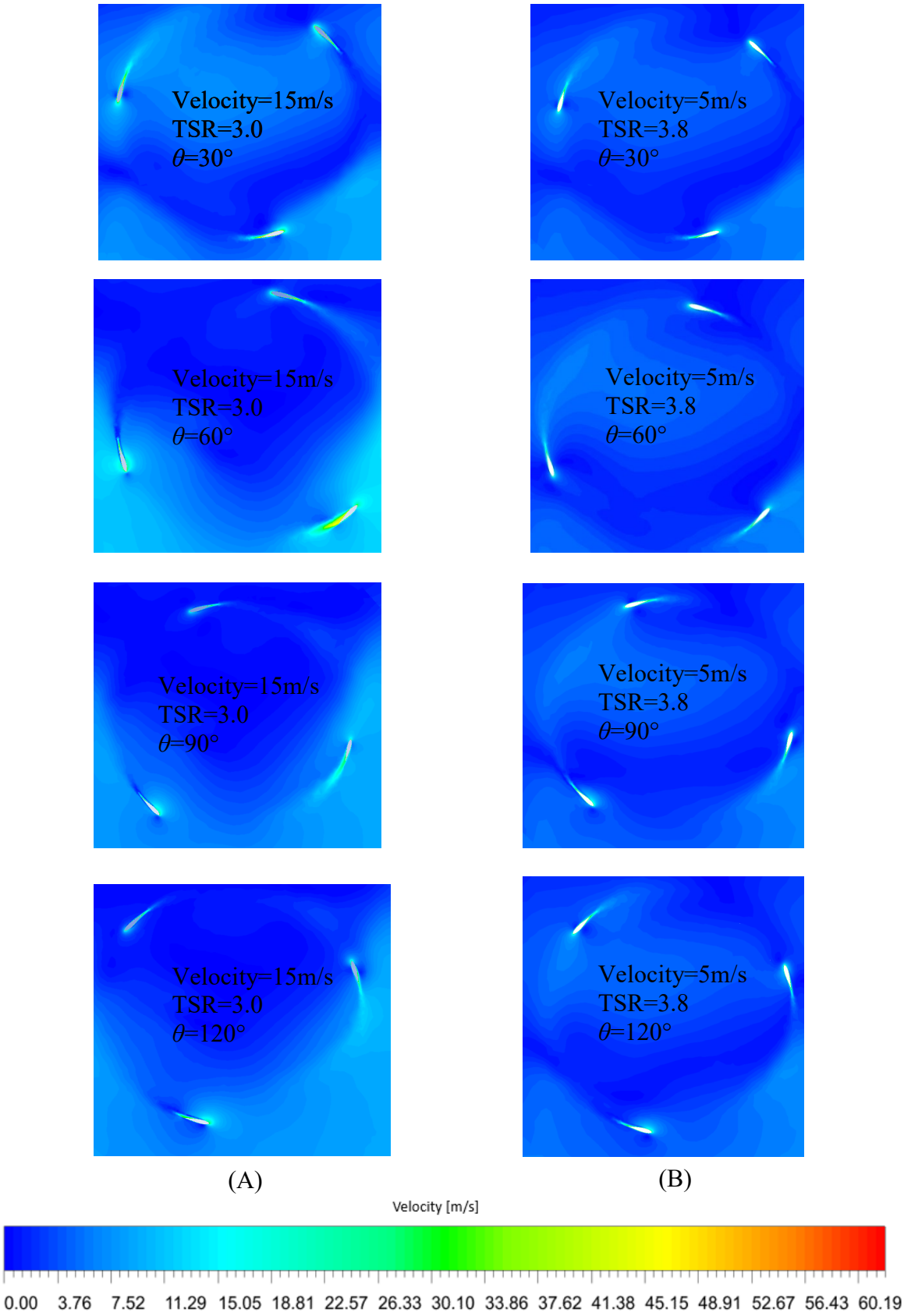

Figure 5.9:Velocity contour of Maximum (A) and Minimum (B) power coefficient

5.2.4 Static Pressure Contour for Helical H-Darrieus

The static pressure contour for the maximum and minimum Coefficient of power was employed and studied to understand the reasoning behind the results. Figure 5.10(A) shows the static pressure contour for the maximum power coefficient with the TSR of 3.0, wind velocity of 15m/s and Figure 5.10(B) shows the static contour pressure for the minimum coefficient of power with TSR3.8, wind velocity of 5m/s. The selected azimuthal angles for the static pressure contour are θ=30°,60°, 90° and 120°. These azimuthal angles were taken from the last rotation where the wake region had been fully developed.

For the static pressure contour of the maximum coefficient of power shown in Figure 4.10(A), the pressure difference for all the azimuthal angles was almost similar where the inner surface of the turbine blades experiences approximately -535 pa while the outer surface of the turbine blades experiences approximately 216pa. Thus, there was an approximate pressure difference of 511pa. For the pressure at the trailing edge. It was clear in Figure 5.10(A), no large pressure region. This indicated the drag force acting on the blade is low.

In addition, for the static pressure contour of the minimum coefficient of power shown in Figure 5.10(B), it was portrayed the inner surface of the turbine blades has higher pressure as compared to the outer surface. This caused the turbine blade to have an approximate pressure difference of 700pa. With the highest pressure difference, it caused an increase in the drag force for the turbine blades thus resulting in the lowest coefficient of power. Also, it was shown that the leading edge of the turbine blades faces a high-pressure region. This was due to the helical blades. As the blade curves, the section before the leading-edge cuts through the airflow causing an increase in the pressure. Thus, this was the reason why the helical turbines could have better starting ability as compared to the standard straight turbines.

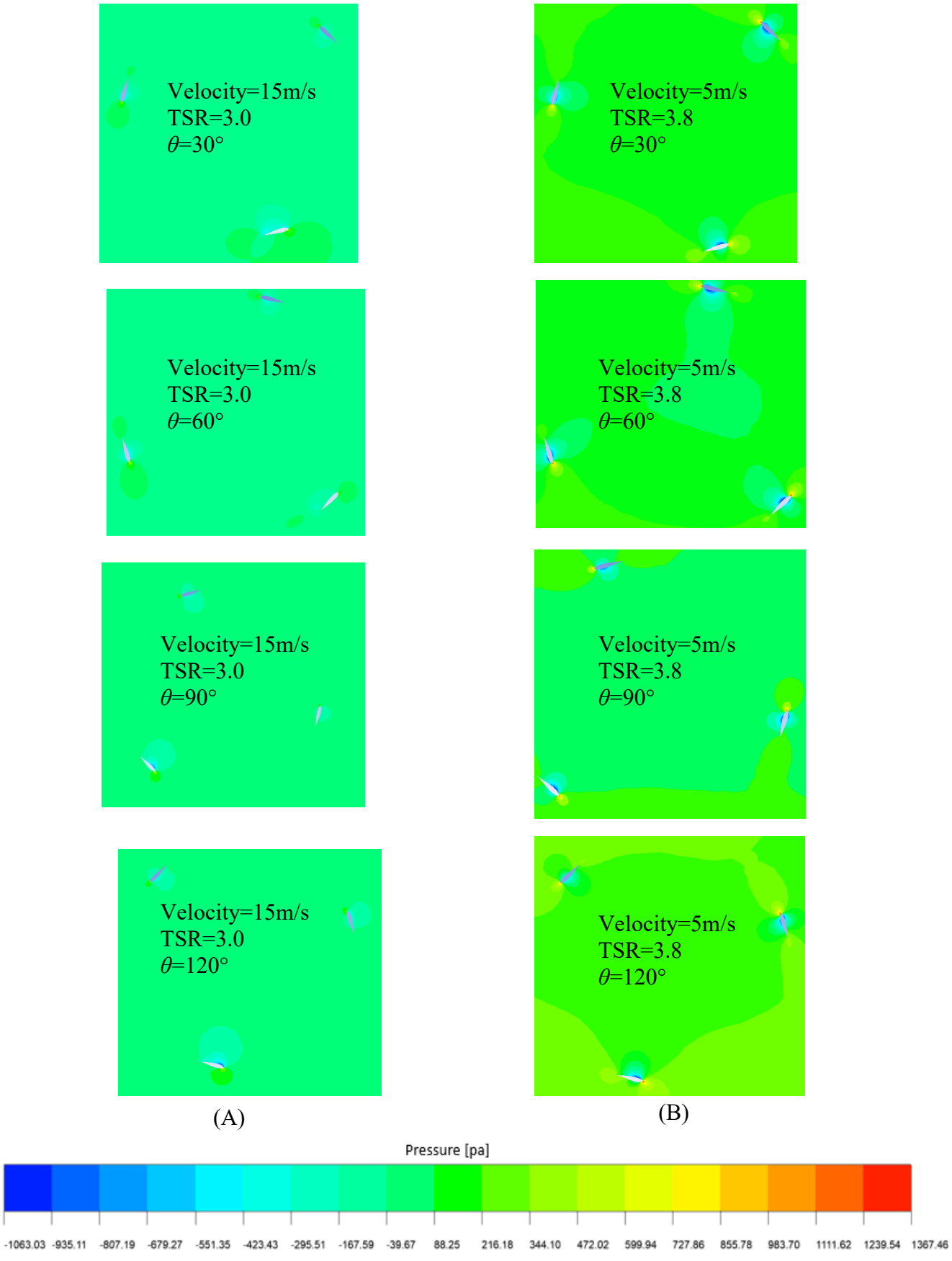

Figure 5.10:Static Pressure contour of Maximum (A) and Minimum (B) power coefficient

5.3 Numerical result for Semi-Elliptical Savonious VAWT

In this section, the overall performance of the Semi-Elliptical Savonious VAWT was studied by analysing the coefficient of moment and coefficient of power. The graphs of the coefficient of moment and the coefficient of power were plotted against the tip speed ratio of 0.4, 0.6, 0.8 and 1.0. To study the flow physics of the turbine, the velocity contour and the pressure contour are employed to have a better visualization of the flow around the turbine at the azimuthal angle of θ= 30°, 60°, 90° and 120° of the final rotation.

5.3.1 Coefficient of moment and power for Semi-Elliptical Savonious VAWT

Figure 5.11 portrays the coefficient of moment for the Semi-Elliptical Savonious VAWT. The Savonious VAWT best performed at the wind speed of 15m/s as compared to the wind speed of 5m/s and 10m/s used in the numerical study. For all three wind speed, it showed the same trend where the coefficient of moment decreases as the increase of tip speed ratio from 0.4 to 1.0 respectively.

In addition, the maximum coefficient of moment was at the tip speed ratio of 0.4 for all the three wind speed selected. The wind speed of 15m/s gave the highest peak coefficient of moment of 0.2487. However, for the wind speed of 10m/s and 5m/s the peak coefficient of moment is 0.2241 and 0.2010.

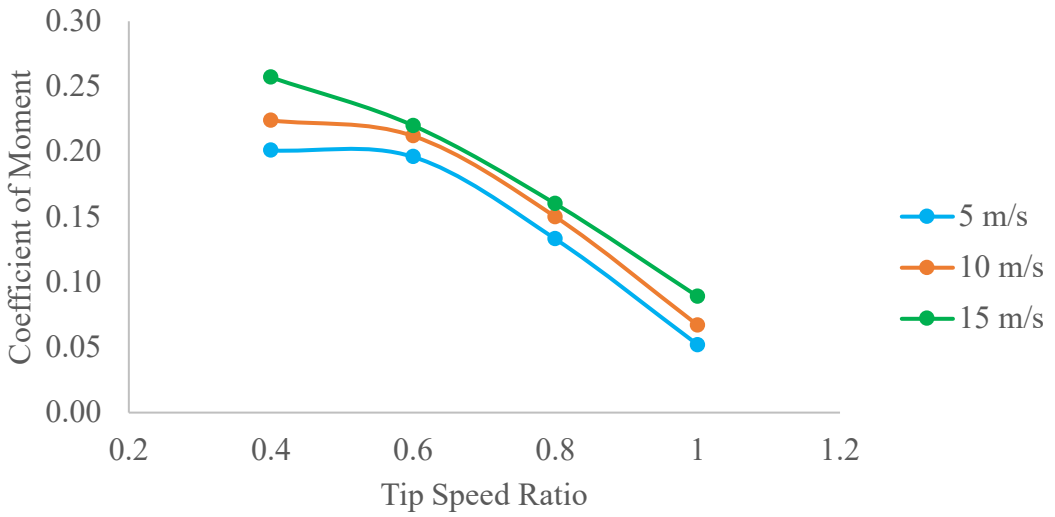

Figure 5.11: Coefficient of Moment for Semi-Elliptical Savonious VAWT at various wind speed

Moreover, Figure 5.12 shows the graph of the power coefficient of the Semi-Elliptical Savonious VAWT. The graph indicated the maximum power coefficient was achieved at 15m/s when compared to the other two wind speeds. A particular behavioural pattern was observed when compared to the coefficient of moment where the power coefficient increases from the tip speed ratio of 0.4 to 0.6 and then decreases as the tip speed ratio increases from 0.6 to 1.0. All three graph lines also shows the Tip speed ratio 0.6 had the peak power coefficient with the wind speed of 15m/s having the highest peak power coefficient of 0.132.

Furthermore, the results obtained from the study were compared to the study conducted by Irabu and Roy (2007). The behaviour of the coefficient of moment was similar where the coefficient of moment decreases as the tip speed ratio increases from 0.4 to 1.0. Also, the power coefficient of the current portrayed a similar characteristic to the study of Irabu and Roy (2007) where the maximum power coefficient lies in the tip speed ratio of 0.6.

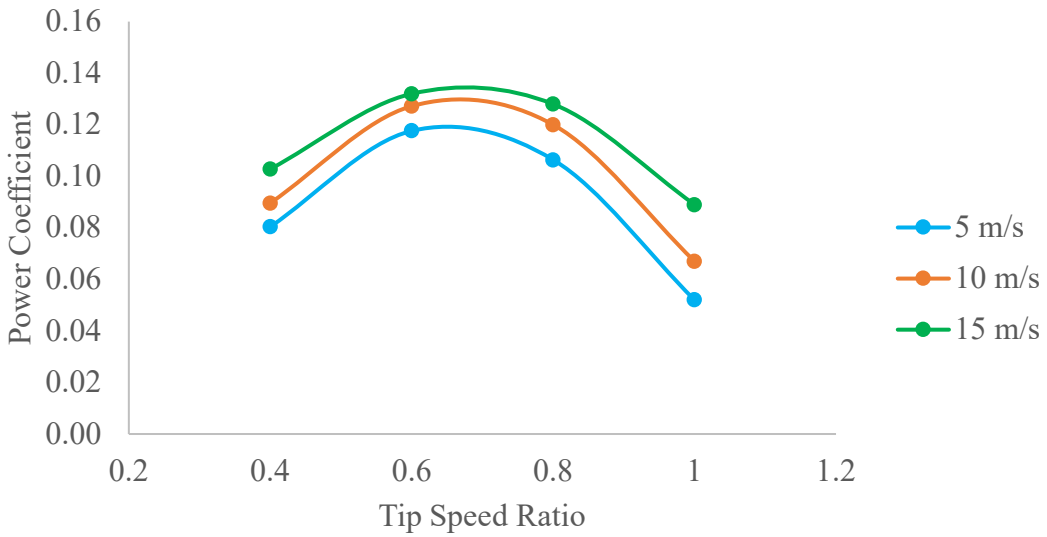

Figure 5.12: Power Coefficient for Semi-Elliptical Savonious VAWT at various wind speed

5.3.2 Instantaneous coefficient of moment for Semi-elliptical Savonious VAWT

The maximum coefficient of moment and the minimum coefficient of moment are shown in Figure 5.13(A) and Figure 5.13(B). This is to underline the coefficient of moment at each angle of the final rotation in the numerical study.

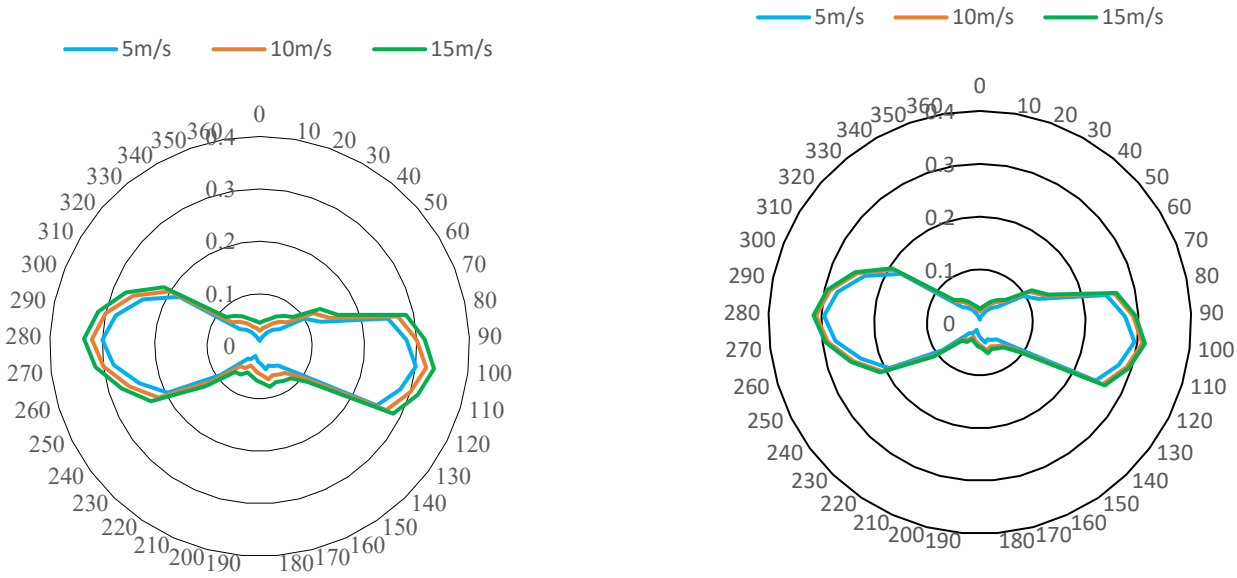

(A)TSR 0.4 (B)TSR 1.0

Figure 5.13: Graph of Instantaneous coefficient of moment (A) Maximum (B) Minimum

5.3.3 Velocity profile for Semi-elliptical Savonious VAWT

The velocity contours of the maximum and minimum coefficient power were extracted. The maximum coefficient of moment was at the TSR of 0.4 with the wind speed of 15m/s shown in Figure 5.14(A). The minimum coefficient of power was from the TSR 1.0 with the wind speed of 5m/s shown in Figure 5.14(B). The azimuthal angles of θ= 30°, 60°, 90° and 120° were chosen.

A clear similarity was seen in both the maximum and minimum instantaneous coefficient of power, at the azimuthal angle of 30°, it had the lowest instantaneous coefficient of moment until it reached 90° and then decreased to 120°. Both maximum and minimum velocity profile did not show any major differences except for the convex part of the returning blade. This was due to the flow on the convex part of the returning blade was weakened by the flow on the concave part of the advancing blade. As the inlet wind velocity increases, the velocity on the convex part of the returning blade increases to a maximum of 23.01m/s.

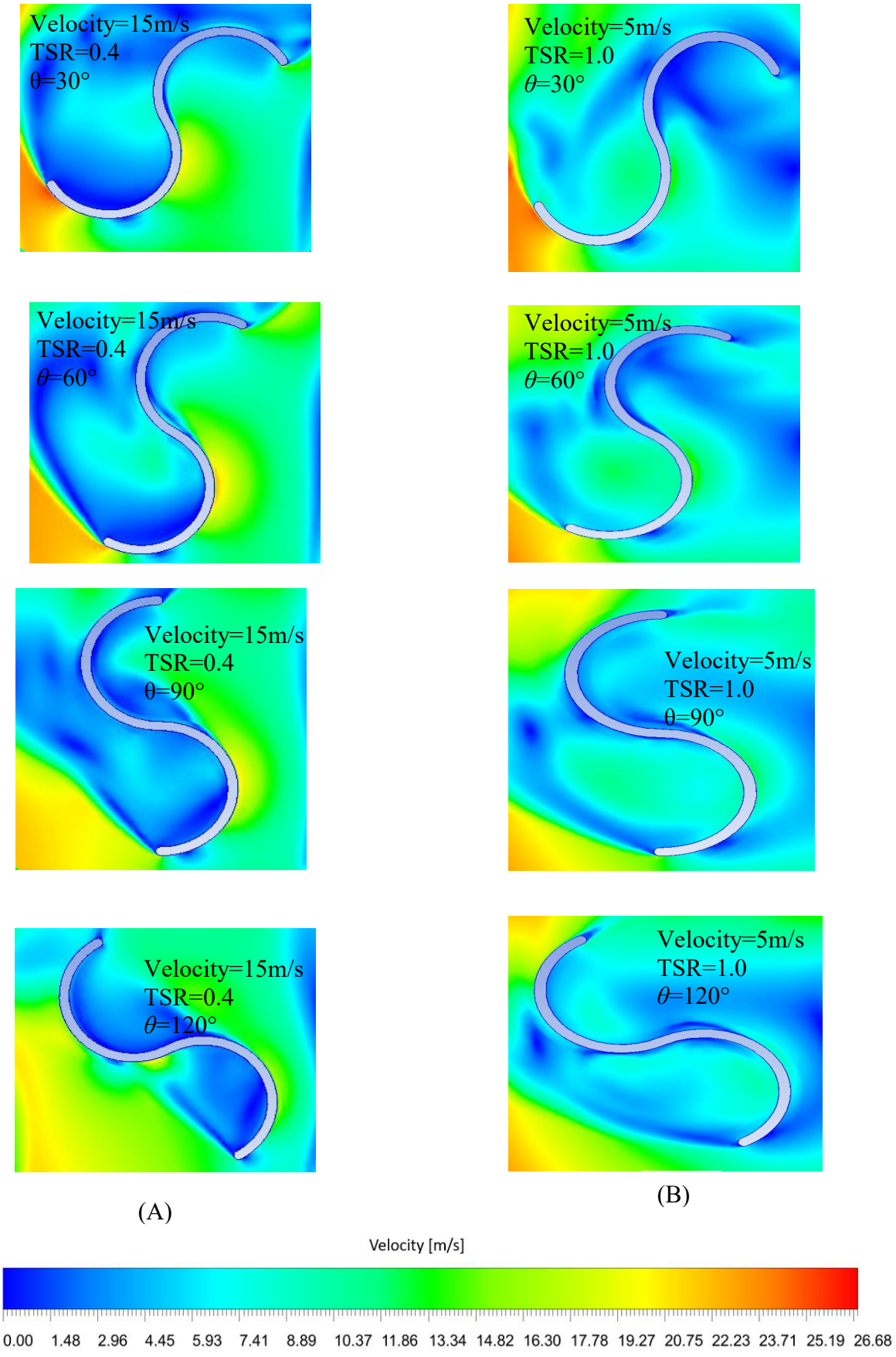

Figure 5.14: Velocity contour of Maximum (A) and Minimum (B) power coefficient

5.3.4 Pressure profile for Semi-elliptical Savonious VAWT

Figure 5.15(A) portrays the static pressure contour for the maximum power coefficient of the TSR 0.4 with the inlet wind velocity of 15m/s. Figure 5.15(B) shows the static pressure contour for the minimum power coefficient of the TSR 1.0 with the inlet wind velocity of 5m/s. Azimuthal angles of 30°,60°, 90° and 120° were taken from the final rotation of the numerical study.

High pressure on the concave sides and low pressure on the convex sides of the advancing blade. These pressure differences led to the increasing torque of the turbine until it reached the azimuthal angle of 90°. When the advancing blade reaches θ=120°, the blade then experiences low pressure on the concave side and higher pressure on the convex side. This then caused the entire turbine to face a negative torque causing the coefficient of power to decrease. At the near maximum coefficient of moment coefficient, θ=90°, there was a huge difference in the pressure magnitude of the convex side and the convex side of the advancing blade.

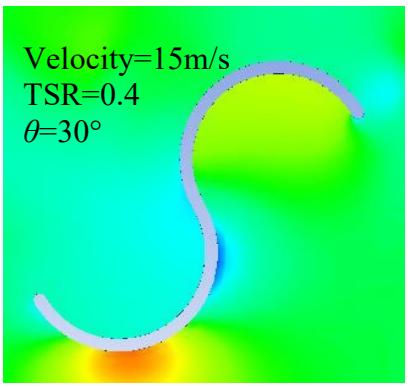

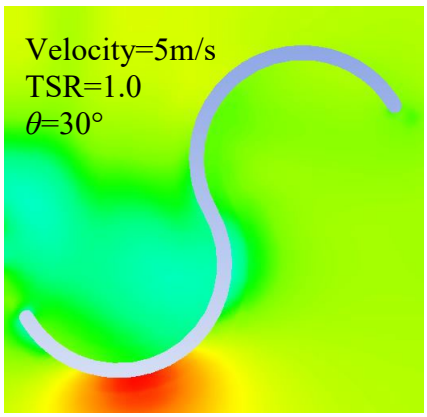

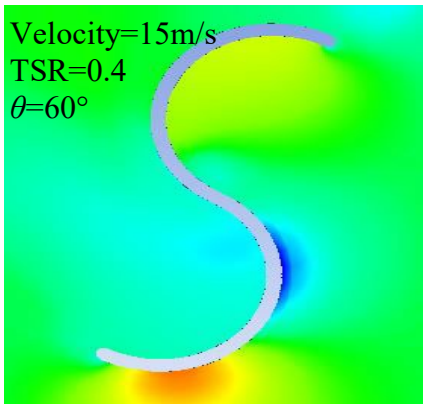

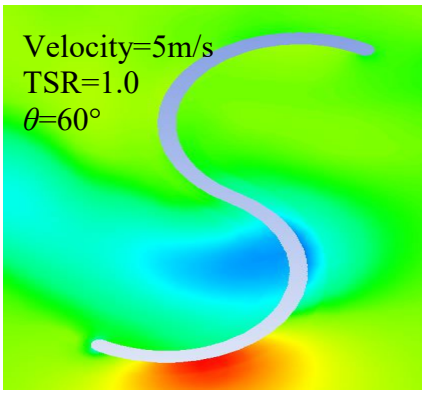

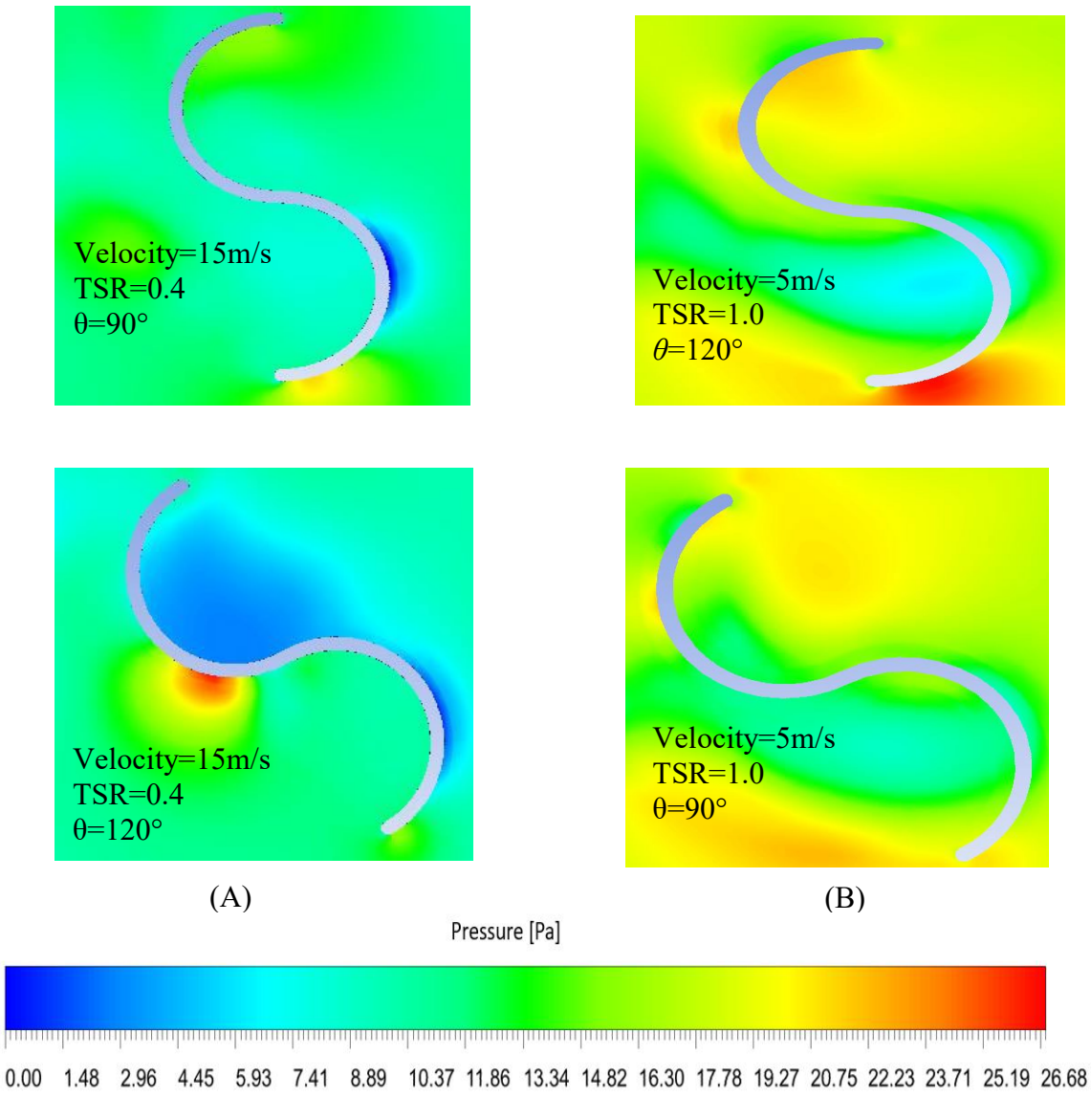

Figure 5.15: Pressure contour of Maximum (A) and Minimum (B) power coefficient

5.4 Numerical result for Helical Savonious VAWT

In this section, the Helical Savonious VAWT performance was analysed through studying the coefficient of moment and coefficient of power. The graphs of each coefficient of moment and the coefficient of power were plotted against the tip speed ratio of 0.4, 0.6, 0.8 and 1.0 respectively. Also, the velocity contour and the pressure contour are deployed to have a better visual of the flow around the turbine at the final rotation azimuthal angle of θ= 30°, 60°, 90° and 120°.

5.4.1 Coefficient of moment and power for Helical Savonious VAWT

Figure 5.16 shows the coefficient of moment of the helical savonious VAWT with the wind speed of 5m/s, 10m/s and 15m/s against the selected tip speed ratio for the study. Generally, the Helical Savonious VAWT performed best with the wind speed of 15m/s followed by the 10m/s and the 5m/s. The graphs of all the three-wind speeds exhibit the same behavior where the coefficient of moment decreased with the rise of the tip speed ratio from the lowest of 0.4 to the highest selected tip speed ratio of 1.0.

Furthermore, the tip speed ratio of 0.4 of all the three-wind speed had the maximum coefficient of moment. The wind speed of 15m/s with the tip speed ratio of 0.4 gave the greatest peak coefficient of moment, 0.1691. In addition, for the wind speed of 10m/s and 5m/s the peak coefficient of moment was 0.1434 and 0.1204 respectively.

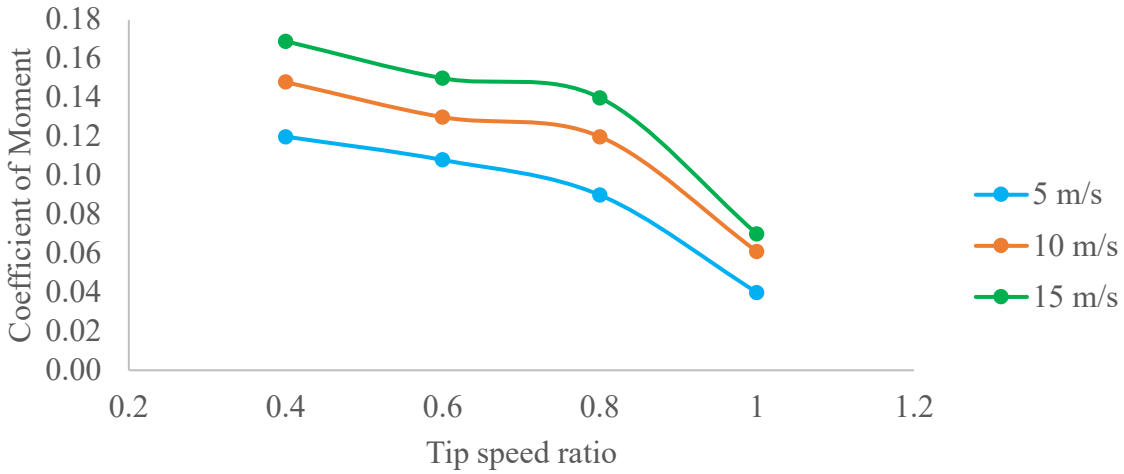

Figure 5.16: Coefficient of Moment for Helical Savonious VAWT at various wind speed

Additionally, Figure 5.17 present the graphs of the power coefficient of the Helical Savonious VAWT and it shows the wind speed of 15m/s had the highest coefficient of power as compared to the other two wind speed of 10m/s and 5m/s. A significant pattern was observed from the power coefficient curves when the tip speed ratio increases from 0.4 to 0.8, the power coefficient increases, and then from 0.8 to 1.0 tip speed ratio, the power coefficient decreases. All three wind speed curves showed the peak power coefficient was at the tip speed ratio of 0.8. The wind speed of

15m/s showed the greatest peak power coefficient of 0.1123 as compared to 0.0964 and 0.0722 was produced by the wind speed of 10m/s and 5m/s respectively.

This current simulation result was comparable to the study conducted by Lajnef et al. (2020). The study of Lajnef et al. (2020) was simulated with the same turbulence model of K-ω SST and was validated with wind tunnel tests. Their result showed at the tip speed ratio of 0.73, the maximum power coefficient of 0.124 was achieved. As their study tested on the wind speed of 10m/s and compared to the current study of with its application in the cooling tower, the results are very close and similar.

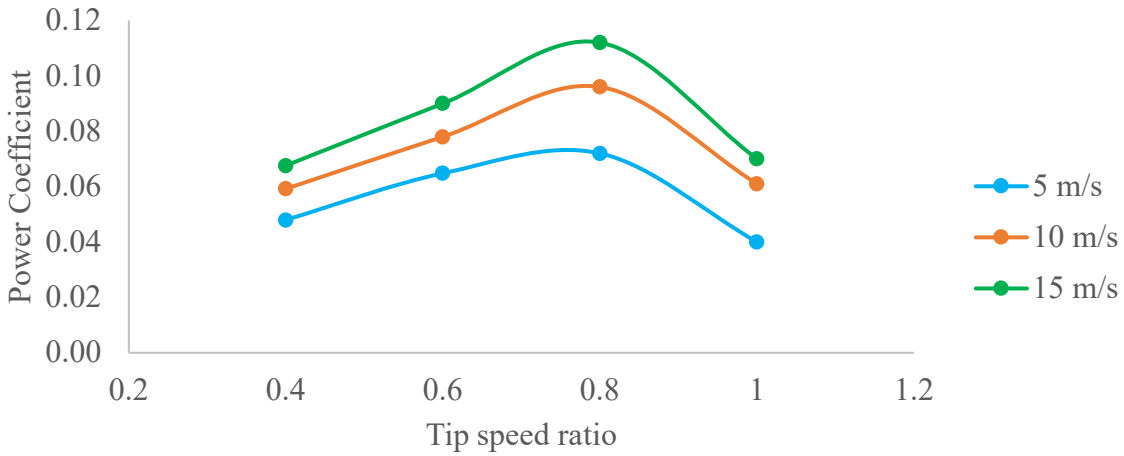

Figure 5.17: Coefficient of Moment for Helical Savonious VAWT at various wind speed

5.4.2 Instantaneous coefficient of moment for Helical Savonious VAWT

The maximum coefficient of moment and the minimum coefficient of moment are shown in Figure 5.18(A) and Figure 5.18(B). This is to underline the coefficient of moment at each angle of the final rotation in the numerical study.

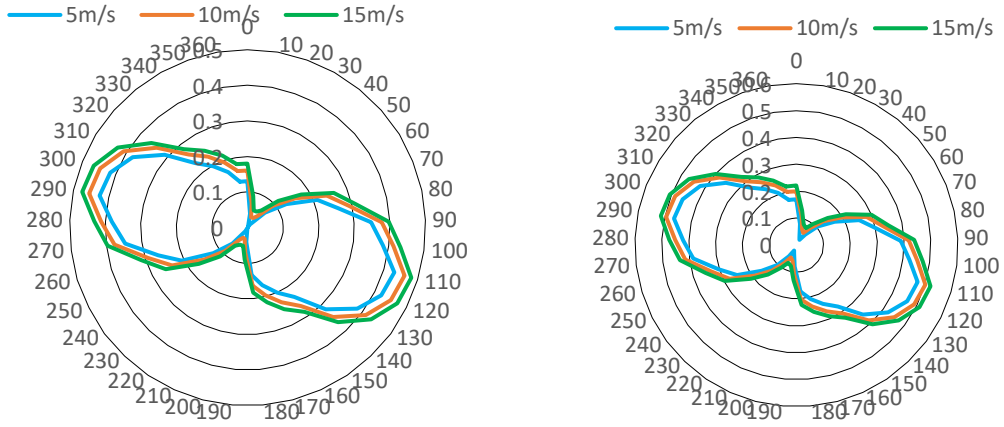

(A)TSR 0.4 (B)TSR 1.0

Figure 5.18: Graph of Instantaneous coefficient of moment (A) Maximum (B) Minimum

5.4.3 Velocity profile for Helical Savonious VAWT

Velocity profile of the Helical Savonious VAWT was extracted for the maximum and minimum coefficient of moment shown in Figure 5.19(A) and Figure 5.19(B). The azimuthal angles selected to portray the velocity profile are θ= 30°, 60°, 90° and 120° as the angles shows the maximum and minimum coefficient of moment.

Both maximum and minimum instantaneous coefficient of power show θ=30°, the coefficient of moment was the lowest and gradually increased until it approached 90°. However, between the range of 90° and 120°, it showed the maximum instantaneous coefficient of moment. This was mainly caused by the velocity difference between the convex side and the concave side of the approaching blade. At the 90° angle, the increase in velocity started to approach the surface of the convex side of the blade. Meanwhile, at a 120° angle, the high velocity of 21.24m/s flowed along the surface of the convex side with a low velocity of 1.02m/s on the concave side of the approaching blade. Due to the velocity difference, it created a drag force. As this turbine is in the Savonious VAWT family, it favored the drag force and is the major factor for the high coefficient of moment over the 90° and 120° angles.

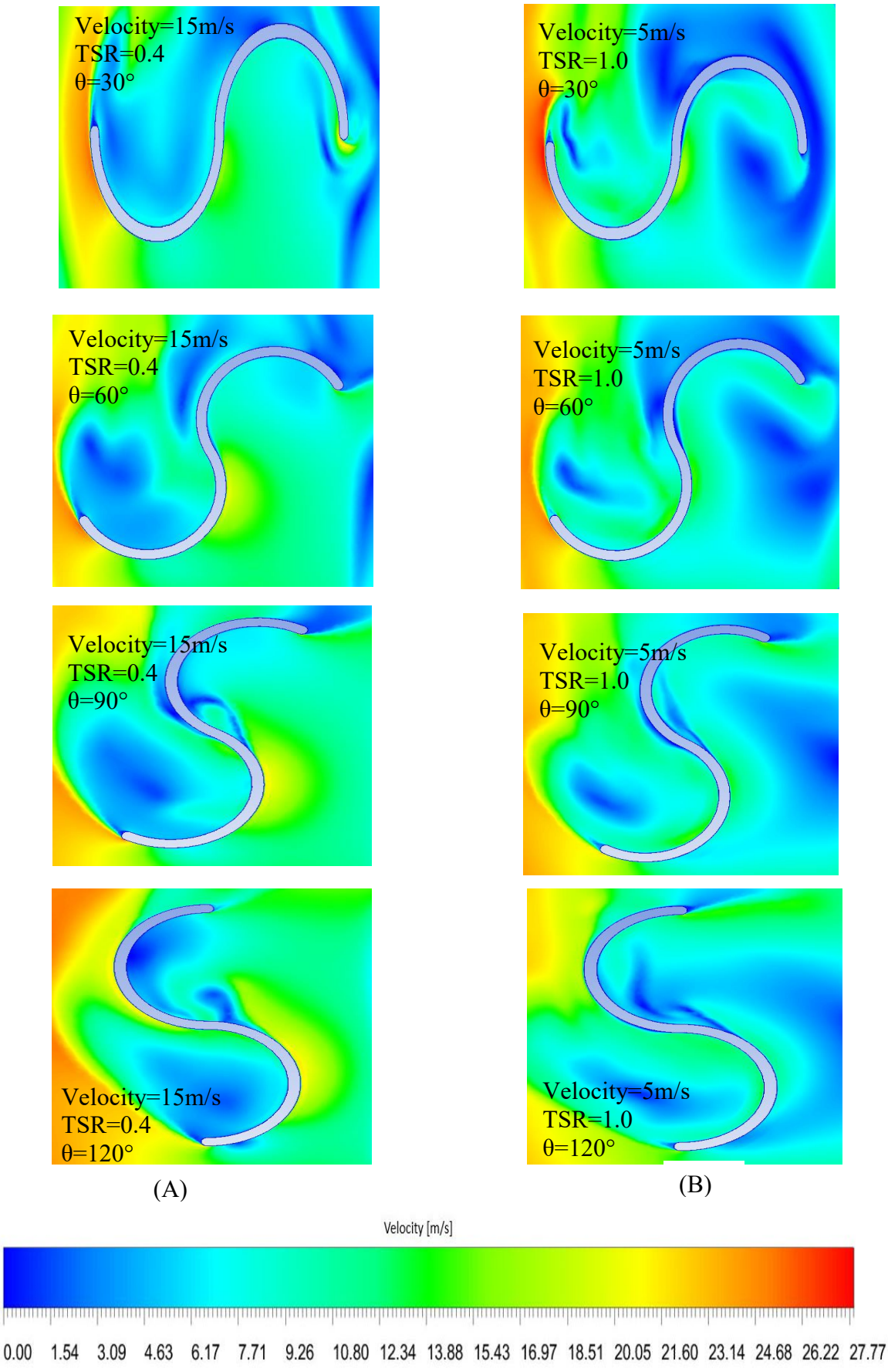

Figure 5.19: Velocity contour of Maximum (A) and Minimum (B) coefficient of moment

5.4.4 Pressure profile for Helical Savonious VAWT

In Figure 5.20(A), the pressure contour for the maximum coefficient of power at the TSR of 0.4 and inlet wind velocity o 15m/s. Also, Figure 5.20(B) shows the pressure contour for the minimum coefficient of power of TSR1.0 with the inlet wind velocity of 5m/s. Critical azimuthal angle, θ of 30°, 60°, 90° and 120°.

From 30° to 90° azimuthal angle, it was clear the concave side of the advancing blade has higher pressure as compared to the convex side of the blade. With this high-pressure difference between both faces of the blades, it increases the coefficient of moment for the turbine at the specific θ of 30° to 90°. As it approaches the 90°, the pressure difference slowly decreases and eventually the pressure differences are near zero as in the θ= 120°. However, at 90° it has more pressure difference as compared to the 120°.

The Savonious turbine favoured the drag force as its operating force. Thus, at higher pressure differences between the blades, the higher the overall coefficient of power. The maximum pressure difference between the concave and the convex face of the blades is approximately 85Pa. By comparing the maximum coefficient of moment pressure contour and the minimum coefficient of moment pressure contour, the pressure difference in the maximum coefficient of moment was far greater as compared to the minimum coefficient of moment pressure contour.

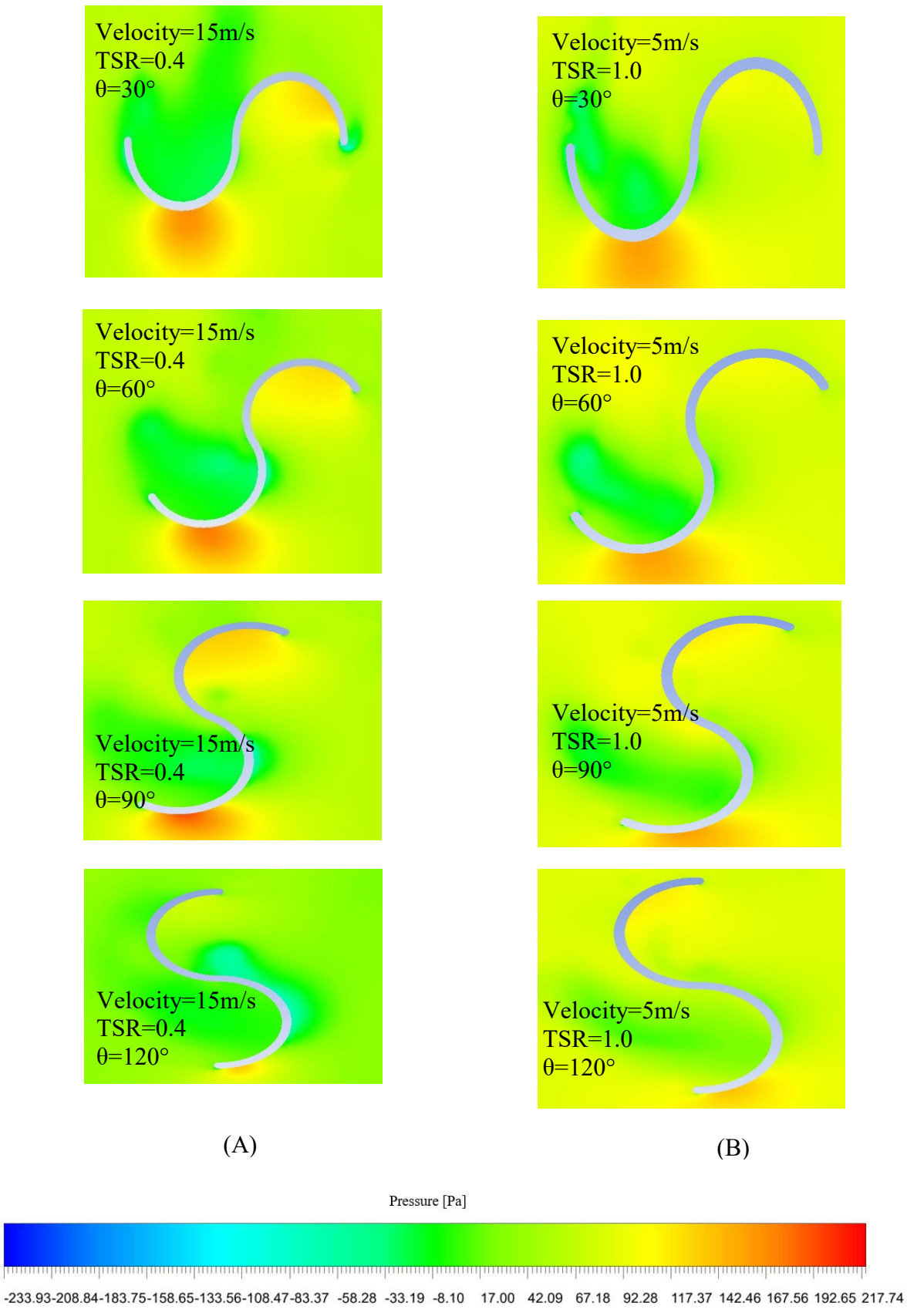

Figure 5.20: Pressure contour of Maximum (A) and Minimum (B) coefficient of moment

5.5 Coefficient of moment and power comparison of tested VAWT

This section will discuss the comparison of the four tested turbines the H-Darrieus VAWT, Helical Darrieus VAWT, Semi-elliptical Savonious VAWT and Helical Savonious VAWT. The maximum coefficient of moment and power graphs was shown in Figure 5.21 and Figure 5.22 respectively. All the results show the 15m/s inlet wind speed had the maximum coefficient of moment and power. Thus, the results from the 15m/s inlet wind speed are discussed in this chapter.

For the graph presented in Figure 5.21 on the coefficient of moment, it showed the semi-elliptical savonious VAWT had achieved the highest overall coefficient of moment at The TSR of 0.6. However, the lowest coefficient of moment presented was from the Helical Savonious at the tip speed ratio of 1.0. An obvious observation seen in this Figure was the Savonious group VAWT runs at a lower TSR while the Darrieus group VAWT performs better at the TSR ranging from 2.0 to 3.0 where the further increment of the TSE would also cause the Coefficient of moment of the VAWT to decrease drastically. For the Savonious group VAWT, it best performed in the low TSR of 0.4 to 0.6. The coefficient of moment for the Savonious VAWTs showed a similar result trend as compared to the study conducted by Torres et al. (2022). In addition, the Darrieus VAWTs coefficient of moment has similar trends to the study by Miliket, Ageze, and Tigabu (2022)

Furthermore, in Figure 5.22. the maximum power coefficient was seen on the H-Darrieus VAWT and the lowest power coefficient is from the Helical Savonious. On the maximum power coefficient curve, the TSR of 3.0 shows the maximum power coefficient of 0.39 for the H-Darrieus VAWT. However, for the minimum power coefficient portrayed in Figure 4.22, the lowest coefficient of power of 0.07 at the TSR of 1.0. The power coefficient graph of the Savonious VAWTs shows similar graph trends as compared to the study by Xu et al. (2022) and the Darrieus VAWTs portray the same trend as the study by Zhang et al. (2022). Thus from Figure 5.22, the turbine achieved a better power coefficient in the cooling tower application of the H-Darrieus with a maximum power coefficient of 0.39.

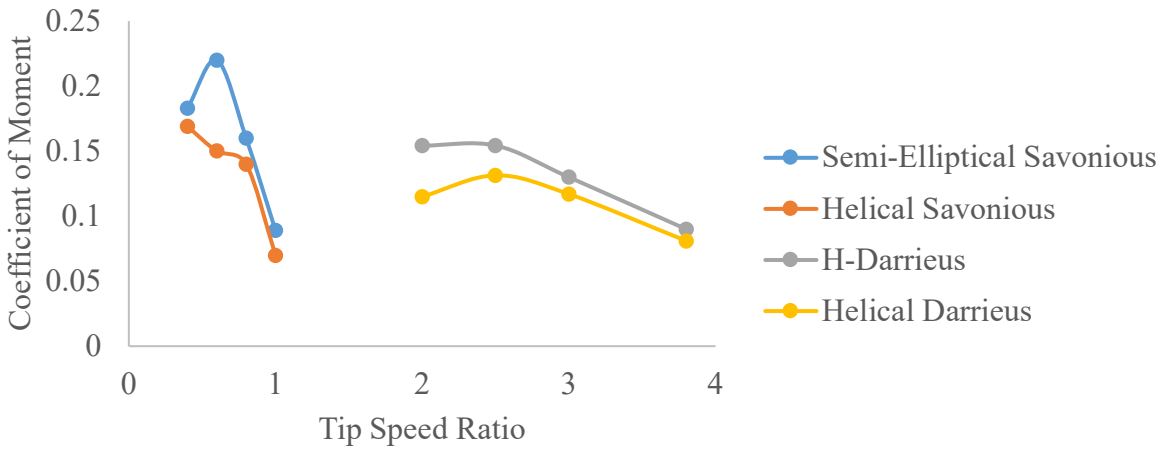

Figure 5.21: Coefficient of Moment comparison graph for the studied turbines.

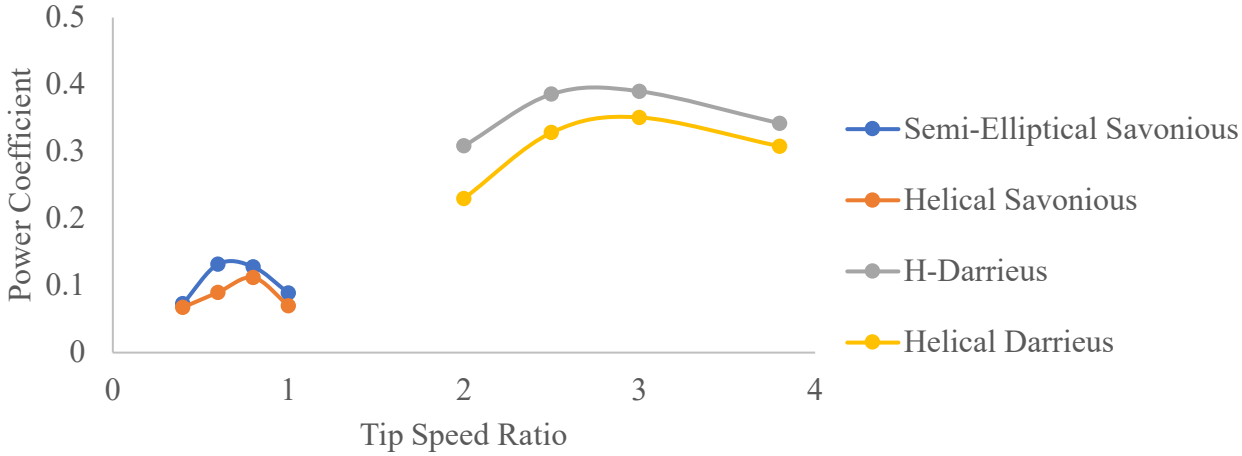

Figure 5.22: Coefficient of Power comparison graph for the studied turbines.

5.6 Further investigation on H-Darrieus and helical Darrieus VAWT

As the H-Darrieus and the helical darrieus VAWT show the maximum coefficient of power, it was selected to study its flow profile and aerodynamics. The instantaneous maximum coefficient of moment for the H-Darrieus and helical Darrieus VAWT was plotted and shown in Figure 5.29 from the results of the turbine operating at the TSR of 2.5 with the wind velocity of 15m/s. At the azimuthal angle of 30° and 60 °, it can be seen from both graph that it was in the maximum instantaneous coefficient of moment region. However, at azimuthal angle of 90° it was the lowest instantaneous coefficient of moment. For the azimuthal angle of 120°, it can be seen both turbines' instantaneous coefficient of moment is slowing increasing. Thus, the critical azimuthal angle of θ=30°, 60°, 90°, and 120° are selected and shown in Figure 5.23 (A) for H-

Darrieus and Figure 5.23 (B) for helical Darrieus. A single blade image was taken from the center of the turbine to further study the flow around the airfoil.

At the azimuthal angle of 30° and 60°, it can be seen the H-Darrieus had a faster wind velocity of 21m/s flowing through the outer surface as compared to the helical Darrieus only about 14.5m/s. At the azimuthal angle θ=90°, it can be seen that both the turbines' inner wall has an increase in wind velocity to 6m/s. The higher wind velocity was seen to be moving closer to the inner wall for booth turbines as compared to the azimuthal angle θ= 60°. However, at azimuthal angle θ=90°, it can be seen that the outer surface wind velocity is slowing down. It was noticeable at the trailing edge of the H-Darrieus that, high-velocity region was still present as compared to the helical Darrieus. For the helical Darrieus, the flow of the trailing edge is short mainly due to the turbulence caused by the blade region before and after the center region.

Due to the Bernoulli's principal, the outer surface of the turbine had lower pressure and the inner surface has higher pressure caused by the wind velocity. Therefore, the higher pressure in the inner surface causes a lift force, an important factor for the Darrieus VAWT. Thus, the H-Darrieus had a greater velocity difference and a greater pressure difference causing greater lift force. The greater lift force in the H-Darrieus as compared to the helical Darrieus caused the overall coefficient of moment for the H-Darrieus is greater than the helical Darrieus.

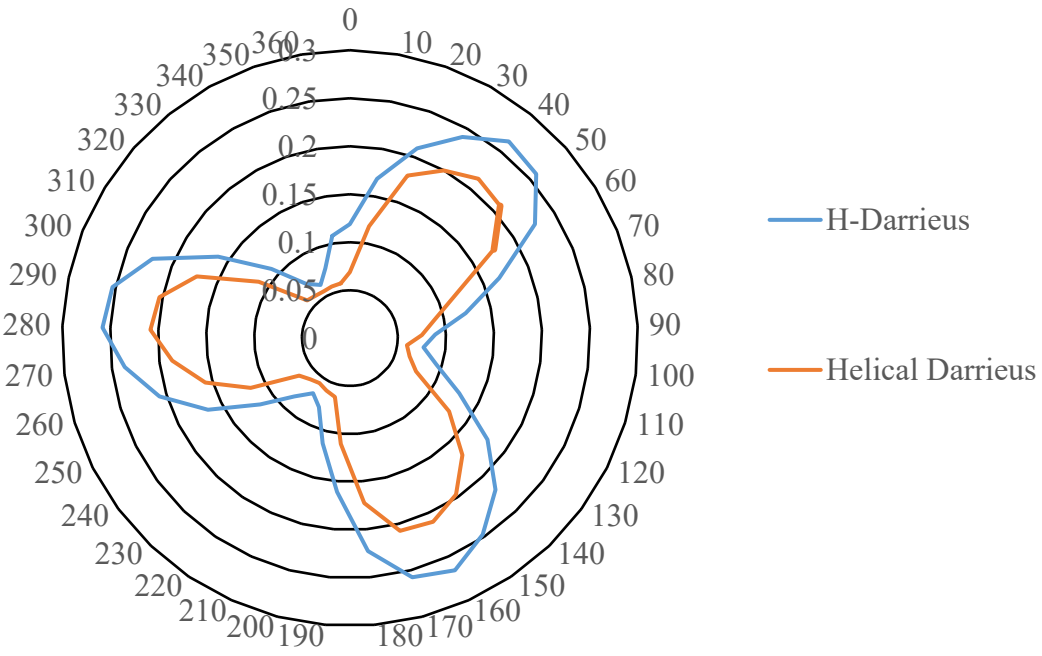

Figure 5.23: Instantaneous coefficient of moment for H-Darrieus and helical Darrieus at TSR2.5 and wind velocity of 15m/s

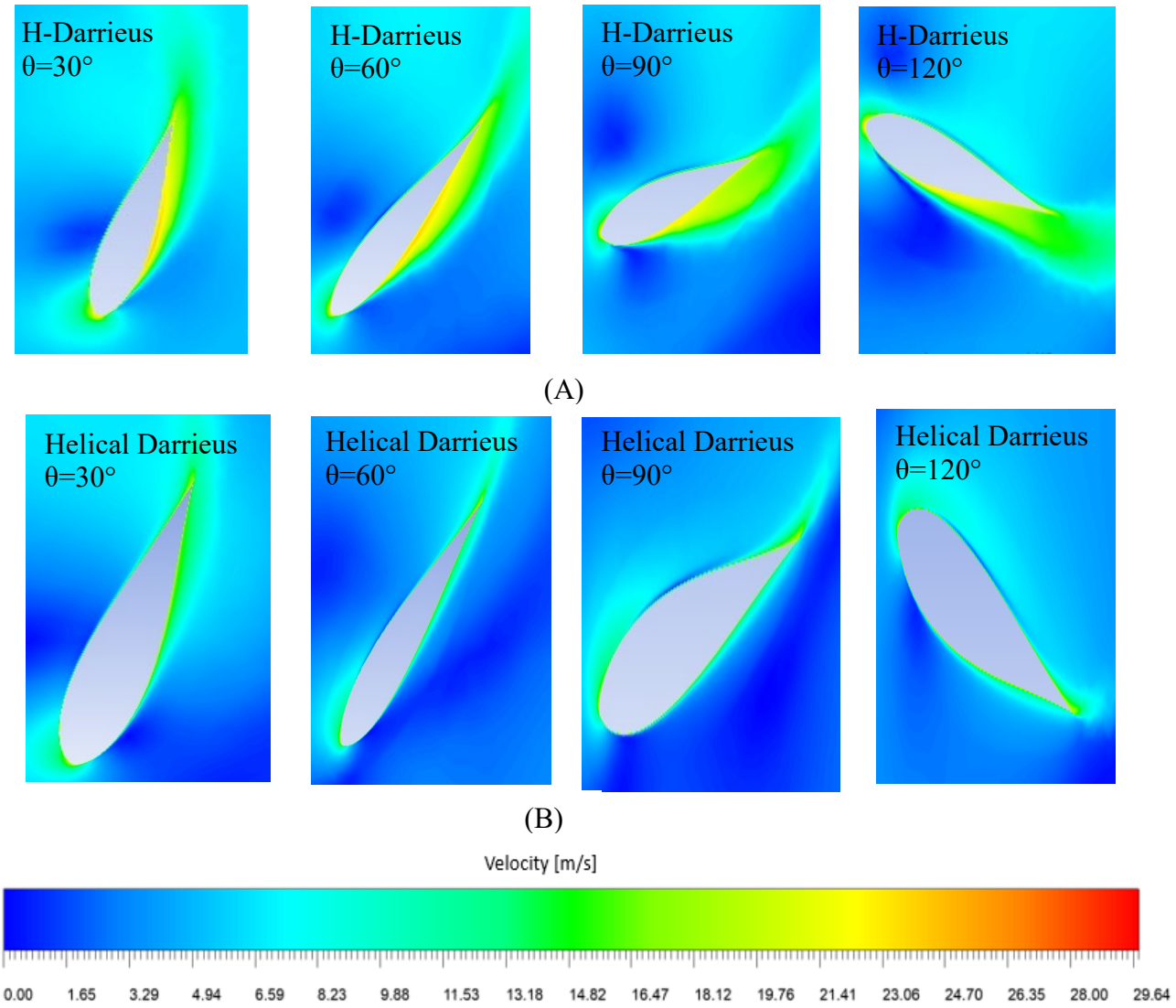

Figure 5.24: Zoom in single blade for (A) H-Darrieus VAWT and (B) Helical Darrieus VAWT

In addition, the aerodynamic performance of the H-Darrieus and helical darrieus was examined by obtaining the graph of coefficient of lift at the last rotation. This is shown in Figure 5.25. Lift generated by the turbine blade was important for the Darrieus type VAWT as it was a lift dependent VAWT. This determined the magnitude of the force making the turbine to rotate. It was shown from the azimuthal angle, θ=90° to 270°, the lift was lower in these regions. This was caused by the angle of attack of the turbine blades in this region was higher than the stall static angle. This condition then leads the turbine blades to experience stalling condition then causes a decrease in the lift coefficient.

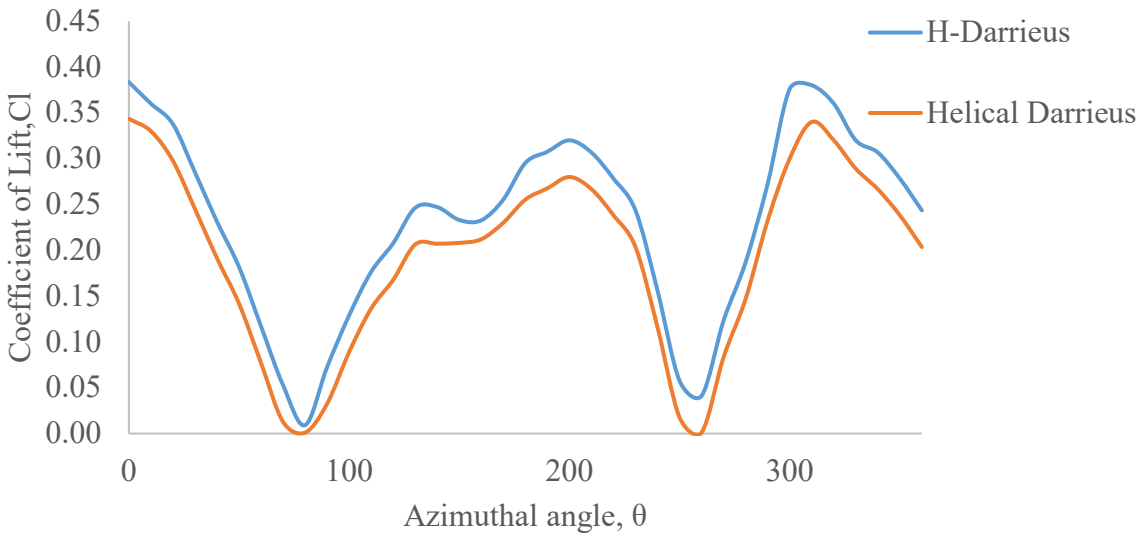

Figure 5.25: Graph of Coefficient of lift against azimuthal angle of last rotation

Additionally, the graph for the coefficient of drag against the azimuthal angle of the final rotation had also been plotted. This is shown in Figure 5.26. It was shown from the graph the H-Darrieus and the helical Darrieus portray almost similar graph characteristic. One major point is noted from the graph is at the azimuthal angle of 40°,180° and 280°. At all the three azimuthal angles, with reference to Figure 5.23, it was where the high coefficient of moment was located. Therefore, the low peak of the coefficient of drag will result in high coefficient of moment.

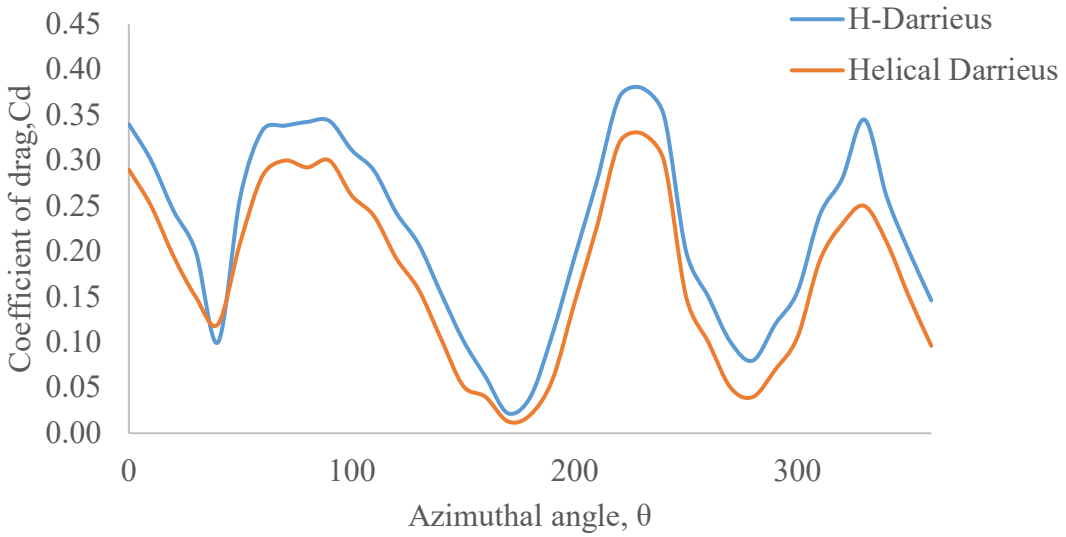

Figure 5.26: Graph of coefficient of drag against azimuthal angle of final rotation

5.7 Testing of H-Darrieus VAWT with altered airfoil

In this section, the H-Darrieus VAWT will be optimized by testing on the altered airfoil. The initial airfoil selected for the study above was the S-1046. However, in this chapter, the S-1048 and the S-1221 will be used. The results were taken from the wind speed of 10m/s inlet wind velocity and the TSR of 2.0, 2.5,3.0 and 3.8 respectively. The results would be discussed based on the coefficient of moment, coefficient of power, together with the velocity and pressure contour.

5.7.1 Coefficient of moment and power for the altered blade H-Darrieus.

Figure 5.27 it shows the coefficient of moment for the H-Darrieus VAWT with the blade configuration of S-1048, S-1221, and S-1046 airfoil profile respectively. Overall, the airfoil profiles of S-1046 and S-1048 portray similar behavior. As the TSR increases from 2 to 2.5, the coefficient of moment increases till its maximum point at TSR 2.5. After the TSR of 2.5, both airfoil profile decreases in coefficient of moment till it reaches the TSR of 3.8. The average difference between the coefficient of moment for the airfoil profile of S-1046 and S-1048 is 0.0112 or a 7.84% difference. However, for the airfoil S-1221, the graph characteristic behaves the same where the coefficient of moment increases from the TSR 2 to 2.5 and decreases from TSR 2.5 to 3.8. The major difference is the sudden increase of the coefficient of moment during the transition from the TSR of 2 to the TSR of 2.5. It shows an increment of 0.05661 from the TSR of 2 to 2.5.

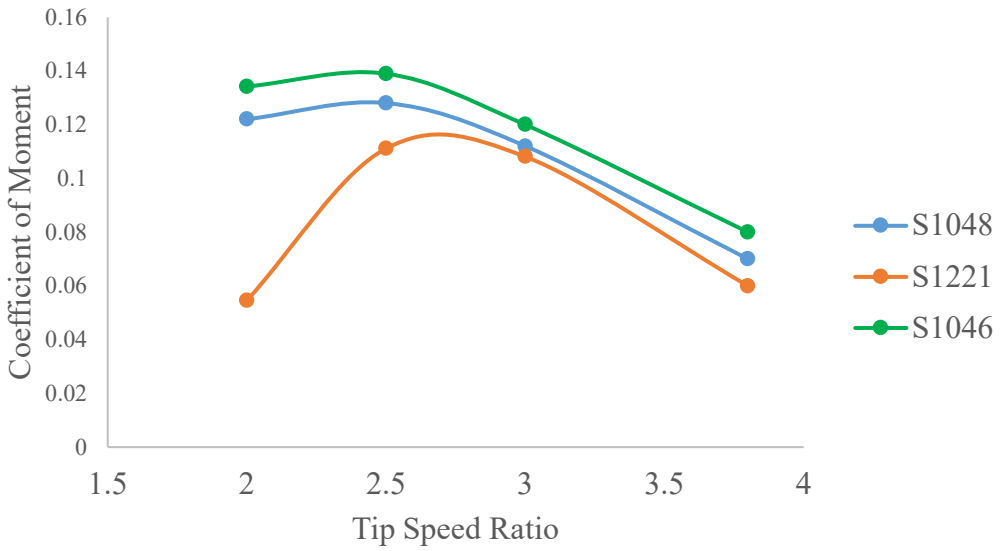

Figure 5.27: Coefficient of Moment comparison graph for altered airfoil profile.

In addition, Figure 5.28 shows the power coefficient of the studied airfoil configuration. It shows the S-1046 airfoil profile had the maximum power coefficient as compared to the S-1048 and the S-1221 airfoil profile. All three airfoil shows the same pattern where the power coefficient increases from the TSR 2 to 2.5 and then decreases as the TSR increase to 3.8. Also, all 3 airfoil profiles have the maximum power coefficient at the TSR of 3.0 and the lowest power coefficient at the TSR of 2. The highest power coefficient generated was from the S-1046 airfoil profile with a power coefficient of 0.359 at the TSR of 3 and the lowest power coefficient was obtained from the S-1221 airfoil profile at the TSR 2 with only 0.1092 as its power coefficient.

Another critical finding to highlight in this research was the airfoil with the similar camber and chord location would have similar graph shapes for both the coefficient of moment and power coefficient even with different maximum chord thickness. This was shown in the two airfoils of S1048 and S1046. Both these airfoils have the camber of 0.01 and its chord is located at the 0 chord. However, the only difference is the airfoils have maximum chord thickness of 0.48 and 0.46 for the airfoil S1048 and S1046 respectively.

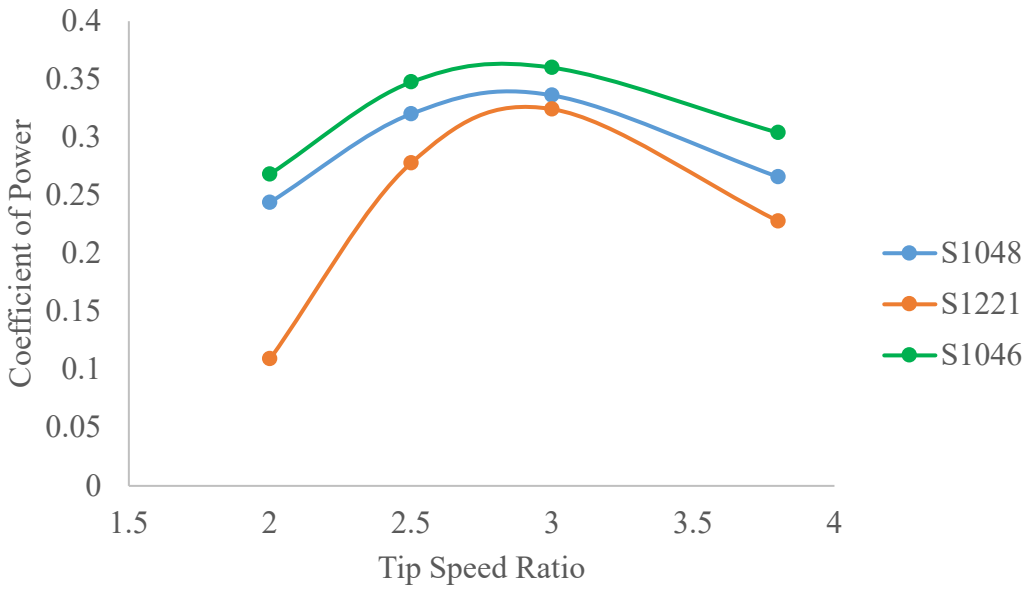

Figure 5.28:Coefficient of Power comparison graph for altered airfoil profile.

5.7.2 Velocity Contour for the altered blade H-Darrieus

In this chapter, the velocity profile of the altered blade H-Darrieus VAWT with the maximum and minimum coefficient of power is presented as shown in Figure 5.29(A) and Figure 5.29(B). The H-Darrieus VAWT selected is with the airfoil S1046 at the TSR of 2.5 for the maximum and the minimum coefficient of power is airfoil S1221 at the TSR of 2. The selected azimuthal angles to study the velocity contour are θ=30°, 60°, 90°, and 120° as these are the critical angles.

Focusing on the maximum power coefficient, it can be seen a higher concentration of high velocity is formed at the lower surface of the airfoils. As the high velocity is formed at the lower surface, the pressure decreases. In addition, the outer surface of the airfoil has lower velocity and thus has a higher pressure. This would then create a higher-pressure difference between the upper and lower surface of the airfoil and thus, increase the lift force generated. However, for the minimum power coefficient, the velocity profile shows minimal change in velocity through the upper and lower surfaces of the turbine.

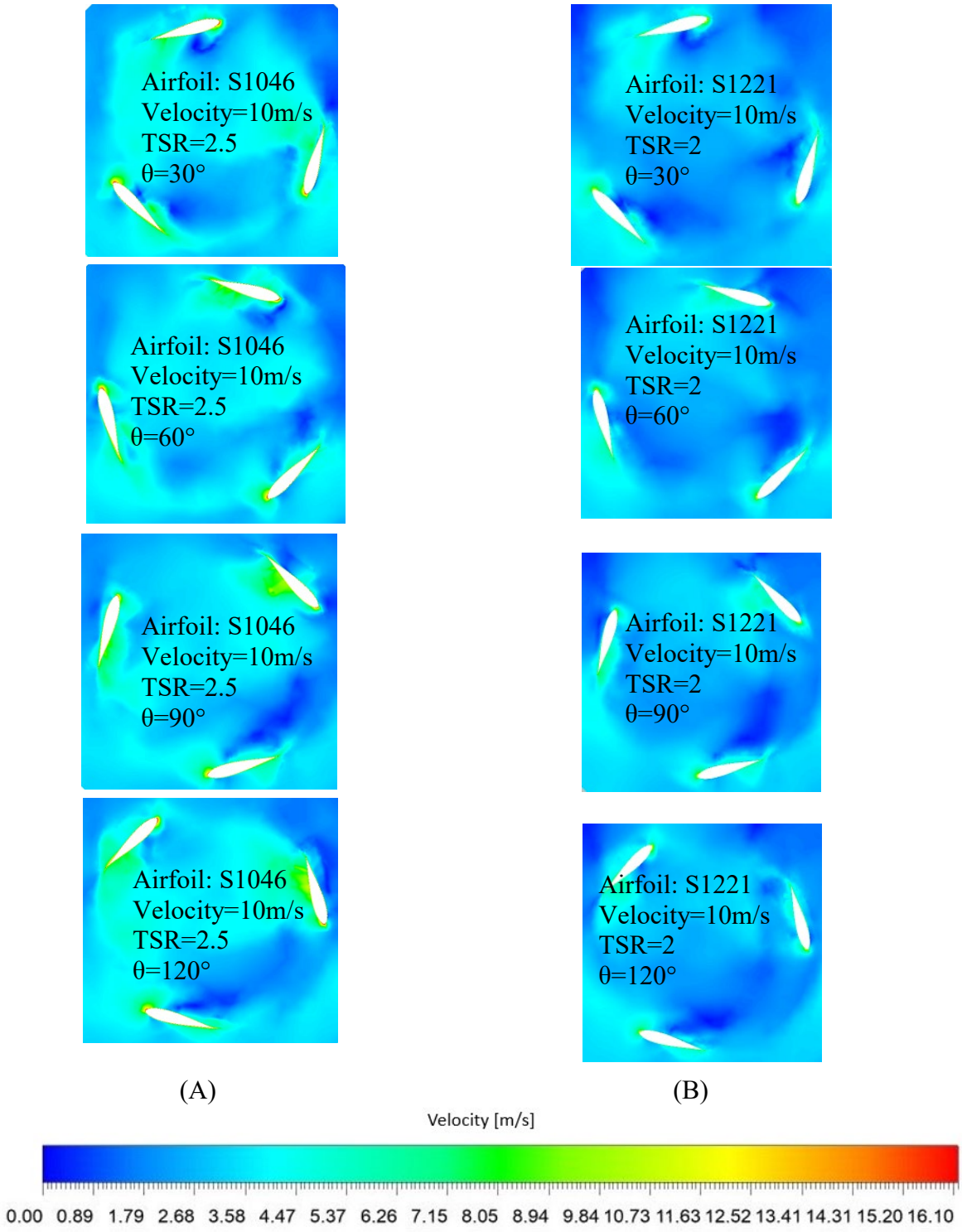

Figure 5.29: Velocity contour of Maximum (A) and Minimum (B) coefficient of moment

5.7.3 Pressure Contour for the altered blade H-Darrieus

To underline the reason of the maximum and minimum power coefficient of the H-Darrieus turbine with altered airfoil profile, the pressure contour was employed. Thus, Figure 5.30(A) and Figure 5.30(B) show the pressure contour for the maximum and minimum power coefficient respectively. The selected azimuthal angle for this part of the study would be θ=30°, 60°, 90° and 120°

The turbine in Figure 5.30(A) shows the maximum power coefficient because of the positive pressure combined with the lower pressure difference. Looking at the trailing edge of the airfoil at θ=30° and 60°, the pressure is approximately 11.01Pa while for the θ =90° and 120°, the pressure is 25.33Pa. Significantly, the pressure difference between the inner and outer surface of the airfoil is relatively small. This showed the airfoil experiences a lower drag -to-lift ratio.

In addition, Figure 5.30(B) shows the minimum power coefficient. It was shown that the trailing edge of the turbines is experiencing a higher pressure region as compared to the inner surface. This indicates a high drag force is being exerted on the blades. As these airfoils were lifted depending on the type of airfoil, drag force would be the factor causing the lower coefficient of power. Thus, with the higher drag-to-lift ratio, the aerodynamic performance of the turbine is highly affected causing the lower coefficient of power being generated by the turbines.

Figure 5.30: Pressure contour of Maximum (A) and Minimum (B) coefficient of moment

5.8 Experimental result

After selecting the most efficient VAWT the S1046 3-bladed configuration, the blade was printed out with a Creality Ender 3 V2 3D Printer with the Polylactic acid (PLA) material. The blade surface was smoothened out by sanding with sandpaper to reduce friction on the blade surface. The selected testing parameter is shown in table 5.1.

Table 5.1: Selected TSR and Wind velocity for experimental setting

Tip speed Ratio	Wind Velocity (m/s)
2.5	5
	10
3.8	5
	10

To achieve the selected TSR with the selected wind velocity, a pulley system with a spring balance was attached to one side of the rotating shaft to create friction to slow down the rotation to achieve the desired rotational speed. A tachometer was used to record the required revolution per minute of the rotating shaft. All the parameters to ensure the tested TSR was achieved are listed in table 5.2.

Table 5.2: Experimental rotation speed with respect to the TSR

Tip speed Ratio	Wind Velocity (m/s)	Rotational speed (rad/s)	Revolution per Minute
2.5	5	125	1193
	10	250	2387
3.8	5	190	1814
	10	380	3628

The result was obtained after one minute after the turbine starts to rotate. This is to ensure the stability of the wind speed effecting on the turbine. After one minute, the torque sensor is turned on and the results is obtained and plotted.

5.8.1 Torque obtained from experimental result

Figure 5.31 shows the result from the TSR 2.5 with the wind velocity of 5m/s. The highest torque achieved was 0.0138Nm. However, the lowest torque achieved was -0.0069Nm. The average torque achieved over the period of one minute was calculated to be 0.0031Nm. In addition, the Figure 5.32 exhibits the result of TSR 2.5 with the

wind velocity of 10m/s. The highest recorded torque was 0.92Nm and the lowest recorded torque was -0.46Nm. Thus, the average torque is 0. 0203Nm.The negative torque is due to the air loading on the surface of the turbine blades.

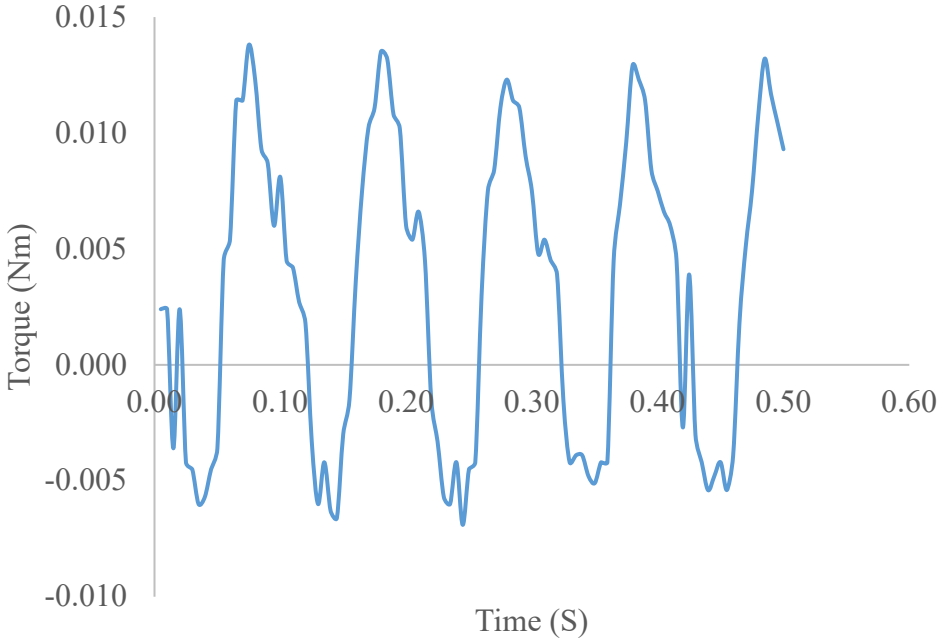

Figure 5.31: Graph of torque against time for TSR2.5, Wind velocity of 5m/s

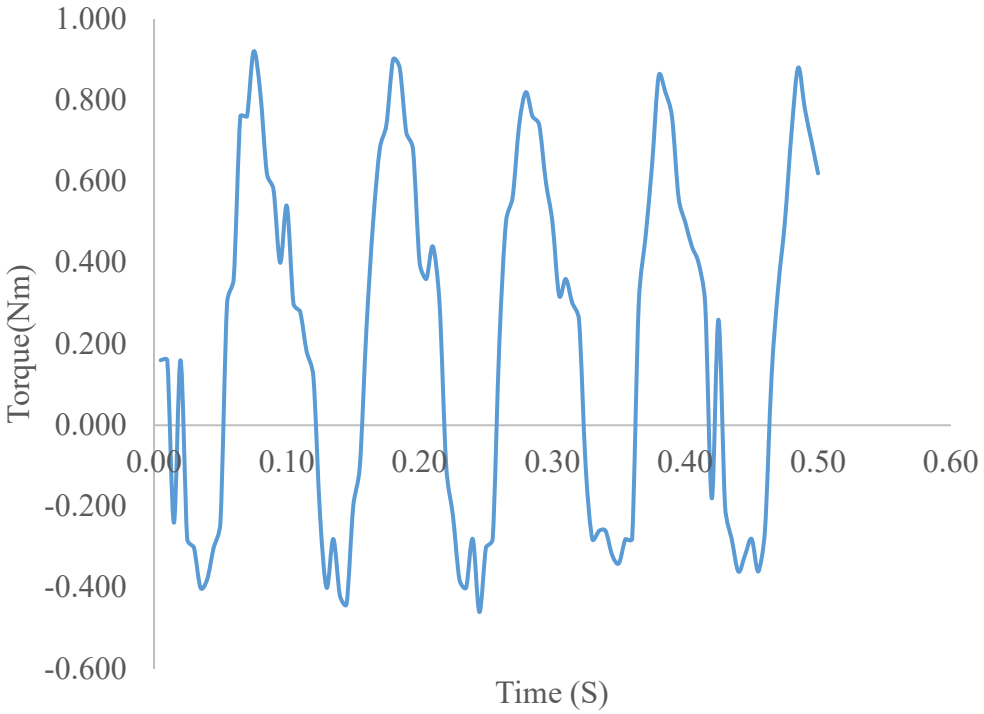

Figure 5.32: Graph of torque against time for TSR2.5, Wind velocity of 10m/s

Also, for TSR 3.8, the maximum torque of the wind velocity of 5m/s shown in Figure 5.33 is 0.005Nm. The minimum torque reported was -0.0018Nm. However, the average torque for the experimental period was 0.0014Nm. Figure 5.34 shows the result from the TSR 3.8 with the wind velocity of 10m/s. The highest torque was 0.46Nm and the lowest torque was -0.23Nm. The average torque obtained was 0.0110Nm. In addition, table 5.3 summarizes the average torque of each TSR with respect to its wind velocity. From the average torque in Table 5.3, it can be seen as the wind velocity doubles, the torque of the turbine increases by almost 7 times.

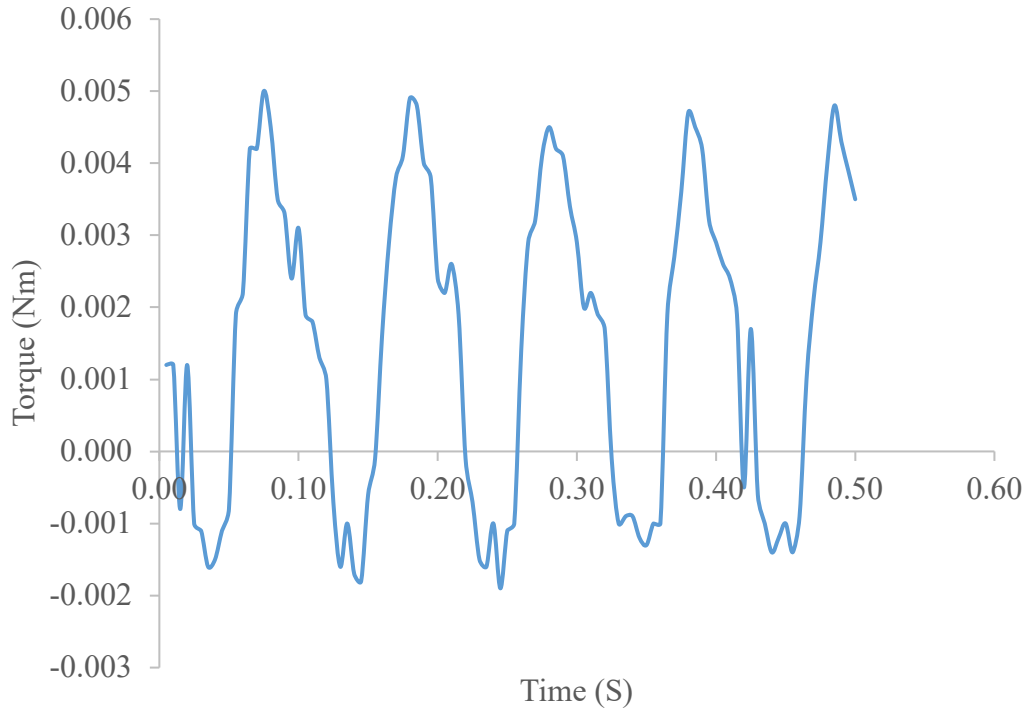

Figure 5.33: Graph of torque against time for TSR3.8, Wind velocity of 5m/s

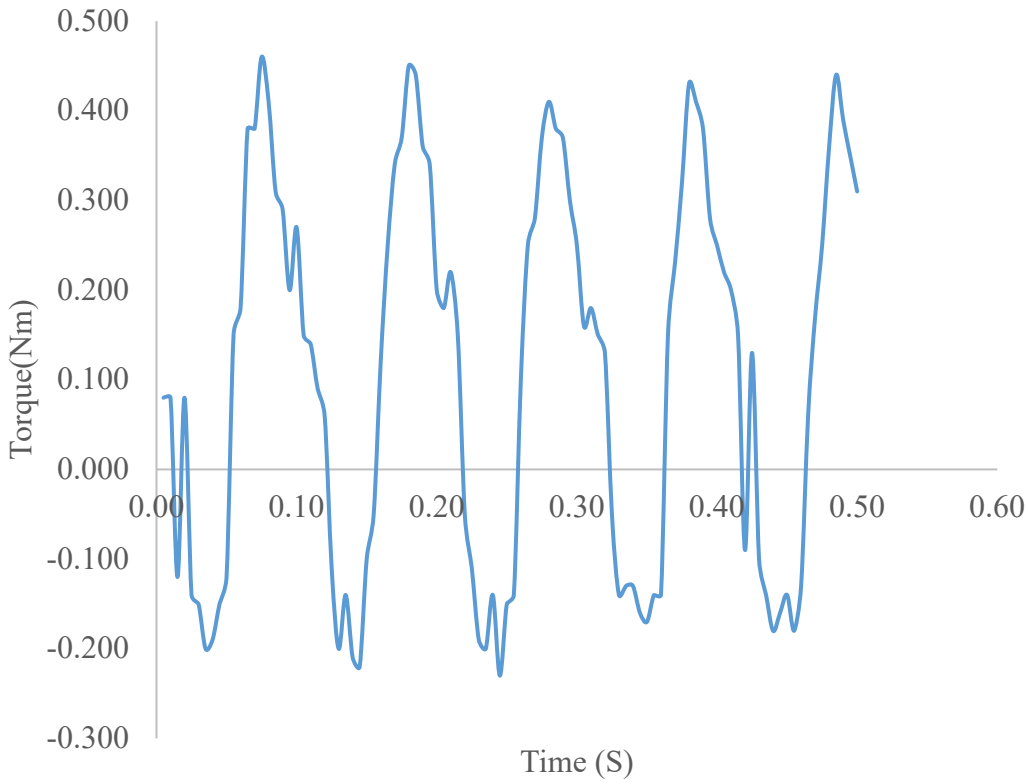

Figure 5.34: Graph of torque against time for TSR3.8, Wind velocity of 10m/s

Table 5.3: Average torque for all the selected experimental parameter

Tip speed Ratio	Wind Velocity (m/s)	Average Torque (Nm)
2.5	5	0.0031
	10	0.0203
3.8	5	0.0014
	10	0.0110

5.8.2 Coefficient of moment for experimental result

The torque obtained from Figure 5.31 to Figure 5.34 then used to calculate the Coefficient of moment with the equation 6,

$$C_m = \frac{2T}{\rho A R V_\infty^2} \quad (6)$$

Where,

ρ is the density of air equals to 1.225kg/m^3

A is the turbine swept area is πr^2=0.0314m^2

R is the radius of the turbine=0.1m

V∞ is the wind velocity for the selected wind speed.

The coefficient of moment for the TSR 2.5 with the wind velocity of 5m/s is portrayed in Figure 5.35. The maximum coefficient of moment achieved was 0.2869 and the minimum coefficient of moment that was recorded was -0.1435. The average coefficient of moment was calculated to be 0.0648. In addition, Figure 5.36 shows the coefficient of moment for the TSR 2.5 and the wind velocity of 10m/s. It achieved the highest coefficient of moment with 0.4781 and the lowest coefficient of moment with -0.2390. This gives an average coefficient of moment of 0.1054.

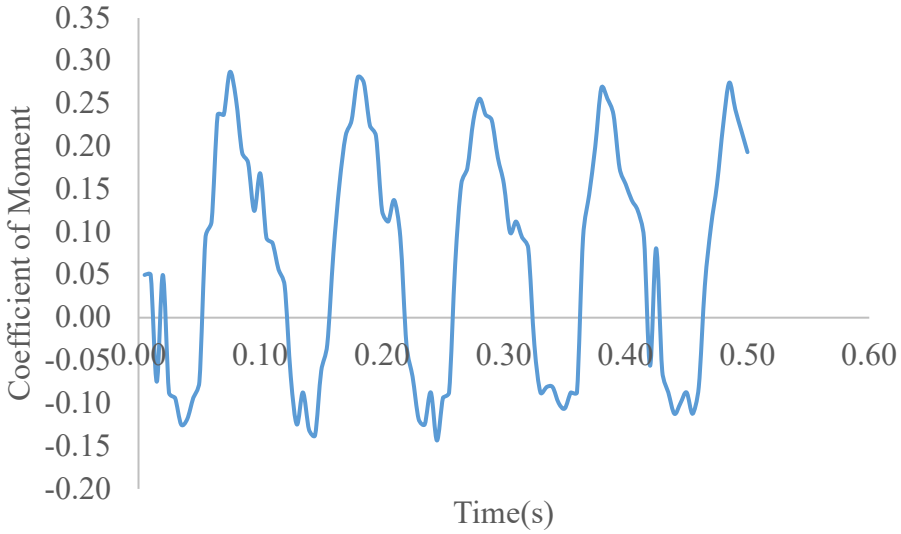

Figure 5.35: Graph of Coefficient of moment against time for TSR2.5, wind velocity of 5m/s

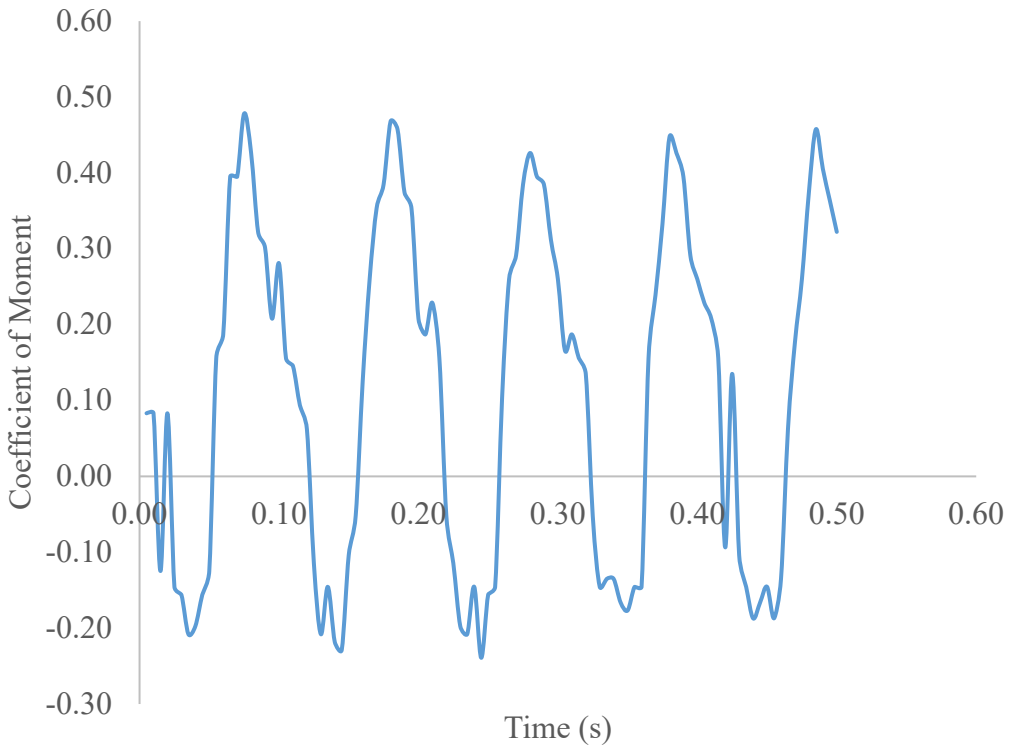

Figure 5.36: Graph of Coefficient of moment against time for TSR2.5, wind velocity of 10m/s

In addition, Figure 5.37 displays the coefficient of moment for the TSR 3.8 with the wind velocity of 5m/s. The minimum achieved coefficient of moment was -0.0395 and the maximum achieved coefficient of moment was 0.1040. The average coefficient of moment obtained was 0.0296. Furthermore, Figure 5.38 shows the coefficient of moment for the TSR 3.8 with the wind velocity of 10m/s. 0.2309 was achieved for the maximum coefficient of moment and -0.1195 was recorded for the minimum coefficient of moment. The average coefficient of moment obtained was 0.0572.

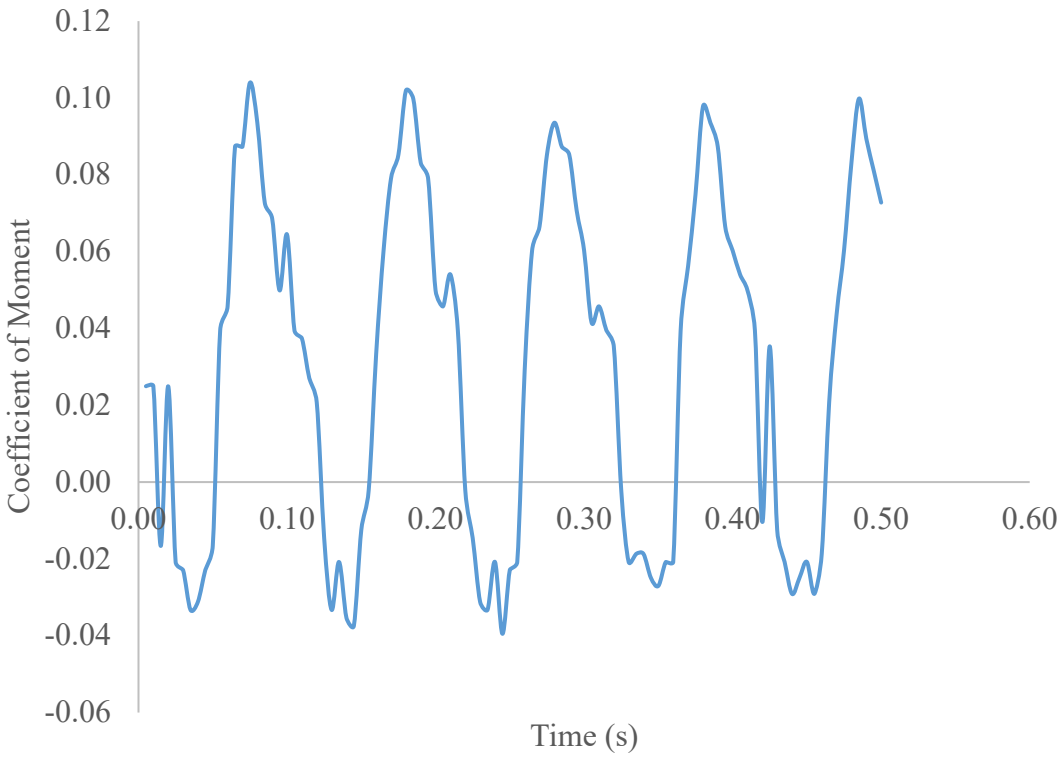

Figure 5.37: Graph of Coefficient of moment against time for TSR3.8, wind velocity of 5m/s

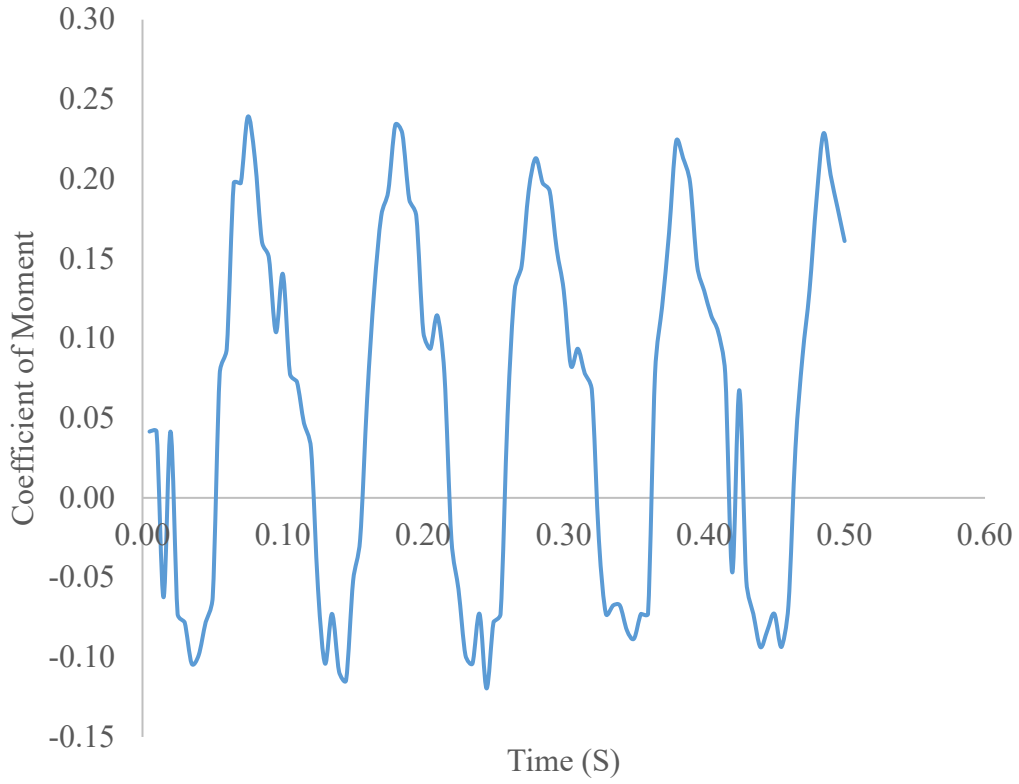

Figure 5.38: Graph of Coefficient of moment against time for TSR3.8, wind velocity of 10m/s

5.8.3 Power coefficient from experimental result

The average coefficient of moment was calculated and tabulated in table 5.4 for each of the TSR and wind velocity together with the average coefficient of power. From the average coefficient of moment and power coefficient obtained, a similar relationship was seen whereas the wind velocity doubles, the average coefficient of moment and power coefficient also increase by a multiply of two.

Table 5.4:Average coefficient of moment and power coefficient

Tip speed Ratio	Wind Velocity (m/s)	Average Coefficient of Moment	Average power coefficient
2.5	5	0.0648	0.1620
	10	0.1054	0.2635
3.8	5	0.0296	0.1125
	10	0.0572	0.2174

5.9 Comparison of Numerical and experimental results

The average numerical coefficient of moment and the average experimental coefficient of moment is tabulated in Table 5.5. The graph comparing the numerical and experimental results was plotted and shown in Figure 5.39. As the numerical and experimental results were compared, it was noticed the experimental results showed an average percentage error of 24.77%. These errors were the accumulative errors from the human error and the machine error. Some of the human errors were not avoidable from the production of the turbine when gluing the parts together. In addition, the machine errors were from the fluctuating wind speed produced by the fan of the cooling tower. Also, the small vibration from the fan in the cooling tower causes a minimal loss of power in the system. In general, the result obtained from the experimental study was acceptable due to the nature and behavior of the torque, and coefficient of moment graph is similar to the numerical study.

Table 5.5: Comparison of experimental and numerical coefficient of moment

Tip speed Ratio	Wind Velocity (m/s)	Average Experiment Coefficient of Moment	Average Numerical Coefficient of Moment
2.5	5	0.0648	0.0815
	10	0.1054	0.1389
3.8	5	0.0296	0.04
	10	0.0572	0.08

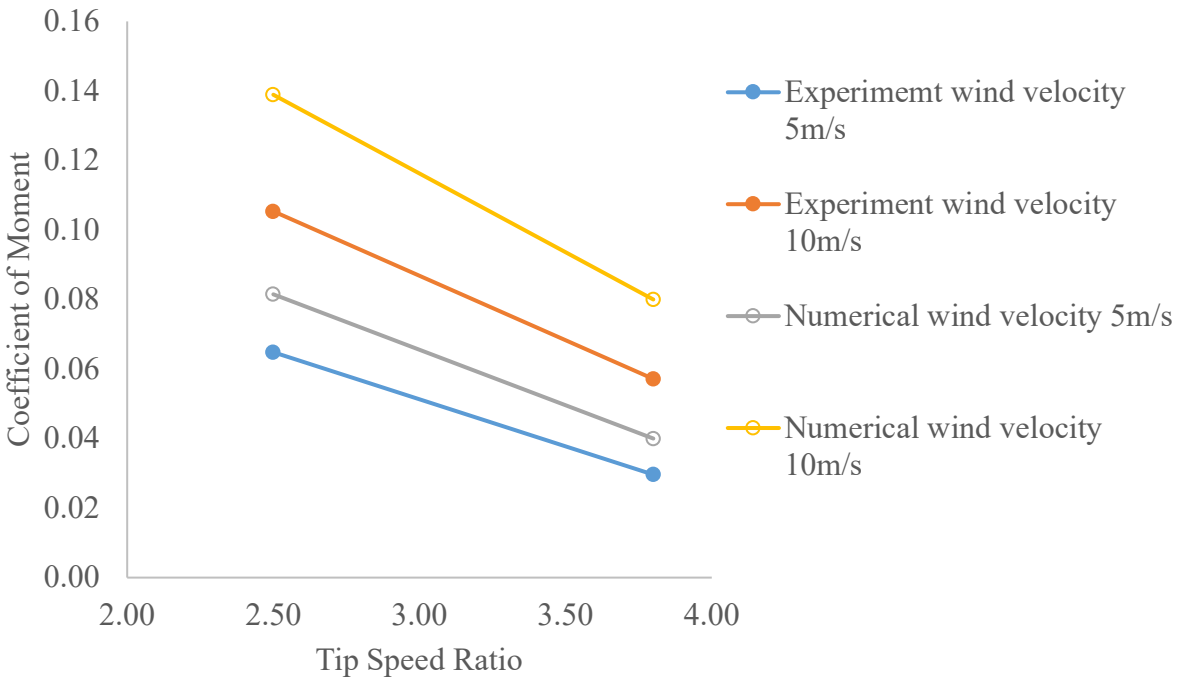

Figure 5.39: Comparison graph of numerical and experimental results

CHAPTER 6: CONCLUSION AND RECOMMENDATION

6.1 Conclusion

The air energy extractor using the vertical axis wind turbine of the H-Darrieus VAWT (S1046 airfoil profile), helical Darrius VAWT, Semi- -elliptical Savonious VAWT, and helical Savonious VAWT had been investigated. The velocity and the pressure contour surrounding the turbine blades an important parameters to determine the performance of the turbine blades. The H-Darrieus VAWT with the S1046 airfoil profile showed the largest velocity and pressure difference at the inner and outer walls of the turbine blade. It was also noticeable the inner surface of the S1046 airfoil has higher pressure as compared to the outer surface. With this pressure difference, it creates a lift force favorable to the H-Darrieus VAWT. However, the Semi-elliptical Savonious VAWT, had a better start-up time as compared to the other selected VAWT. This is due to the concave shape of the turbine blades which capture the wind energy at a lower wind speed as compared to the other VAWTs.

The numerical results of the four selected VAWTs (H-Darrieus VAWT, helical Darrieus VAWT, Semi- elliptical Savonious VAWT, and helical Savonious VAWT) in the air energy extractor gave a maximum power coefficient of 36.11%,32.41% 13.20% and 9.60% respectively. In addition, the Darrieus type VAWT performed best at the higher TSR ranging from 2 to 3. In addition, as the wind velocity for the output of the cooling tower increases, the coefficient of moment and power increases. For every increment of 5m/s in wind velocity, the coefficient of moment and power increase approximately 1.5 times. The low efficiency of the air energy extractor was found in the case of the Savonious VAWT. This is because they have a high drag-to-lift ratio as compared to the Darrieus VAWT.

The optimization of the blade with altered airfoil profile (S1046, S1048, and S1221) was conducted. The S1046 airfoil profile was the chosen airfoil profile for its optimum balance between the lift and drag ratio. The maximum power coefficient achieved for the S1046, S1048, and S1221 airfoil profiles are 36.11%, 33.61%, and 32.43% respectively. It was also seen the S1046 airfoil profile had slower flow separation at the trailing edge shown in the velocity and pressure contour.

In the experimental study, a cooling tower was set up to investigate the optimized energy extractor design the experimental results show a 24.77 % difference as compared to the numerical study. The 3D printed VAWT tested on the cooling tower shows a maximum power coefficient of 16.21% and 26.34% for the TSR of 2.5 and wind velocity of 5m/s and 10m/s. Also, the maximum power coefficient for the tested TSR of 3.8 was 11.26% and 21.72% for 5m/s and 10m/s wind velocity respectively.

6.2 Recommendation

Derived from this work and the available literature, the following recommendations were envisaged to be able to provide further opportunities in this research area.

1. The turbulence modeling techniques such as Large Eddy Simulation (LES) or Detached Eddy Simulations (DES) are highly recommended to further investigate the turbulence structure.
2. The different distances of the VAWT and the cooling tower outlet in the cooling tower application.
3. Further optimization of the VAWT with various types of surfaces of the turbine blades, for example, dotted or slitted surfaces.
4. Application of airfoiled arms of the VAWT would aid in the increase of the lift force for the Darrieus type VAWT.
5. The turbine blades are to be connected to the arms with diverse pitch angles. This will aid in finding the optimum angle of attack to increase the overall performance.
6. Combining the Savonious VAWT and the Darrieus VAWT into the same configuration. This is to leverage the better self-starting capability of the Savonious VAWT and the high performance of the Darrieus VAWT.
7. For the experimental test, it is recommended other printing materials are used such as Acrylonitrile butadiene styrene (ABS) or Polyethylene terephthalate glycol (PETG). ABS and PETG have distinctive mechanical properties as compared to PLA.
8. The testing of the air energy extractor is to be conducted on a full-scale cooling tower to increase the accuracy of the outcome.

REFERENCES

Abdullah, Wan Syakirah Wan, Miszaina Osman, Mohd Zainal Abidin Ab Kadir, and Renuga Verayiah. 2019. "The potential and status of renewable energy development in Malaysia." *Energies* no. 12 (12):2437.

Ali, Sajid, Sang-Moon Lee, and Choon-Man Jang. 2018. "Effects of instantaneous tangential velocity on the aerodynamic performance of an H-Darrieus wind turbine." *Energy Conversion and Management* no. 171:1322-1338.

Anwar, Khairil, Syukri Himran, Luther Sule, Nasruddin %J Journal of Mechanical Engineering Research Azis, and Developments. 2018. "Numerical Investigation Of Modified Savonius Wind Turbine with Various Straight Blade Angle." no. 41 (3):38-42.

Armstrong, Shawn, Andrzej Fiedler, and Stephen %J Renewable Energy Tullis. 2012. "Flow separation on a high Reynolds number, high solidity vertical axis wind turbine with straight and canted blades and canted blades with fences." no. 41:13-22.

Asnaghi, Abolfazl, Urban Svennberg, and Rickard E Bensow. 2019. "Evaluation of curvature correction methods for tip vortex prediction in SST k− ω turbulence model framework." *International Journal of Heat and Fluid Flow* no. 75:135-152.

Borhanazad, H, S Mekhilef, R Saidur, and G Boroumandjazi. 2013. "Potential application of renewable energy for rural electrification in Malaysia." *Renewable energy* no. 59:210-219.

Castelli, Marco Raciti, and Ernesto Benini. 2012. "Effect of blade inclination angle on a Darrieus wind turbine." *Journal of turbomachinery* no. 134 (3).

Castelli, Marco Raciti, Alessandro Englaro, and Ernesto Benini. 2011. "The Darrieus wind turbine: Proposal for a new performance prediction model based on CFD." *Energy* no. 36 (8):4919-4934.

Chan, Chun Man, HL Bai, and DQ He. 2018. "Blade shape optimization of the Savonius wind turbine using a genetic algorithm." *Applied energy* no. 213:148-157.

Chong, Wen Tong, SY Yip, A Fazlizan, Sin Chew Poh, Wooi Ping Hew, Ee Peng Tan, and TS %J Renewable energy Lim. 2014. "Design of an exhaust air energy recovery wind turbine generator for energy conservation in commercial buildings." no. 67:252-256.

Chong, WT, WP Hew, SY Yip, A Fazlizan, SC Poh, CJ Tan, HC %J Energy conversion Ong, and management. 2014. "The experimental study on the wind turbine's guide-vanes and diffuser of an exhaust air energy recovery system integrated with the cooling tower." no. 87:145-155.

Chong, WT, SC Poh, A Fazlizan, SY Yip, CK Chang, and WP %J Applied energy Hew. 2013. "Early development of an energy recovery wind turbine generator for exhaust air system." no. 112:568-575.

Emmanuel, Binyet, and Wang Jun. 2011. "Numerical study of a six-bladed Savonius wind turbine." *Journal of Solar Energy Engineering* no. 133 (4).

Fazlizan, Ahmad, Wen Tong Chong, Sook Yee Yip, Sin Chew Poh, Wan Khairul %J International Journal of Precision Engineering Muzammil, and Manufacturing-Green Technology. 2017. "Double multiple stream tube analysis of non-uniform wind stream of exhaust air energy recovery turbine generator." no. 4 (4):401-407.

Fazlizan, Ahmad, Wen Chong, Sook Yip, Wooi Hew, and Sin %J Energies Poh. 2015. "Design and experimental analysis of an exhaust air energy recovery wind turbine generator." no. 8 (7):6566-6584.

Haddad, Hassan Z, Mohamed H Mohamed, Yasser M Shabana, and Khairy Elsayed. 2023. "Optimization of Savonius wind turbine with additional blades by surrogate model using artificial neural networks." *Energy* no. 270:126952.

Hashem, I, and MH %J Energy Mohamed. 2018. "Aerodynamic performance enhancements of H-rotor Darrieus wind turbine." no. 142:531-545.
Irabu, Kunio, and Jitendro Nath Roy. 2007. "Characteristics of wind power on Savonius rotor using a guide-box tunnel." *Experimental thermal and fluid science* no. 32 (2):580-586.
Kumar, Rakesh, Kaamran Raahemifar, Alan S %J Renewable Fung, and Sustainable Energy Reviews. 2018. "A critical review of vertical axis wind turbines for urban applications." no. 89:281-291.
Lajnef, Mariem, Mabrouk Mosbahi, Youssef Chouaibi, and Zied Driss. 2020. "Performance Improvement in a Helical Savonius Wind Rotor." *Arabian Journal for Science and Engineering* no. 45 (11):9305-9323.
Lee, Jae-Hoon, Young-Tae Lee, and Hee-Chang %J Renewable Energy Lim. 2016. "Effect of twist angle on the performance of Savonius wind turbine." no. 89:231-244.
Li, Qing'an, Takao Maeda, Yasunari Kamada, Junsuke Murata, Kazuma Furukawa, and Masayuki %J Energy Yamamoto. 2015. "Effect of number of blades on aerodynamic forces on a straight-bladed Vertical Axis Wind Turbine." no. 90:784-795.
Liu, Zhenqing, Chong Zhang, and Takeshi Ishihara. 2018. "Numerical study of the wind loads on a cooling tower by a stationary tornado-like vortex through LES." *Journal of Fluids and Structures* no. 81:656-672.
Ma, Ning, Hang Lei, Zhaolong Han, Dai Zhou, Yan Bao, Kai Zhang, Lei Zhou, and Caiyong %J Energy Chen. 2018. "Airfoil optimization to improve power performance of a high-solidity vertical axis wind turbine at a moderate tip speed ratio." no. 150:236-252.
Mahmoud, NH, AA El-Haroun, E Wahba, and MH Nasef. 2012. "An experimental study on improvement of Savonius rotor performance." *Alexandria Engineering Journal* no. 51 (1):19-25.
Mehrpooya, Mehdi, Mohammadreza Asadbeigi, Farzad Ghafoorian, and Shayan Farajyar. 2023. "Investigation and Optimization on Effective Parameters of a H-rotor Darrieus Wind Turbine, Using CFD Method." *Iranian Journal of Chemistry and Chemical Engineering*.
Miliket, Temesgen Abriham, Mesfin Belayneh Ageze, and Muluken Temesgen Tigabu. 2022. "Aerodynamic performance enhancement and computational methods for H-Darrieus vertical axis wind turbines." *International Journal of Green Energy*:1-38.
Oerlemans, Stefan, Pieter Sijtsma, B Méndez %J Journal of sound López, and vibration. 2007. "Location and quantification of noise sources on a wind turbine." no. 299 (4-5):869-883.
Pope, K, GF Naterer, I Dincer, and E %J International Journal of Energy Research Tsang. 2011. "Power correlation for vertical axis wind turbines with varying geometries." no. 35 (5):423-435.
Qamar, Sayyad Basim, and Isam %J Energy Procedia Janajreh. 2017. "Investigation of effect of cambered blades on Darrieus VAWTs." no. 105:537-543.
Razali, Ahmad Mahir, Mohammad Syafiq Sapuan, Kamarulzaman Ibrahim, Azami Zaharim, and Kamaruzzaman Sopian. 2010. Mapping of annual extreme wind speed analysis from 12 stations in Peninsular Malaysia. Paper read at Proceedings of the 9th WSEAS international conference on System science and simulation in engineering.
REN21. 2019. "Renewables 2019: Global status report." *REN21 Secretariat*.
Roy, Sukanta, and Ujjwal K %J Procedia Engineering Saha. 2013. "Computational study to assess the influence of overlap ratio on static torque characteristics of a vertical axis wind turbine." no. 51:694-702.
Saad, Ahmed S, Ibrahim I El-Sharkawy, Shinichi Ookawara, and Mahmoud Ahmed. 2020. "Performance enhancement of twisted-bladed Savonius vertical axis wind turbines." *Energy Conversion and Management* no. 209:112673.

Sagharichi, A, M Zamani, and A %J Energy Ghasemi. 2018. "Effect of solidity on the performance of variable-pitch vertical axis wind turbine." no. 161:753-775.
Singh, Enderaaj, Sukanta Roy, and Yam Ke San. 2020. Numerical Analysis of Exhaust Air Energy Extractor for Cooling Tower Applications. Paper read at IOP Conference Series: Materials Science and Engineering.
Sørensen, Jens Nørkær. 2016. *General momentum theory for horizontal axis wind turbines*. Vol. 4: Springer.
Subramanian, Abhishek, S Arun Yogesh, Hrishikesh Sivanandan, Abhijit Giri, Madhavan Vasudevan, Vivek Mugundhan, and Ratna Kishore %J Energy Velamati. 2017. "Effect of airfoil and solidity on performance of small scale vertical axis wind turbine using three dimensional CFD model." no. 133:179-190.
Tabatabaeikia, Seyedsaeed, Nik Bin Nik-Ghazali, Wen Chong, Behzad Shahizare, Ahmad Fazlizan, Alireza Esmaeilzadeh, and Nima Izadyar. 2016. "A Comparative Computational Fluid Dynamics Study on an Innovative Exhaust Air Energy Recovery Wind Turbine Generator." *Energies* no. 9 (5). doi: 10.3390/en9050346.
Tabatabaeikia, Seyedsaeed, Nik Nazri Bin Nik Ghazali, Wen Tong Chong, Behzad Shahizare, Nima Izadyar, Alireza Esmaeilzadeh, Ahmad %J Energy conversion Fazlizan, and management. 2016. "Computational and experimental optimization of the exhaust air energy recovery wind turbine generator." no. 126:862-874.
Thé, Jesse, and Hesheng Yu. 2017. "A critical review on the simulations of wind turbine aerodynamics focusing on hybrid RANS-LES methods." *Energy* no. 138:257-289.
Tian, Wenlong, Zhaoyong Mao, Baoshou Zhang, and Yanjun Li. 2018. "Shape optimization of a Savonius wind rotor with different convex and concave sides." *Renewable Energy* no. 117:287-299. doi: 10.1016/j.renene.2017.10.067.
Torres, Sebastian, Agustín Marulanda, Miguel F Montoya, and Camilo Hernandez. 2022. "Geometric design optimization of a Savonius wind turbine." *Energy Conversion and Management* no. 262:115679.
Xu, Wen, Cheng-cheng Li, Sheng-xian Huang, and Ying Wang. 2022. "Aerodynamic performance improvement analysis of Savonius Vertical Axis Wind Turbine utilizing plasma excitation flow control." *Energy* no. 239:122133.
Yusri, Haziq Fahmi Muhamad, Firzana Amira Ramsay, Teo Wee Xuan, Ng Zhi Yong, Pang Ming Khai, Djamal Hissein Didane, and Bukhari Manshoor. 2023. "2D Numerical Simulation of H-type Darrieus Vertical-Axis Wind Turbine (VAWT)." *Journal of Design for Sustainable and Environment* no. 5 (1):11-16.
Zhang, Yanfeng, Zhiping Guo, Xinyu Zhu, Yuan Li, Xiaowen Song, Chang Cai, Yasunari Kamada, and Takao Maeda. 2022. "Investigation of aerodynamic forces and flow field of an H-type vertical axis wind turbine based on bionic airfoil." *Energy* no. 242:122999.

Appendix A

Line diagram of fabricated cooling tower.